91602
new 82-10

LEGAL NOTICE

This report was prepared by Ontario Hydro and, while effort has been made to assure the accuracy and applicability of the material contained herein, neither Ontario Hydro nor any person acting on its behalf:

(a) makes any warranty, express or implied with respect to the use of any information, apparatus, method or process disclosed in this report or that such use may not infringe privately owned rights; or

(b) assumes any liabilities with respect to the use of, or for damages resulting from the use of, any information, apparatus, method or process disclosed in this report.

ontario hydro
research division

EFFICIENT SHELL ELEMENTS FOR THREE-DIMENSIONAL NON-LINEAR EXPLICIT TRANSIENT DYNAMIC ANALYSIS

Report No. 89-222-K

R.G. Sauvé
Engineer
Applied Mechanics Section
Mechanical Research Department

ABSTRACT

The transient dynamic analysis of three-dimensional structures undergoing severe deformation represents a complex field in solid mechanics which is computationally very demanding. The use of explicit schemes, in this area, provide distinct advantages in terms of reliability and efficiency when applied to problems involving impact, shock and finite deformation. Some applications at Ontario Hydro, include the simulation of accidental impacts of radioactive waste transportation packages in support of licensing and design, impulsive loading of reactor components and reactor component interaction using dynamic relaxation techniques. In this report, an efficient three-dimensional bi-linear quadrilateral shell element for use in explicit transient dynamic analysis is presented. Salient features of this element include the use of one point quadrature for in-plane integration, thickness modification, and a co-rotational coordinate system which is attached to the element in order to account for the rigid body rotation of the material. The element is incorporated into the Ontario Hydro finite element code H3DMAP. A number of test cases along with experimental verifications are included which demonstrate the efficiency and applicability of the element to a variety of problems involving finite deformation.

job	file	date	report no.
21-562-051	825.2	January 26, 1990	89-222-K

91602
new 82-10

90-06653/

ontario hydro
research division

EXECUTIVE SUMMARY

EFFICIENT SHELL ELEMENTS FOR THREE-DIMENSIONAL NON-LINEAR EXPLICIT TRANSIENT DYNAMIC ANALYSIS

R.G. Sauvé
Applied Mechanics Section
Mechanical Research Department

The transient dynamic analysis of three-dimensional structures undergoing severe deformation represents a complex field in solid mechanics which is computationally very demanding. The use of explicit schemes, in this area, provide distinct advantages in terms of reliability and efficiency when applied to problems involving impact, shock and finite deformation. Some applications at Ontario Hydro, include the simulation of accidental impacts of radioactive waste transportation packages in support of licensing and design, impulsive loading of reactor components and reactor component interaction using dynamic relaxation techniques. In this report, an efficient three-dimensional bi-linear quadrilateral shell element for use in explicit transient dynamic analysis is presented.

Salient features of this element include the use of one point quadrature for in-plane integration, thickness modification, and a co-rotational coordinate system which is attached to the element in order to account for the rigid body rotation of the material. The spurious kinematic (hourglass) modes, which arise from the use of reduced integration, are controlled with a simple yet effective hourglass resisting force vector.

The co-rotational rate of deformation formulation permits the element to represent finite strain in a consistent fashion. Both elastic and elastic-plastic plane-stress constitutive laws are considered. The element is incorporated into the Ontario Hydro finite element code H3DMAP.

A number of test cases along with experimental verifications are included which demonstrate the efficiency and applicability of the element to a variety of problems involving finite deformation.

JC

job	file	date	report no.
21-562-051	825.2	January 26, 1990	89-222-K

TABLE OF CONTENTS

Page

EXECUTIVE SUMMARY

TABLE OF CONTENTS

1.0 INTRODUCTION 1

2.0 EXPLICIT TRANSIENT DYNAMIC ANALYSIS 2

2.1 Governing Equations 2
2.2 Discretization of Equations 5
2.3 Explicit Temporal Integration 7

3.0 ISOPARAMETRIC QUADRILATERAL SHELL ELEMENT FORMULATION 8

3.1 Element Geometry 8
3.2.1 Element Interpolation Function 10
3.2.2 Element Velocity Field 11
3.3 Velocity Gradient Relations 13
3.4 Rate of Deformation Components 14
3.5 Internal Force Vector 18
3.6 Stress Computation 19
3.6.1 Recovery of Normal Strain 20
3.6.2 Elastic Material Model 21
3.6.3 Elastic-Plastic Material Model 22
3.6.4 Shell Thickness Modification 27
3.7 Lumped Mass Matrix 28
3.8 Stable Time Step 29
3.9 Hourglass Stabilization 30
3.9.1 Rank Deficiency of the Strain-Rate Velocity Matrix B 31
3.9.2 Hourglass Control 35
3.9.3 Hourglass γ Operator 36
3.9.4 Hourglass Resisting Force 38
3.9.5 Hourglass Stiffness Control 39
3.9.6 Hourglass Viscosity Control 41
3.10 Pressure Boundary 41

4.0 COMPUTER IMPLEMENTATION 43

4.1 Shell Element Implementation 44
4.2 Hourglass Control Implementation 46

Table of Contents cont'd

Page

5.0 VERIFICATION CASES 48

5.1 Uniformly Loaded Cantilever Plate 48
5.2 Moment Loaded Cantilever Plate (Non-Linear Geometric) 49
5.3 Corner Supported Plate 49
5.4 Uniformly Loaded Elastic-Plastic Square Plate 50
5.5 Impulsively Loaded Circular Plate 50
5.6 Impulsively Loaded Cylindrical Shell 50
5.7 Punch Verification Test 51
5.8 Pipe Impact on Rigid Surface 52

ACKNOWLEDGMENTS 53

REFERENCES 54

LIST OF FIGURES:

3.1 Bilinear Degenerated Isoparametric Thin/Thick Shell Element
3.2 Shell Element Co-Rotational Coordinate System
3.3 Stress/Strain Measures - Elasto-Plastic Material Model
3.4 Typical Hourglass Modes for Membrane and Bending Deformations
3.5 Example of Hourglass Modes in Plate Bending
4.1 Shell Element Routines for Explicit Analysis (H3DMAP Module SHEX)
5.1.1 Geometric Non-Linear Cantilever Shell Test - P=2.85 psi Displacement Response of Node 6 and 12 in the Y-Direction
5.1.2 Geometric Non-Linear Cantilever Shell Test - P=2.85 psi Response at Time = 4ms
5.2.1 Moment Load Test for Non-Linear Shell (Dynamic Relaxation) - Model and Load
5.2.2 Displacement of Node 13 in Both X and Y Directions
5.2.3 Response at Time = 0.1 sec.
5.2.4 Response at Time = 0.4 sec.
5.3.1 Corner Supported Flat Plate Under Pressure Load H3DMAP Model
5.3.2 Response at Time = 0.2 sec.
5.3.3 Uncontrolled Hourglassing for Corner Supported Plate View A
5.3.4 Uncontrolled Hourglassing for Corner Supported Plate View B
5.3.5 Uncontrolled Hourglassing for Corner Supported Plate View C
5.3.6 Vertical Deflection of Node 73
5.4.1 Simply Supported Square Plate Test - Model, Material Properties and Applied Load
5.4.2 Displacement at Node 25 in the Y-Direction Elastic-Plastic Material
5.4.3 Displacement at Node 25 in the Y-Direction Elastic Material
5.4.4 Response at Time = 0.7 ms
5.5.1 Impulsively Loaded Circular Plate - Experimental Test Rig and Material Properties

Table of Contents (cont'd)

LIST OF FIGURES (cont'd):

5.5.2 Impulsively Loaded Circular Plate - Node Numbers
5.5.3 Impulsively Loaded Circular Plate - Element Numbers
5.5.4 Impulsively Loaded Circular Plate - Displacement in Y-Direction at Node 1 - Comparison of Theoretical and Experimental Results
5.5.5 Impulsively Loaded Circular Plate Response at Time = 0.2 ms
5.6.1 Impulsively Loaded Cylindrical Shell Model and Material Properties
5.6.2 Impulsively Loaded Cylindrical Shell Deformed Shape of Crown Line
5.6.3 Impulsively Loaded Cylindrical Shell Vertical Deflection of Node 273 and 409
5.6.4 Impulsively Loaded Cylindrical Shell Deformed Shape at X = 6.28
5.6.5 Impulsively Loaded Cylindrical Shell Response at Time = 0.8 ms
5.6.6 Effective Plastic Strain - View A
5.6.7 Effective Plastic Strain - View B
5.7.1 Punch Verification Tests
5.7.2 Punch Verification Test - Node Numbering
5.7.3 Punch Verification Test - Node Numbering - Close-up of Impact Area
5.7.4 Yield vs. Pressure Curve for Polyurethane Foam Model
5.7.5 Pressure/Volumetric Strain Curve for Polyurethane Foam Model
5.7.6 Punch Verification Test - Deformed Geometry - Response at Time = 0.028 sec
5.7.7 Punch Verification Test - Vertical Displacement at the Periphery (Node 1474)
5.7.8 Punch Verification Test - Impact Force Time History
5.7.9 Plastic Strain in Shell Element No. 10, Sampling Pt No. 3
5.7.10 Hydrostatic Stress in Solid Element No. 417
5.7.11 Plastic Strain in Metal Sheet - Outer Shell - Time: 28 ms
5.7.12 Plastic Strain in Metal Sheet - Inner Shell - Time: 28 ms
5.7.13 von Mises Stress in Foam at Time: 28 ms
5.7.14 Hydrostatic Stress in Foam at Time: 28 ms
5.8.1 Pipe Whip Test - Model and Material Properties
5.8.2 Pipe Whip Test - Deformed Structure - Response at Time = 0.0035 sec
5.8.3 Effective Plastic Strain - Outer Shell - Time = 3.5 ms
5.8.4 Effective Plastic Strain - Inner Shell - Time = 3.5 ms
5.8.5 von Mises Stress - Outer Shell - Time = 3.5 ms
5.8.6 von Mises Stress - Inner Shell - Time = 3.5 ms
5.8.7 Pipe Whip Test - X-Displacement Time History of Node 1

APPENDIX A1: Central Difference Operator Non-Linear Structural Dynamics

APPENDIX A2: Three-Dimensional Elastic-Plastic Material Model with Isotropic Hardening

APPENDIX A3: Simplification of Gradients in One Point Gauss Quadrature

ontario hydro
research division

To Dr. D. Mills
Director of Research

EFFICIENT SHELL ELEMENTS FOR THREE-DIMENSIONAL NON-LINEAR EXPLICIT TRANSIENT DYNAMIC ANALYSIS

1.0 INTRODUCTION

Although the development of general shell elements has been the topic of numerous publications over the years/3/, the focus on efficient shell elements for use with explicit time integration operators has been limited. The use of explicit operators, such as the central difference scheme, provide distinct advantages in terms of computational efficiency and reliability in the non-linear transient dynamic analysis of structures. In this report, non-linearity implies finite deformation which includes both geometric and material non-linearity.

At Ontario Hydro, a major effort is underway in the area of radioactive waste management. One important facet of this program is the design and construction of transportation packages for high and low level radioactive waste. These packages must survive various accidental impact scenarios/15/ such as a 9m drop onto an unyielding target, as part of the regulatory requirements governing the safe transport of solid and liquid radioactive materials. Many of these containers utilize thin shell structures, some containing fluid such as heavy water, which undergo severe deformation during impact. Predictions of response under these conditions are necessary in order to improve and verify structural integrity economically prior to licensing tests. Explicit techniques are well suited to such impulsively loaded structural and crackworthiness problems involving large deformation and fluid structure interaction. In addition, the use of explicit temporal operators in conjunction with dynamic relaxation techniques can be used to accurately simulate the response of nuclear reactor components/18/.

In this report, an efficient three-dimensional bi-linear quadrilateral shell element for use in non-linear structural problems such as those previously described is presented. The element is an extension of the formulation given in /2/, which is currently used for implicit analyses in the Ontario Hydro general purpose three dimensional finite element computer code H3DMAP/1,2/.

Following the direction proposed in /6,12/, modifications to the element in /2/, are made which result in an efficient, flexible, and fairly accurate, yet simple shell element. Simplicity is one of the salient features of the formulation. The use of more complicated higher order elements in explicit time integration necessitates the use of a severely restricted stable time

step due to the high frequency content of these elements. Although more mesh refinement is required using the simple elements, this formulation still provides the most accurate solutions for the same computer run time.

In the explicit time integration of the equations of motion, a major portion of the computation time is spent in the evaluation of the element internal force vector at each time step. This requires the numerical evaluation of strain components for use in material constitutive calculations at each element integration point. At each sampling point of the mid-surface, through-thickness integration is necessary in order to capture the combined bending-membrane response. Thus, the use of exact integration using 2x2 Gauss quadrature is prohibitively expensive, especially in problems involving a non-linear constitutive law (i.e. elastic-plastic material). Following /6/, one point quadrature is adopted in the plane of the element which leads to more than a four-fold decrease in constitutive computations. This is particularly attractive for efficient explicit time integration.

Unfortunately, the use of reduced integration allows kinematic or zero energy modes which are not represented in the formulation of the element matrices. This rank deficiency leads to the possibility of spurious behaviour known as hourglassing/11/. Hourglass control is developed, for the element described herein, in the form of a resisting hourglass force vector based on either viscous or stiffness control. Work in /11,10/ proposes a method of controlling hourglassing for membrane and plate bending quadrilateral elements. The hourglass control described in this report differs from this work in the definition of hourglass stress. The approach developed here leads to a more computationally attractive yet effective scheme.

One of the salient features of the element is the use of the rate of deformation formulation, in which computations are performed directly in terms of rates and velocities. A velocity strain tensor is used in conjunction with a co-rotational coordinate system which is attached to the element in order to account for the rigid body rotation of the material. This avoids the difficulties surrounding the question of objectivity and frame invariance which arise in finite deformation problems. A benefit of this approach arises in the definition of stress measures. In the version of the shell element developed for implicit problems in /2,5/, the Lagrangian formulation leads to Green-St Venant strain and its conjugate the 2nd Piola-Kirchhoff stress. The use of a co-rotational rate of deformation formulation leads to the Cauchy stress which is desirable since it is a physical stress and is simple to compute. In addition, the constitutive law is easily given in terms of true stress and logarithmic strain which is compatible with these tensors. The disadvantage with this formulation is the mandatory use of smaller time steps. This is not a problem since explicit temporal operators require a stable time step whose magnitude precludes significant errors in the integration of the rate equations.

A plane stress constitutive law is used for elastic and elastic-plastic materials. In keeping with the general applicability of this shell element, modification of the thickness is considered using the normal strain component. This is consistent with the stress-strain measures used. The single step

radial return method/8,9/ is used to model elastic-plastic materials. The plane stress condition necessitates a modification to this method in the form of an iterative scheme to enforce this condition in a yielded material.

The shell element developed in this report has been incorporated into the explicit transient dynamic analysis option available in the computer code H3DMAP Version 4/1/. This option enables the prediction of large deformation response of structures undergoing shock and impact. The element library includes continuum elements, analog elements and non-linear beam elements which may be used in conjunction with the present shell elements, to model complex geometries. The hydrodynamic formulation used in the code permits materials such as foams and fluids as well as conventional elastic and elastic-plastic materials to be modelled.

This report presents the details of the formulation including the discretization of the momentum equations, the derivation of the element matrices, hourglass control, the computer implementation, and a number of verification cases including cases where comparisons with experimental results have been made.

2.0 EXPLICIT TRANSIENT DYNAMIC ANALYSIS

2.1 Governing Equations

Consider a body undergoing time dependent deformations in a reference Cartesian coordinate system x_i. Initially at time t=0;

$$x_i^t = x_i^o$$

$$\dot{x}_i^t = \dot{x}_i^o$$

where x_i^o = initial coordinates $\begin{Bmatrix} x^o \\ y^o \\ z^o \end{Bmatrix}$

$$\dot{x}_i^o = \frac{dx_i^o}{dt} = \text{initial velocities } \begin{Bmatrix} \dot{x}^o \\ \dot{y}^o \\ \dot{z}^o \end{Bmatrix}$$

In general,

$$x_i^{t+\Delta t} = x_i^t + u_i^{t+\Delta t}$$

where $u_i^{t+\Delta t}$ is the displacement during time step Δt.

Using the momentum principle/4/ which states that the time rate of change of the total momentum on a given collection of particles is equal to the vector sum of all external forces acting on these particles, and performing a momentum balance leads to the following momentum equations in three dimensions;

$$\rho\frac{d\dot{x}}{dt} = F_x + \frac{\partial\sigma_{xx}}{\partial x} + \frac{\partial\sigma_{xy}}{\partial y} + \frac{\partial\sigma_{xz}}{\partial z}$$

$$\rho\frac{d\dot{y}}{dt} = F_y + \frac{\partial\sigma_{yx}}{\partial x} + \frac{\partial\sigma_{yy}}{\partial y} + \frac{\partial\sigma_{yz}}{\partial z}$$

$$\rho\frac{d\dot{z}}{dt} = F_z + \frac{\partial\sigma_{zx}}{\partial x} + \frac{\partial\sigma_{zy}}{\partial y} + \frac{\partial\sigma_{zz}}{\partial z}$$

where;

ρ - mass density

$\dot{x}$, $\dot{y}$, $\dot{z}$ - velocity with respect to x, y, z, directions respectively

F_x, F_y, F_z - body force components per unit volume in the x, y, z directions respectively.

σ_{ij} - Cauchy stress

These equations are known as the Cauchy Equations of Motion and are alternatively expressed as;

$$\rho\frac{d\dot{x}_i}{dt} = F_i + \frac{\partial\sigma_{ij}}{\partial x_j}$$

where i = 1,2,3 denotes the x,y,z directions and the summation convention is used.

A solution to the equations are sought subject to the following boundary conditions;

Kinematic boundary conditions at time t on boundary b_d:

$$u_i^t = d_i^t$$

where d_i^t are imposed displacements on boundary b_d.

Traction boundary conditions at time t on boundary b_p:

$$\sigma_{ij} n_j = P_i$$

where b_p represents the boundary upon which the tractions P_i are specified and n_j is a unit outward normal to the boundary of b_p.

In addition, jump conditions at contact discontinuities must satisfy:

$$(\sigma_{ij}^{+} - \sigma_{ij}^{-}) n_j = 0 \quad \text{on boundary } b_c$$

In this case, b_c is the contact surface where $x_i^{+} = x_i^{-}$. The superscripts '+' and '-' denote the two sides of the contact surface.

The continuity equation is given by /4/:

$$\dot{\rho} + \rho \frac{\partial \dot{x}_i}{\partial x_i} = 0$$

In the absence of mass transport, the continuity equation is stated as;

$$\rho^t V^t = \rho_o V_o$$

where ρ^t, V^t and ρ_o, V_o are the density and volume at time t and in the initial configuration respectively.

2.2 Discretization of Equations

Using the Galerkin method of weighted residuals/3,4/, a set of weighting functions $\bar{N}$ are selected and the weighted average of the residual is set to zero. The interior R_I and boundary R_B residuals for the equations in section 2.1 are written as;

$$R_I = \int_v \bar{N} \left[\rho \frac{d\dot{\bar{x}}_i}{dt} - \frac{\partial \bar{\sigma}_{ij}}{\partial x_j} - F_i \right] dV$$

in Region V and:

$$R_B = \int_{b_p} \bar{N}(\bar{\sigma}_{ij} n_j - P_i)\, ds + \int_{b_c} \bar{N}(\bar{\sigma}_{ij}^{+} - \bar{\sigma}_{ij}^{-})\, n_j ds$$

on boundaries b_p and b_c of V,

where $\dot{\bar{x}}_i^t$ and $\bar{\sigma}_{ij}$ are approximations of $\dot{x}_i^t$ and σ_{ij} respectively.

$$R_i = R_{I_i} + R_{B_i} = 0$$

The integration of the terms associated with $\bar{\sigma}_{ij}$ proceeds as follows;

$$\partial \frac{(\bar{N}\,\bar{\sigma}_{ij})}{\partial x_j} = \frac{\partial \bar{N}}{\partial x_j}\,\bar{\sigma}_{ij} + \frac{\partial \bar{\sigma}_{ij}}{\partial x_j}\,\bar{N}$$

Thus,

$$\int_v \bar{N}\,\frac{\partial \bar{\sigma}_{ij}}{\partial x_j}\,dV = \int_v \partial \frac{(\bar{N}\,\bar{\sigma}_{ij})}{\partial x_j}\,dV - \int_v \frac{\partial \bar{N}}{\partial x_j}\,\bar{\sigma}_{ij}\,dV$$

From Gauss's Theorem/4,7/, the integral of the divergence of a vector over a volume bounded by a closed surface is equal to the integral of the outer normal component of the vector over the closed surface. Therefore,

$$\int_v \partial \frac{(\bar{N}\,\bar{\sigma}_{ij})}{\partial x_j}\,dV = \int_s (\bar{N}\,\bar{\sigma}_{ij}) n_j\,ds$$

Substitution into the expression for R_i leads to;

$$R_i = \int_v \bar{N}\,\rho \frac{d\dot{\bar{x}}_i}{dt}\,dV + \int_v \frac{\partial \bar{N}}{\partial x_j}\,\bar{\sigma}_{ij}\,dV - \int_v \bar{N} F_i\,dV - \int_{b_p} \bar{N} P_i\,ds = 0$$

This represents a weak form of the equilibrium equations.

Summing over NE elements;

$$\sum_{k=1}^{NE} \left[\int_{v_k} \rho\,\bar{N}^k \frac{d\dot{\bar{x}}_i}{dt}\,dV + \int_{v_k} \frac{\partial \bar{N}^k}{\partial x_j}\,\bar{\sigma}^k_{ij}\,dV - \int_{v_k} \bar{N}^k F^k_i\,dV - \int_{b_{pk}} \bar{N}^k p^k_i\,ds \right] = 0$$

Considering $\bar{N}$ is an interpolation function;

$$\bar{N}^k = (N_1, N_2 \ldots N_n)^k$$

where N_1, N_2 ... N_n are the interpolation functions for an element with 'n' nodes.

The value of $\dot{\bar{x}}_i$ at a point within element k is then obtained by interpolation of nodal values $\dot{x}_i^j$;

$$\dot{\bar{x}}_i = \sum_{j=1}^{n} N_j^k \dot{x}_i^j \quad \text{at time 't'.}$$

Using matrix representation;

$$\sum_{k=1}^{NE} \left[\int_{v_k} \rho N^T N \, dV \frac{d\dot{x}}{dt} + \int_{v_k} B^T \sigma \, dV - \int_{v_k} N^T F \, dV - \int_{b_{pk}} N^T p ds \right] = 0$$

The derivation of each of the terms given above is unique to the type of element considered (i.e. beam, shell, continuum element).

Neglecting body forces, the discretized equations of motion for an element are as follows;

$$M \frac{d\dot{x}}{dt} + F_{int}^t = F_{ext}^t$$

where M is the mass matrix, F_{int}^t, F_{ext}^t are the element internal and external force vectors respectively.

2.3 Explicit Temporal Integration

The time integration of the equations of motion is performed using the central difference operator.

The integration operator is summarized as follows;

- $\frac{d\dot{x}^t}{dt} = \ddot{x}^t = M^{-1} \left[F_{ext}^t - F_{int}^t \right]$
- $\Delta t^{\frac{1}{2}} = \frac{\Delta t1 + \Delta t2}{2}$
- $\dot{x}^{t+\Delta t2/2} = \dot{x}^{t-\Delta t1/2} + \Delta t^{\frac{1}{2}} \ddot{x}^t$
- $x^{t+\Delta t2} = x^t + \Delta t2 \, \dot{x}^{t+\Delta t2/2}$
- update time $t+\Delta t2$
- obtain $F_{int}^{t+\Delta t2}$ and repeat above steps.

where $\ddot{x}^t$, $\dot{x}^t$, x^t are the nodal acceleration, velocity and coordinate vectors respectively.

This operator is explicit and as such is conditionally stable so that values of the time step Δt must be maintained at values below a critical time step based on the Courant stability limit Δt_{cr}:

$$\Delta t_{cr} \leq \frac{2}{\omega_{max}}$$

where ω_{max} is the highest eigenvalue of the system. The values of Δt_{cr} used for the elements are given in section 3. Further details are given in Appendix 1.

3.0 ISOPARAMETRIC QUADRILATERAL SHELL ELEMENT FORMULATION

3.1 Element Geometry

One of the salient features of the element (figure 3.1) described herein is the simplicity introduced by the use of a co-rotational coordinate system. This local system, denoted by x'y'z', is attached to the element in order to account for the rigid body rotation of the material. This avoids the difficulties surrounding the question of objectivity or frame invariance associated with finite deformation problems.

Referring to figure 3.2, the direction vectors ${}^t\vec{v}_z$ and ${}^t\vec{v}_y$ defining the element co-rotational system at time 't' are obtained using the following vector cross products:

$$\text{unit vector } \vec{v}_x = \frac{\vec{V}_x}{|\vec{V}_x|} = \frac{(x_4-x_3)\vec{I} + (y_4-y_3)\vec{J} + (z_4-z_3)\vec{k}}{((x_4-x_3)^2 + (y_4-y_3)^2 + (z_4-z_3)^2)^{0.5}}$$

$$\vec{v}_Q = \frac{\vec{V}_Q}{|\vec{V}_Q|}$$

$$\vec{v}_z = \vec{v}_x \times \vec{v}_Q$$

$$\vec{v}_y = \vec{v}_z \times \vec{v}_x$$

$x'^t = Tx^t$ current local nodal coordinates

$\dot{x}'^{t+\Delta t/2} = T\dot{x}^{t+\Delta t/2}$ current local velocity components

where;

$$T = \begin{bmatrix} v_{x1} & v_{x2} & v_{x3} \\ v_{y1} & v_{y2} & v_{y3} \\ v_{z1} & v_{z2} & v_{z3} \end{bmatrix}$$

This is the time varying transformation matrix of direction cosines relating the global reference frame to the element co-rotational coordinate system, and

$$\dot{x}'^{,t+\Delta t/2} = \begin{Bmatrix} \dot{x}'_1 \\ \dot{y}'_1 \\ \dot{z}'_1 \\ R\dot{x}'_1 \\ R\dot{y}'_1 \end{Bmatrix}^{t+\Delta t/2} \quad \text{at node 1}$$

The shell local coordinates must be obtained in the x'y'z' system at time 't' since the strain-displacement relation is based on the convected coordinates at each time step. These local coordinates are obtained at each step as follows:

- Referring to figure 3.2, the local origin is located at node 3 (i.e. x'_3-y'_3-0)
- Using the components of matrix T, obtain the local coordinates at nodes 1, 2 and 4 relative to the local origin at node 3;

$$q_1 = (t_{11} \quad t_{12} \quad t_{13})$$

$$q_2 = (t_{21} \quad t_{22} \quad t_{23})$$

$$x'_4 = q_1 \cdot \bar{v}_{43} = t_{11}(x_4 - x_3) + t_{12}(y_4 - y_3) + t_{13}(z_4 - z_3)$$

$$y'_4 = q_2 \cdot \bar{v}_{43}$$

$$x'_2 = q_1 \cdot \bar{v}_{23}$$

$$y'_2 = q_2 \cdot \bar{v}_{23}$$

$$x'_1 = q_1 \cdot \bar{v}_{12} + x'_2$$

$$y'_1 = q_2 \cdot \bar{v}_{12} + y'_2$$

3.2.1 Shell Interpolation Function

The shell element shown in figure 3.1, is defined in natural coordinates r,s,t. The position of any point within the element in terms of nodal thickness, and local coordinates is given as:

$$\begin{Bmatrix} x'(r,s,t) \\ y'(r,s,t) \\ z'(r,s,t) \end{Bmatrix} = \sum_{i=1}^{4} N_i(r,s) \begin{Bmatrix} x'_i \\ y'_i \\ 0.5th_i \end{Bmatrix}$$

where;

h_i - thickness at node i

x'_i, y'_i, z'_i - local coordinates at node "i" at point r,s,t from section 3.1.

The bi-linear shape functions for the mid-plane (t=0) are/2,3/:

$$N_i(r,s) = 0.25\ (1 + r_i r)(1+s_i s)$$

where r_i, s_i are the natural coordinates of node i;

$N_1 = 0.25(1+r)(1+s)$	$r_1 = 1$	$s_1 = 1$
$N_2 = 0.25(1-r)(1+s)$	$r_2 = -1$	$s_2 = 1$
$N_3 = 0.25(1-r)(1-s)$	$r_3 = -1$	$s_3 = -1$
$N_4 = 0.25(1+r)(1-s)$	$r_4 = 1$	$s_4 = -1$

Since reduced integration in the mid-plane using single point Gauss quadrature is considered, the sampling points r=s=0 result in simplification for N_i.

For 1 point quadrature, r=s=0, $N_i = 0.25$ for i=1,4

Transformation to the local plane x'y' of the element leads to a 2-D Jacobian; (i.e. z'=0).

For single point quadrature;

$$J_{11} = \frac{\partial x'}{\partial r} = \sum_{i=1}^{4} \frac{\partial N_i(0,0)}{\partial r}\, x'_i = \sum_{i=1}^{4} 0.25 r_i x'_i$$

$$J_{21} = \frac{\partial x'}{\partial s} = \sum_{i=1}^{4} 0.25 s_i x'_i$$

$$J_{12} = \frac{\partial y'}{\partial r} = \sum_{i=1}^{4} 0.25 r_i y'_i$$

$$J_{22} = \frac{\partial y'}{\partial s} = \sum_{i=1}^{4} 0.25 s_i y'_i$$

$$z'_i = 0.5 th_i$$

$$J = \begin{bmatrix} J_{11} & J_{12} \\ J_{21} & J_{22} \end{bmatrix}$$

3.2.2 Element Velocity Field

The element local velocity field at a point (r,s,t) within the element is given as:

$$\dot{u}'(r,s,t) = \sum_{i=1}^{4} N_i(r,s) \left[\dot{u}'_i + \dot{u}'_{rel_i}(t) \right]$$

where $\dot{u}'_i$ = mid surface local nodal velocity vector at node 'i'

$$= \begin{Bmatrix} \dot{x}'_i \\ \dot{y}'_i \\ \dot{z}'_i \end{Bmatrix}$$

$\dot{u}'_{rel_i}(t)$ = relative local nodal velocity vector produced by a rotation at node i

In the local or material axis, the relative velocity components are as shown;

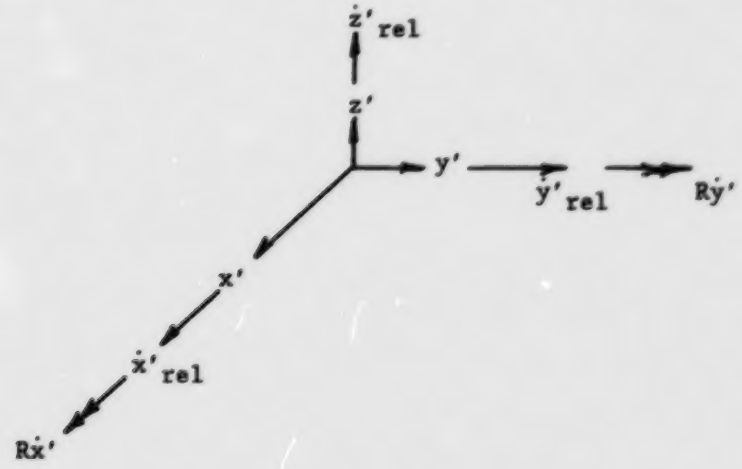

$$\dot{x}'_{rel_i} = 0.5th_i R\dot{y}'_i$$

$$\dot{y}_{rel_i} = -0.5th_i R\dot{x}'_i$$

$$\dot{z}'_{rel} = 0.$$

$$\dot{u}'(r,s,t) = \sum_{i=1}^{4} N_i(r,s) \left[\dot{u}'_i + 0.5th_i \phi \hat{\theta}'_i \right]$$

where $\phi = \begin{bmatrix} 0 & 1 & 0 \\ -1 & 0 & 0 \\ 0 & 0 & 0 \end{bmatrix}$

$\hat{\theta}'_i$ = local rotational velocity vector

$$= \begin{Bmatrix} R\dot{x}'_i \\ R\dot{y}'_i \\ 0 \end{Bmatrix}$$

$$\dot{x}'(r,s,t) = \sum_{i=1}^{4} N_i(r,s) \left[\dot{x}'_i + 0.5 th_i R \dot{y}'_i \right]$$

$$\dot{y}'(r,s,t) = \sum_{i=1}^{4} N_i(r,s) \left[\dot{y}'_i - 0.5 th_i R \dot{x}'_i \right]$$

$$\dot{z}'(r,s,t) = \sum_{i=1}^{4} N_i(r,s)\, \dot{z}'_i$$

3.3 Velocity Gradient Relations

The velocity derivatives in the local system are obtained from the displacement derivatives in the natural system (r,s,t) as follows:

Using the chain rule of differentiation:

$$\frac{\partial \dot{x}'}{\partial r} = \frac{\partial \dot{x}'}{\partial x'} \cdot \frac{\partial x'}{\partial r} + \frac{\partial \dot{x}'}{\partial y'} \cdot \frac{\partial y'}{\partial r} + \frac{\partial \dot{x}'}{\partial z'} \cdot \frac{\partial z'}{\partial r}$$

$$\frac{\partial \dot{x}'}{\partial s} = \frac{\partial \dot{x}'}{\partial x'} \cdot \frac{\partial x'}{\partial s} + \frac{\partial \dot{x}'}{\partial y'} \cdot \frac{\partial y'}{\partial s} + \frac{\partial \dot{x}'}{\partial z'} \cdot \frac{\partial z'}{\partial s}$$

$$\frac{\partial \dot{x}'}{\partial t} = \frac{\partial \dot{x}'}{\partial x'} \cdot \frac{\partial x'}{\partial t} + \frac{\partial \dot{x}'}{\partial y'} \cdot \frac{\partial y'}{\partial t} + \frac{\partial \dot{x}'}{\partial z'} \cdot \frac{\partial z'}{\partial t}$$

$$\begin{Bmatrix} \partial\dot{x}'/\partial r \\ \partial\dot{x}'/\partial s \\ \partial\dot{x}'/\partial t \end{Bmatrix} = \begin{bmatrix} \partial x'/\partial r & \partial y'/\partial r & \partial z'/\partial r \\ \partial x'/\partial s & \partial y'/\partial s & \partial z'/\partial s \\ \partial x'/\partial t & \partial y'/\partial t & \partial z'/\partial t \end{bmatrix} \begin{Bmatrix} \partial\dot{x}'/\partial x' \\ \partial\dot{x}'/\partial y' \\ \partial\dot{x}'/\partial z' \end{Bmatrix} = J \begin{Bmatrix} \partial\dot{x}'/\partial x' \\ \partial\dot{x}'/\partial y' \\ \partial\dot{x}'/\partial z' \end{Bmatrix}$$

Similarly for $\partial\dot{y}'/\partial x'$, $\partial\dot{y}'/\partial y'$, ----------, $\partial\dot{z}'/\partial z'$

$$\begin{Bmatrix} \partial\dot{x}'/\partial x' \\ \partial\dot{x}'/\partial y' \\ \partial\dot{x}'/\partial z' \end{Bmatrix} = J^{-1} \begin{Bmatrix} \partial\dot{x}'/\partial r \\ \partial\dot{x}'/\partial s \\ \partial\dot{x}'/\partial t \end{Bmatrix}$$

where J is the Jacobian matrix and J^{-1} is its inverse.

The complete set of velocity gradients in the natural coordinates are related to those in local coordinates as:

$$\begin{Bmatrix} \partial\dot{x}'/\partial x' \\ \partial\dot{x}'/\partial y' \\ \partial\dot{x}'/\partial z' \\ \partial\dot{y}'/\partial x' \\ \partial\dot{y}'/\partial y' \\ \partial\dot{y}'/\partial z' \\ \partial\dot{z}'/\partial x' \\ \partial\dot{z}'/\partial y' \\ \partial\dot{z}'/\partial z' \end{Bmatrix} = \underset{(9x9)}{\begin{bmatrix} J^{-1} & & \\ & J^{-1} & \\ & & J^{-1} \end{bmatrix}} \cdot \begin{Bmatrix} \partial\dot{x}'/\partial r \\ \partial\dot{x}'/\partial s \\ \partial\dot{x}'/\partial t \\ \partial\dot{y}'/\partial r \\ \cdot \\ \cdot \\ \cdot \\ \cdot \\ \partial\dot{z}'/\partial t \end{Bmatrix}$$

3.4 Rate of Deformation Components

The components of the rate of deformation or velocity strain, $\dot{\epsilon}$, are given in the material or co-rotational coordinate system following the shell assumption of plane stress as:

in tensor notation; $$\dot{\epsilon}_{ij} = \frac{1}{2}\left(\frac{\partial\dot{x}_i}{\partial x_j} + \frac{\partial\dot{x}_j}{\partial x_i}\right)$$

in component form;

$$\dot{\epsilon}(r,s,t) = \begin{Bmatrix} \dot{\epsilon}'_{11} \\ \dot{\epsilon}'_{22} \\ 2\dot{\epsilon}'_{12} \\ 2\dot{\epsilon}'_{13} \\ 2\dot{\epsilon}'_{23} \end{Bmatrix} = \begin{Bmatrix} \dfrac{\partial\dot{x}'}{\partial x'} \\ \dfrac{\partial\dot{y}'}{\partial y'} \\ \dfrac{\partial\dot{x}'}{\partial y'} + \dfrac{\partial\dot{y}'}{\partial x'} \\ \dfrac{\partial\dot{x}'}{\partial z'} + \dfrac{\partial\dot{z}'}{\partial x'} \\ \dfrac{\partial\dot{y}'}{\partial z'} + \dfrac{\partial\dot{z}'}{\partial y'} \end{Bmatrix}$$

where $\dot{\epsilon}(r,s,t)$ = velocity strain.

The stress measure corresponding to these rate of deformation components is the Cauchy stress which is the physical stress component/4,8/.

The components are obtained from the velocity gradients using the planar Jacobian:

$$\begin{Bmatrix} \frac{\partial N_i}{\partial x'} \\ \frac{\partial N_i}{\partial y'} \end{Bmatrix} = [J]^{-1} \begin{Bmatrix} \frac{\partial N_i}{\partial r} \\ \frac{\partial N_i}{\partial s} \end{Bmatrix}$$

$$\frac{\partial \dot{x}'}{\partial x'} = \sum_{i=1}^{4} \frac{\partial N_i(r,s)}{\partial x'} \left[\dot{x}'_i + 0.5 th_i \, R\dot{y}'_i \right]$$

$$\frac{\partial \dot{y}'}{\partial y'} = \sum_{i=1}^{4} \frac{\partial N_i(r,s)}{\partial y'} \left[\dot{y}'_i - 0.5 th_i \, R\dot{x}'_i \right]$$

$$\frac{\partial \dot{x}'}{\partial y'} + \frac{\partial \dot{y}'}{\partial x'} = \sum_{i=1}^{4} \left[\frac{\partial N_i(r,s)}{\partial y'} \left[\dot{x}'_i + 0.5 th_i \, R\dot{y}'_i \right] + \frac{\partial N_i(r,s)}{\partial x'} \left[\dot{y}'_i - 0.5 th_i \, R\dot{x}'_i \right] \right]$$

$$\frac{\partial \dot{x}'}{\partial z'} + \frac{\partial \dot{z}'}{\partial x'} = \sum_{i=1}^{4} \left[\frac{\partial N_i(r,s)}{\partial x'} \dot{z}'_i + N_i(r,s) \, Ry'_i \right]$$

$$\frac{\partial \dot{y}'}{\partial z'} + \frac{\partial \dot{z}'}{\partial y'} = \sum_{i=1}^{4} \left[\frac{\partial N_i(r,s)}{\partial y'} \dot{z}'_i - N_i(r,s) \, Rx'_i \right]$$

A matrix, B, relating the velocity strain components to nodal velocities can now be derived.

The velocity strains are given by:

$$\dot{\epsilon}' = \underset{5x5}{\mathbf{B}}\dot{x}'$$

$$\begin{Bmatrix} \dot{\epsilon}'_{11} \\ \dot{\epsilon}'_{22} \\ 2\dot{\epsilon}'_{12} \\ 2\dot{\epsilon}'_{13} \\ 2\dot{\epsilon}'_{23} \end{Bmatrix} = \sum_{i=1}^{4} \begin{bmatrix} \frac{\partial N_i(r,s)}{\partial x'} & 0 & 0 & 0 & \frac{\partial N_i(r,s)0.5th_i}{\partial x'} \\ 0 & \frac{\partial N_i(r,s)}{\partial y'} & 0 & -\frac{\partial N_i(r,s)0.5th_i}{\partial y'} & 0 \\ \frac{\partial N_i(r,s)}{\partial y'} & \frac{\partial N_i(r,s)}{\partial x'} & 0 & -\frac{\partial N_i(r,s)0.5th_i}{\partial x'} & \frac{\partial N_i(r,s)0.5th_i}{\partial y'} \\ 0 & 0 & \frac{\partial N_i(r,s)}{\partial x'} & 0 & N_i(r,s) \\ 0 & 0 & \frac{\partial N_i(r,s)}{\partial y'} & -N_i(r,s) & 0 \end{bmatrix} \begin{Bmatrix} \dot{x}'_i \\ \dot{y}'_i \\ \dot{z}'_i \\ R\dot{x}'_i \\ R\dot{y}'_i \end{Bmatrix}$$

where the transpose of B(r,s,t) at node "i" is given as:

$$\mathbf{B}_i^T = \begin{bmatrix} \frac{\partial N_i}{\partial x'} & 0 & \frac{\partial N_i}{\partial y'} & 0 & 0 \\ 0 & \frac{\partial N_i}{\partial y'} & \frac{\partial N_i}{\partial x'} & 0 & 0 \\ 0 & 0 & 0 & \frac{\partial N_i}{\partial x'} & \frac{\partial N_i}{\partial y'} \\ 0 & -\frac{\partial N_i}{\partial y'}0.5th_i & -\frac{\partial N_i}{\partial x'}0.5th_i & 0 & -N_i \\ \frac{\partial N_i}{\partial x'}0.5th_i & 0 & \frac{\partial N_i}{\partial y'}0.5th_i & N_i & 0 \end{bmatrix}$$

As demonstrated in Appendix A3, 1 pt Gauss Quadrature in-plane (r-s-0), results in significant simplification of the previous relations. For r-s-0, at the element centroid:

$$J_{11} = \sum_{i-1}^{4} 0.25\, r_i x'_i \qquad J_{12} = \sum_{i-1}^{4} 0.25\, r_i y'_i$$

$$J_{21} = \sum_{i-1}^{4} 0.25\, s_i x'_i \qquad J_{22} = \sum_{i-1}^{4} 0.25\, s_i y'_i$$

$$J = \begin{bmatrix} J_{11} & J_{12} \\ J_{21} & J_{22} \end{bmatrix} \qquad [J]^{-1} = \frac{\begin{bmatrix} J_{22} & -J_{12} \\ -J_{21} & J_{11} \end{bmatrix}}{|J|}$$

where: $|J| = (J_{11}J_{22} - J_{12}J_{21})$

$$N_i(0,0) = 0.25$$

$$\frac{\partial N_i(0,0)}{\partial x'} = J_{11}^{-1} \frac{\partial N_i}{\partial r} + J_{12}^{-1} \frac{\partial N_i}{\partial s}$$

$$= J_{11}^{-1}\, 0.25 r_i + J_{12}^{-1}\, 0.25\, s_i$$

$$\frac{\partial N_i(0,0)}{\partial y'} = J_{21}^{-1} \frac{\partial N_i}{\partial r} + J_{22}^{-1} \frac{\partial N_i}{\partial s}$$

$$= J_{21}^{-1}\, 0.25 r_i + J_{22}^{-1}\, 0.25\, s_i$$

In Appendix A3, closed form expression for $\frac{\partial N_i}{\partial x'}$, $\frac{\partial N_i}{\partial y'}$ are derived.

Typically, the velocity strain $\dot{\epsilon}$, is obtained using the B matrix applied to the local nodal variables of velocity and the stresses obtained as follows:

$$\sigma_{ij}^{t+\Delta t} = \sigma_{ij}^{t} + C_{ijkl}\dot{\epsilon}_{kl}^{t+\Delta t/2}\Delta t$$

where the stress, σ, is computed in the corotational system x', y', z' using a constitutive law C_{ijkl} as discussed in section 3.6. Since the central difference operator is used in the time integration, the rate components are obtained at the mid-step (t+Δt/2).

3.5 Internal Force Vector

As described in section 2.2, the local internal force vector F'^{t}_{int} at time 't' is given as:

$$F'^{t}_{int} = \int_{vol} B^{T}\sigma^{t} dv$$

where superscript T denotes transpose of the matrix.

Using 1 pt. Gauss Quadrature in the mid-plane (i.e. r=s=0);

$$F'^{t}_{int} = \frac{h}{2} \sum_{k=1}^{nl} \bar{\alpha}_k \, B^{T}(0,0,t_k) \, \sigma^{t}(0,0,t_k) \, |J^{t}(0,0)|$$

where nl = order of Gauss Quadrature in the local thickness direction

t_k = sampling point

$\bar{\alpha}_k$ = weighting constant

The plane area of the element at time 't' is approximated by $A^{t} = 4|J^{t}(0,0)|$

In order to capture the material non-linearity, numerical integration through the thickness is required. Typically, nl=3 for elastic and nl=4 for hypoelastic problems is used. For membrane resistance only, nl=1 is specified since this ignores all bending contributions.

The global element internal force vector F^{t}_{int} is obtained using the transformation matrix T derived in section 3.1 as:

$$F^{t}_{int_i} = T^{T} F'^{t}_{int_i}$$

for each node and assembled into the global internal system force vector.

At each time step, the current coordinates are used to evaluate B, J and T. In the computer implementation, the constant terms of B, $\dot{\epsilon}$, A are evaluated only once prior to entering the thickness integration.

3.6 Stress Computation

The Cauchy stresses are computed in terms of the co-rotational components defined by the transformation given in section 3.1 which relates the material or local element axis x', y', z' to the global reference axis. Once the velocity strains, $\dot{\epsilon}$, are obtained from the nodal velocities using the B matrix, the stresses, σ, at time t+Δt are obtained from a constitutive relation $C(\sigma)$ as follows:

$$\sigma_{ij}^{t+\Delta t} = \sigma_{ij}^{t} + C_{ijkl}\, \dot{\epsilon}_{kl}^{t+\Delta t/2}\, \Delta t$$

Note that the rate quantities are accurately evaluated at the mid-step (t+Δt/2) using the central difference operator.

Following the shell assumption of plane stress;

$$\sigma = \begin{Bmatrix} \sigma_{11} \\ \sigma_{22} \\ \sigma_{12} \\ \sigma_{13} \\ \sigma_{23} \end{Bmatrix}$$

The components σ_{13} and σ_{23} are basically taken as penalty parameters to discretely enforce the Kirchhoff conditions/6/. In applications involving thin plates or shells, they do not function as material parameters but as numerical constants to enforce the associated kinematic behaviour. In the implementation described herein, σ_{13} and σ_{23} are obtained exclusively with an elastic constitutive law, whereas the remaining components may be derived using either elastic or inelastic constitutive relations as described in the following sections.

The hydrostatic or spherical component of stress is treated separately from the deviatoric components. A typical computation at time t+Δt follows:

- Obtain the increment in hydrostatic stress ΔP;

$$\dot{\epsilon}_v^{t+\Delta t/2} = (\dot{\epsilon}_{11} + \dot{\epsilon}_{22} + \dot{\epsilon}_{33})^{t+\Delta t/2}$$

$$\Delta P^{t+\Delta t} = K \dot{\epsilon}_v^{t+\Delta t/2}\, \Delta t$$

where K = material bulk modulus.

- The deviatoric components $\dot{\varepsilon}'_{ij}$, $\Delta\varepsilon'_{ij}$ are then obtained;

$$\dot{\varepsilon}'_{ij}{}^{t+\Delta t/2} = \dot{\varepsilon}_{ij}{}^{t+\Delta t/2} - \frac{1}{3}\delta_{ij}\dot{\varepsilon}_{v}{}^{t+\Delta t/2}$$

$$\Delta\varepsilon'_{ij} = \Delta t\ \dot{\varepsilon}'_{ij}$$

- The stresses $\sigma^{t+\Delta t}$ at time $t+\Delta t$ are obtained using the constitutive law;

$$\sigma_{ij}{}^{t+\Delta t} = \sigma_{ij}{}^{t} + \Delta P^{t+\Delta t} + C_{ijkl}\Delta\varepsilon'_{kl}{}^{t+\Delta t}$$

where $\Delta\varepsilon'_{ij}$ is the increment in deviatoric strain and δ_{ij} is the Kronecker delta.

3.6.1 Recovery of Normal Strain

The constitutive formulation adopted herein must accommodate the plane stress condition inherent in the shell element proposed in this work. The final stress state in the element co-rotational material coordinates must be such that the normal stress $\sigma_{33}{}^{t}$ at any time t must be zero.

Thus, it is necessary to evaluate the normal strain component ε_{33} prior to applying the constitutive law and updating the stress state.

The strain components for an elastic material in the plane stress condition ($\sigma_{33} = 0$) are given as:

$$\varepsilon_{11} = \frac{\sigma_{11}}{E} - \mu\frac{\sigma_{22}}{E}$$

$$\varepsilon_{22} = \frac{\sigma_{22}}{E} - \mu\frac{\sigma_{11}}{E}$$

$$\varepsilon_{33} = -\mu\frac{\sigma_{11}}{E} - \mu\frac{\sigma_{22}}{E}$$

$$\varepsilon_{12} = \sigma_{12}/2G$$

where E, μ, and G are the modulus of elasticity, Poisson's ratio and shear modulus respectively.

Rearranging the equations in matrix form:

$$\frac{1}{E}\begin{bmatrix} 1 & -\mu \\ -\mu & 1 \end{bmatrix}\begin{Bmatrix} \sigma_{11} \\ \sigma_{22} \end{Bmatrix} = \begin{Bmatrix} \epsilon_{11} \\ \epsilon_{22} \end{Bmatrix}$$

$$\begin{Bmatrix} \sigma_{11} \\ \sigma_{22} \end{Bmatrix} = \frac{\begin{bmatrix} 1 & \mu \\ \mu & 1 \end{bmatrix} E}{(1-\mu^2)} \begin{Bmatrix} \epsilon_{11} \\ \epsilon_{22} \end{Bmatrix}$$

$$\sigma_{11} = \frac{E}{(1-\mu^2)}\epsilon_{11} + \frac{\mu E}{(1-\mu^2)}\epsilon_{22}$$

$$\sigma_{22} = \frac{\mu E \epsilon_{11}}{(1-\mu^2)} + \frac{E\epsilon_{22}}{(1-\mu^2)}$$

Substituting into the expression for ϵ_{33}:

$$\epsilon_{33} = \frac{-\mu}{E}\left[\frac{E\epsilon_{11}}{(1-\mu^2)} + \frac{\mu E\epsilon_{22}}{(1-\mu^2)}\right] - \frac{\mu}{E}\left[\frac{E\epsilon_{22}}{(1-\mu^2)} + \frac{\mu E\epsilon_{11}}{(1-\mu^2)}\right]$$

$$= \epsilon_{11}\left[\frac{-\mu}{(1-\mu^2)} - \frac{\mu^2}{(1-\mu^2)}\right] + \epsilon_{22}\left[\frac{-\mu^2}{(1-\mu^2)} - \frac{\mu}{(1-\mu^2)}\right]$$

$$\epsilon_{33} = -\left(\epsilon_{11} + \epsilon_{22}\right)\left[\frac{u}{(1-u)}\right]$$

In addition, the first Invariant of the Stress Deviator = 0, thus

$$\sigma'_{33} = -\sigma'_{11} - \sigma'_{22}$$

3.6.2 Elastic Material Model

For the elastic isotropic material model, the Cauchy stress in the element co-rotational system is obtained using the convention in section 3.6;

$$\sigma_{ij}^{t+\Delta t} = \sigma_{ij}^{t} + \Delta P^{t+\Delta t} + 2G\Delta\epsilon'^{t+\Delta t}_{ij}$$

where G is the shear modulus. Regardless of the material law used, this model is also used for updating the penalty parameter stresses σ_{13} and σ_{23}.

3.6.3 Elastic Plastic Material Model

For elastic-plastic material models, the non-linear description of the material behaviour in the post yield region entails the following:

(a) A yield criterion to determine the threshold at which plastic flow begins;

(b) A flow rule to relate plastic strain increments with total strain and stress increments;

(c) A hardening rule to specify the modification of the yield condition during plastic flow.

For models used in the computer code H3DMAP, a von Mises yield surface and associated flow rule are adopted. The von Mises yield function is given as:

$$f(\sigma_{ij}) = J_2 - k^2$$

where J_2 is the second invariant of the stress deviator

k is the yield stress in pure shear.

The bi-linear hardening model used to represent the stress strain curve is given in figure 3.3.

The deviatoric components of velocity strain and stress are given as;

$$\dot{\varepsilon}'_{ij}{}^{t+\Delta t/2} = \dot{\varepsilon}_{ij}{}^{t+\Delta t/2} - \frac{1}{3}\delta_{ij}\dot{\varepsilon}_{kk}{}^{t+\Delta t/2}$$

$$\sigma'_{ij}{}^{t+\Delta t} = \sigma_{ij}{}^{t} - \delta_{ij}P^{t+\Delta t}$$

$$P^{t+\Delta t} = P^{t} + K\,\dot{\varepsilon}_{ii}{}^{t+\Delta t/2}\,\Delta t$$

The radial return method/8,9/ for isotropic hardening is used in H3DMAP for the elastic plastic material models. In this method, a trial elastic deviatoric stress, S, is established. The plastic strain vector is assumed to be parallel to S. The yield condition is used to determine the effective plastic strain increment $\Delta\bar{\varepsilon}_p$. The updated radius of the yield surface is found and the trial elastic stress vector is returned to the new yield surface.

Details of the development for a three dimensional state of stress is given in Appendix A2.

For the shell described herein, the elastic-plastic constitutive law governs the state of plane stress associated with shell behaviour whereas an elastic law governs the transverse shear stresses σ_{23}, σ_{13} which are considered penalty constraints as previously discussed.

A difficulty arises when the method described in Appendix A2 is applied to a state of plane stress (i.e. $\sigma_{33}=0$).

In this case the final stress state at time t+Δt must yield a normal stress $\sigma_{33}^{t+\Delta t}=0$. An adaptation of the radial return method to elasto-plasticity involving plane stress is presented.

The essential difference lies in the iterative scheme used to enforce the plane stress condition ($\sigma_{33}=0$) in the yielded material.

The development of the algorithm as implemented in H3DMAP follows.

i) At time t+Δt, calculate a trial stress, S_{ij} by updating σ'^{t}_{ij} elastically;

$$S_{ij}^{t+\Delta t} = \sigma'^{t}_{ij} + 2G\dot{\epsilon}'^{t+\Delta t}_{ij}\Delta t$$

where the normal strain $\epsilon_{zz} = -(\epsilon_{xx} + \epsilon_{yy})\frac{\mu}{(1-\mu)}$

ii) Obtain the effective trial stress $\bar{S}$;

$$\bar{S} = \left[3J_2\right]^{1/2} = \left[\frac{3}{2}S_{ij}S_{ij}\right]^{1/2}$$

iii) The current yield stress σ_y^t is calculated using the initial yield stress σ_y^o, the effective plastic strain $\bar{\epsilon}_p^t$ and the plastic modulus E_H (figure 3.3);

$$\sigma_y^t = \sigma_y^o + \bar{\epsilon}_p^t E_H$$

iv) Test the yield condition;

If $\bar{S} \le \sigma_y^t$, then no yielding has occurred and the trial stresses are the required stresses.

$$\sigma^{t+\Delta t} = \begin{Bmatrix} \sigma_{11} \\ \sigma_{22} \\ 0 \\ \sigma_{12} \end{Bmatrix} \qquad \text{and } \Delta\bar{\epsilon}_p = 0$$

If $\bar{S} > \sigma_y^t$, then yielding has occurred and the trial stress must be scaled back to the yield surface.

v) In order to scale back the trial stress to the yield surface and maintain $\sigma_{33} = 0$, an iterative scheme is required when yielding is detected.

Initialization; $^{0}\sigma_{33} = K\frac{1}{3}\dot{\varepsilon}_{ii}^{t+\Delta t}\Delta t + 2G\dot{\varepsilon}_{33}^{\prime t+\Delta t}\Delta t$

$$\overset{0}{\dot{\varepsilon}}_{33} = -\dot{\varepsilon}_{11} - \dot{\varepsilon}_{22} \quad \text{(note: incompressibility condition } \mu = 0.5)$$

vi) Up to fifteen iterations are allowed, although converged solutions using five are normally observed.

Iteration i=1,15

$$^{i}\dot{\bar{\varepsilon}} = \frac{1}{3}\left(\dot{\varepsilon}_{11} + \dot{\varepsilon}_{22} + \dot{\varepsilon}_{33}^{i}\right)$$

The increment in hydrostatic pressure is given as;

$$^{i}\Delta p^{t+\Delta t} = 3K\dot{\bar{\varepsilon}}\Delta t$$

$$^{i}\sigma_{11} = \sigma_{11}^{t} + {}^{i}\Delta p^{t+\Delta t} + 2G\left(\dot{\varepsilon}_{11}^{t+\Delta t} - {}^{i}\dot{\bar{\varepsilon}}\right)\Delta t$$

$$^{i}\sigma_{22} = \sigma_{22}^{t} + {}^{i}\Delta p^{t+\Delta t} + 2G\left(\dot{\varepsilon}_{22}^{t+\Delta t} - {}^{i}\dot{\bar{\varepsilon}}\right)\Delta t$$

$$^{i}\sigma_{33} = {}^{i}\Delta p^{t+\Delta t} + 2G\left({}^{i}\dot{\varepsilon}_{33}^{t+\Delta t} - {}^{i}\dot{\bar{\varepsilon}}\right)\Delta t$$

$$^{i}p = \frac{1}{3}\,{}^{i}\sigma_{kj}\delta_{kj}$$

$$^{i}S'_{11} = {}^{i}\sigma_{11} - {}^{i}p$$

$$^{i}S'_{22} = {}^{i}\sigma_{22} - {}^{i}p$$

$$^{i}S'_{33} = -{}^{i}S'_{11} - {}^{i}S'_{22}$$

$$^{i}S'_{12} = \sigma_{12}$$

Calculate the effective trial stress, $\bar{S}$, at iteration i;

$$^{i}\bar{S} = \left[\frac{3}{2} \, {}^{i}S'_{kj} \, {}^{i}S'_{kj} \right]^{1/2}$$

Obtain the effective plastic strain increment, $\Delta\bar{\varepsilon}_p$, at iteration i;

$$^{i}\Delta\bar{\varepsilon}_p = \frac{^{i}\bar{S} - \sigma_y{}^{t}}{3G + E_H}$$

The yield σ_y at iteration i is determined and the trial stress S'_{33} at iteration i is scaled back to the yield surface;

$$^{i}\sigma_y = \sigma_y{}^{t} + E_H \, {}^{i}\Delta\bar{\varepsilon}_p$$

$$^{i}\sigma_{33} = \frac{^{i}\sigma_y}{^{i}\bar{S}} \, {}^{i}S'_{33} + {}^{i}p$$

vii) Referring to the following figure;

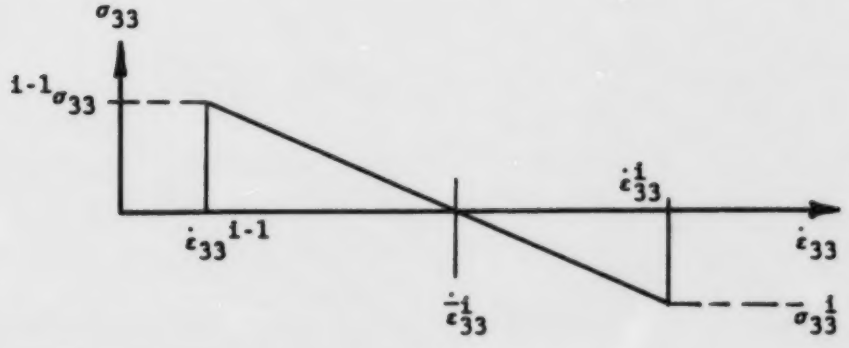

$$\frac{\dot{\bar{\varepsilon}}_{33}^{i} - \dot{\varepsilon}_{33}^{i-1}}{0 - {}^{i-1}\sigma_{33}} = \frac{(\dot{\varepsilon}_{33}^{i} - \dot{\varepsilon}_{33}^{i-1})}{({}^{i}\sigma_{33} - {}^{i-1}\sigma_{33})}$$

$$\therefore \dot{\bar{\varepsilon}}_{33}^{i} = \dot{\varepsilon}_{33}^{i-1} - {}^{i-1}\sigma_{33} \frac{(\dot{\varepsilon}_{33}^{i} - \dot{\varepsilon}_{33}^{i-1})}{({}^{i}\sigma_{33} - {}^{i-1}\sigma_{33})}$$

$\dot{\bar{\varepsilon}}_{33}$ is an estimate of $\dot{\varepsilon}_{33}$ which corresponds to $\sigma_{33} = 0$

viii) Check for convergence;

Convergence is achieved when:

$$\left| \frac{\dot{\varepsilon}_{33}^{i} - \dot{\varepsilon}_{33}^{i-1}}{\dot{\bar{\varepsilon}}_{33}^{i}} \right| \leq 0.0001$$

If no convergence, go to (vi) and repeat for next iterate i.

ix) Upon convergence, the stresses are obtained in the shell co-rotational system as;

$$\sigma_{11} = p + \frac{\sigma_y}{\bar{s}} s'_{11}$$

$$\sigma_{22} = p + \frac{\sigma_y}{\bar{s}} s'_{22}$$

$$\sigma_{33} = 0$$

$$\sigma_{12} = \frac{\sigma_y}{\bar{s}} s'_{12}$$

Update effective plastic strain $\bar{\varepsilon}_p$ at time t+Δt;

$$\bar{\varepsilon}_p^{t+\Delta t} = \bar{\varepsilon}_p^{t} + \Delta\bar{\varepsilon}_p$$

These stresses are then used to obtain the internal force vector, F_{int}, described in section 3.5.

Failure Model

A simple failure model is used with this material characterization. At each time step, the effective plastic strain $\bar{\epsilon}_p^{t+\Delta t}$ is compared to a specified failure strain $\bar{\epsilon}_{pf}$. Failure is deemed to have occurred when;

$$\bar{\epsilon}_p^{\,t+\Delta t} > \bar{\epsilon}_{pf}$$

Once failure has occurred the deviatoric components are set to zero and the element is permitted to carry compressive loads only for the remainder of the loading history. Improvements in the failure model are possible by using, for example, the work described in reference /16/ in which the failure can be tracked with respect to the principal axes.

3.6.4 Shell Thickness Modification

The thickness modification is achieved using the normal strain component ϵ_{33} which is derived from the plane stress components of strain ϵ_{11}, ϵ_{22}.

In elasto-plastic material models, the thickness modification is applied using the condition of incompressibility (constant volume) when $\bar{\sigma}^t > \bar{\sigma}_y^{\,t}$, where $\bar{\sigma}^t$ is the effective stress based on the deviatoric part of stress and $\bar{\sigma}_y^{\,t}$ is the current yield.

The increment in normal strain $\Delta\epsilon_{33}^t$ is used to obtain a mean normal strain $\Delta\bar{\epsilon}_{33}^t$ through the thickness. The first law of the mean for integrals is used to obtain the mean component $\Delta\bar{\epsilon}_{33}^t$ as:

$$\Delta\bar{\epsilon}_{33}^{\,t} = \left(\int_{-1}^{+1} \Delta\epsilon_{33}^t \, dh \right) / 2$$

using Gauss Quadrature;

$$\bar{\Delta}\epsilon_{33}^{\,t} = \left[\sum_{k=1}^{n1} \Delta\epsilon_{33}(t_k)\, \bar{\alpha}_k \right] / 2$$

where t_k, $\bar{\alpha}_k$ are the sampling and weighting components of the Gauss Quadrature respectively and n_1 is the order of quadrature which is taken to be the same as the through-thickness quadrature rule specified for the constitutive law.

The strain in terms of thickness h is;

$$\Delta\bar{\epsilon}_{33}^{\,t} = \frac{\Delta h^{t+\Delta t}}{h^t}$$

Thus, the updated thickness of the shell at time t+Δt is;

$$h^{t+\Delta t} = h^{t}\,(1 + \Delta\varepsilon_{33}^{t})$$

Thus, the new thickness $h^{t+\Delta t}$ is obtained for use in the next time step where h lags one time step behind.

3.7 Lumped Mass Matrix

In order to exploit the advantages of an explicit solution technique, the mass matrix, M, described in section 2 is diagonalized. That is, by lumping the mass of the element at the nodes, the mass matrix is diagonal and the inversion of the mass matrix becomes trivial, i.e.;

$$M_{ii}^{-1} = \frac{1}{m_{ii}}$$

For the four noded shell element formulation described herein, the following mass matrix is used;

$$M = \begin{bmatrix} m_1 & 0 & 0 & 0 \\ & m_2 & 0 & 0 \\ & & m_3 & 0 \\ \text{symmetric} & & & m_4 \end{bmatrix}$$

where the m_k are sub matrices for each node of the element given as follows;

$$m_k = \frac{\rho A h}{4} \begin{bmatrix} 1 & & & & & \\ & 1 & & & & \\ & & 1 & & & \\ & & & m_R & & \\ & & & & m_R & \\ & & & & & m_R \end{bmatrix}$$

where ρ = mass density of the element material

A = area of the element at the mid-plane

h = element thickness

Thus, the lumping of the mass for the translational degrees of freedom is straightforward and consists of placing one quarter of the total element mass at each of the four nodes in the global x, y and z directions. The inertial components, m_R, for the rotational degrees of freedom, though relatively unimportant, must have non-zero entries in order to permit the inversion of M. An expression for the rotary inertia of a cross section of a square plate is used. This gives a value of m_R;

$$m_R = \frac{(h^2 + A)}{12}$$

This is valid for elements in a fine mesh or for thick elements. In reference /6/, an alternative value for the lumped rotary inertia for thin plate/shell elements which provides reasonable accuracy is given as;

$$m_R = \frac{A}{8}$$

In the computer code, m_R is determined as follows:

$$m_R = \max\left[\frac{A}{8}, \frac{(h^2 + A)}{12}\right]$$

The diagonal mass matrix M is stored in vector form in the computer code since non-zero entries lie on the diagonal and the remaining entries are null.

3.8 Stable Time Step

As discussed in section 2.3 and demonstrated in appendix A2, the central difference operator used to integrate the equations of motion is explicit and as a result is conditionally stable. This requires that the Courant condition is satisfied. That is;

$$\Delta t_{cr} \leq \frac{2}{w_{max}}$$

where w_{max} is the highest eigenvalue in the mesh of elements and Δt_{cr} is the maximum time step which renders a stable solution.

The estimate of the critical time step size used in H3DMAP in conjunction with this element is based on the transit time of a dilatational wave, /4/, over the shortest element dimension in a mesh. The form used is;

$$\Delta t_{cr} = SCT \cdot \frac{L_{min}}{C}$$

where;

C - speed of sound (dilatational wave) in the material

$$= \sqrt{\frac{K + \frac{4}{3}G}{\rho}}$$

K - bulk modulus

G - shear modulus

ρ - mass density

SCT - scale factor on stable time step (normally = 0.9)

L_{min} - minimum element dimension

Referring to figure 3.2,

$$L_{min} = \min(|\vec{v}_{12}|, |\vec{v}_{23}|, |\vec{v}_{34}|, |\vec{v}_{41}|, |\vec{v}_{24}|, |\vec{v}_{13}|)$$

In this case, $|\vec{v}_{ij}|$ represents the length of the vector $\vec{v}_{ij}$ joining nodes i and j. The algorithm implemented includes automatic time stepping to ensure a stable solution. This entails a prediction of the critical time step to be used in the next increment of time. Any reduction in the stable time step over a single step is compensated by the scale factor SCT which is generally taken as 90 percent.

3.9 Hourglass Stabilization

In the explicit time integration of the equations of motion described in section 2.3 a solution to

$$\ddot{x}^t = M^{-1} [F^t_{ext} - F^t_{int}]$$

is sought. The major portion of the computation is spent in the evaluation of the element internal force vector F_{int} at each time step. This requires the numerical evaluation of the velocity strain components for use in constitutive calculations. As described in section 3.5, the integration of the internal force vector is obtained using one point Gauss quadrature in the plane of the element and a user specified rule in the local thickness direction to capture the desired response depending on whether bending and/or membrane action is required. In references /2,5,6/ selective/reduced integration was used to prevent shear locking. In this case the membrane/bending components were integrated using a 2x2 Gauss rule while the shear component was under integrated with a one point rule.

This results in constitutive calculations at nl sample points in the thickness direction at each of the four sample points in-plane.

The use of reduced one point quadrature is desirable since it leads to a four-fold decrease in computations at the element level. This is particularly attractive for efficient explicit time integration. However, the use of reduced integration leads to kinematic or zero energy modes which are not represented in the formulation of the B matrix. This rank deficiency leads to the possibility of spurious behaviour known as hourglassing.

If the imposed boundary conditions and loads leads to a rank sufficient gradient matrix B in the global system, this oscillatory behaviour may not occur in the assembled system of equations. One approach of recognizing rank deficiency would be to examine the eigenvalues of the system. There will be one or more zero eigenvalues if the global B matrix is rank deficient. Unfortunately, an eigensolution of the complete problem is not practical so the approach adopted herein is to check the rank deficiency at the element level and check for hourglassing directly. This approach is based in part on /10,11/, with extension to the efficient element formulation described in this report and an alternative definition of hourglass stress.

3.9.1 Rank Deficiency of the Strain Rate-Velocity Matrix B

In section 3.4, the strain-rate-velocity matrix B was derived for one-point Gauss quadrature. The expression for the B matrix re-written in appendix A3, using the simplification arising from one-point quadrature yields:

$$B_i = \left[\begin{array}{cc|ccc} b_{1i} & 0 & 0 & 0 & zb_{1i} \\ 0 & b_{2i} & 0 & -zb_{2i} & 0 \\ b_{2i} & b_{1i} & 0 & -zb_{1i} & zb_{2i} \\ \hline 0 & 0 & b_{1i} & 0 & N_i \\ 0 & 0 & b_{2i} & -N_i & 0 \end{array}\right] \begin{array}{l} \} \text{ membrane} \\ \\ \\ \} \text{ transverse shear} \end{array}$$

where: B_i is the B matrix at node i
$z = 0.5\ th_i$
$N_i = 0.25$
h_i = thickness at node i

$$b_1 = \left\{\begin{array}{c} b_{11} \\ b_{12} \\ b_{13} \\ b_{14} \end{array}\right\} = \frac{1}{2A} \left\{\begin{array}{c} y'_2 - y'_4 \\ y'_3 - y'_1 \\ y'_4 - y'_2 \\ y'_1 - y'_3 \end{array}\right\}$$

$$b_2 = \begin{Bmatrix} b_{21} \\ b_{22} \\ b_{23} \\ b_{24} \end{Bmatrix} = \frac{1}{2A} \begin{Bmatrix} x'_4 - x'_2 \\ x'_1 - x'_3 \\ x'_2 - x'_4 \\ x'_3 - x'_1 \end{Bmatrix}$$

$A = 4|J|$ = plane area of the element.

The local coordinate vectors X, Y are given as;

$$X = \begin{Bmatrix} x'_1 \\ x'_2 \\ x'_3 \\ x'_4 \end{Bmatrix} \quad ; \quad Y = \begin{Bmatrix} y'_1 \\ y'_2 \\ y'_3 \\ y'_4 \end{Bmatrix}$$

The zero-energy in-plane and out-of-plane modes of displacement for this shell element which comprise the null space of the B matrix are given as follows:

In-Plane Zero Energy Modes (Membrane)

Mode	Strain	Strain Energy	Type
x'-translation	zero	zero	rigid body
y'-translation	zero	zero	rigid body
x'-y' rotation	zero	zero	rigid body
x'-hourglass	non-zero	zero	hourglass
y'-hourglass	non-zero	zero	hourglass

Out-of-Plane Zero Energy Modes (Bending)

Mode	Strain	Strain Energy	Type
z'-translation	zero	zero	rigid body
Ru'-rotation	zero	zero	rigid body
Rv'-rotation	zero	zero	rigid body
z'-hourglass	non-zero	zero	hourglass
Ru'-hourglass	non-zero	zero	hourglass
Rv'-hourglass	non-zero	zero	hourglass
twist	non-zero	zero	hourglass

The hourglass modes for membrane and bending deformations are shown in figure 3.4.

Considering first the in-plane displacement modes, the rigid body displacement vector Σ_I is given as;

$$\Sigma_I = \begin{Bmatrix} 1 \\ 1 \\ 1 \\ 1 \end{Bmatrix}$$

and the hourglass base vector Γ_I is given as;

$$\Gamma_I = \begin{Bmatrix} 1 \\ -1 \\ 1 \\ -1 \end{Bmatrix}$$

For rigid body modes, zero strain is obtained as expected;

$$b_1^T \Sigma_I = 0$$

$$b_2^T \Sigma_I = 0$$

$$b_1^T Y = 0$$

$$b_2^T X = 0$$

where superscript T denotes transpose of the matrix. However, the hourglass modes Γ_I are troublesome since they result in zero strain representation where non-zero strain is present;

$$b_1^T \Gamma_I = 0$$

$$b_2^T \Gamma_I = 0$$

Note also that;

$$\Gamma_I^T \Sigma_I = 0$$

$$b_1^T X = 1$$

$$b_2^T Y = 1$$

Thus, Γ_I and Σ_I are orthogonal to all of the other vectors.

Considering the out-of-plane displacement w-mode, the rigid body displacement vector Σ_w is given as;

$$\Sigma_w = \begin{Bmatrix} 1 \\ 1 \\ 1 \\ 1 \end{Bmatrix}$$

and the hourglass base vector Γ_w is given as;

$$\Gamma_w = \begin{Bmatrix} 1 \\ -1 \\ 1 \\ -1 \end{Bmatrix}$$

For rigid body modes, zero strain is obtained as expected;

$$b_1^T \Sigma_w = 0$$

$$b_2^T \Sigma_w = 0$$

However, the hourglass modes Γ_w, as with Γ_I, are troublesome since they result in zero strain where non-zero strain is present;

$$b_1^T \Gamma_w = 0$$

$$b_2^T \Gamma_w = 0$$

Also,

$$\Gamma_w^T \Sigma_w = 0$$

Considering the x' and y' rotational deformation Ru'-mode and Rv'-mode, the rigid body displacement vectors Σ_{Ru}, Σ_{Rv}, are given as;

$$\Sigma_{Ru} = \begin{Bmatrix} 1 \\ 1 \\ 1 \\ 1 \end{Bmatrix} \quad ; \quad \Sigma_{Rv} = \begin{Bmatrix} 1 \\ 1 \\ 1 \\ 1 \end{Bmatrix}$$

which results in rigid body displacements $\Sigma_{w\text{-}Ru}$, $\Sigma_{w\text{-}Rv}$ in the out-of-plane direction w as;

$$\Sigma_{w\text{-}Ru} = Y \quad ; \quad \Sigma_{w\text{-}Rv} = -X$$

where $\Sigma_{w\text{-}Ru}$ is the rigid body displacement in the out-of-plane w-direction due to rigid body rotation in Ru. Similarly, $\Sigma_{w\text{-}Rv}$ is the rigid body displacement in the out-plane w-direction due to rigid body rotation in Rv. The hourglass base vectors Γ_{Ru} and Γ_{Rv} are given as;

$$\Gamma_{Ru} = \begin{Bmatrix} 1 \\ -1 \\ 1 \\ -1 \end{Bmatrix} \quad ; \quad \Gamma_{Rv} = \begin{Bmatrix} 1 \\ -1 \\ 1 \\ -1 \end{Bmatrix}$$

For rigid body modes, zero strain is obtained;

$$b_1^T \Sigma_{Ru} = 0$$

$$b_2^T \Sigma_{Rv} = 0$$

$$b_1^T \Sigma_{w\text{-}Rv} + N\Sigma_{Rv} = 0$$

$$b_2^T \Sigma_{w\text{-}Ru} - N\Sigma_{Ru} = 0$$

where; $b_1^T \Sigma_{w\text{-}Rv} = -1$

$b_2^T \Sigma_{w\text{-}R} = 1$

$$N\Sigma_{Rv} = 0.25 \begin{bmatrix} 1 & 1 & 1 & 1 \end{bmatrix} \begin{Bmatrix} 1 \\ 1 \\ 1 \\ 1 \end{Bmatrix} = 1$$

$$N\Sigma_{Ru} = 1$$

The twist kinematic mode is not controlled so that there still exists a rank deficiency of one. However, as pointed out in /10/ this mode is a non-communicable mode which is not possible in a mesh of two or more elements.

As demonstrated, the use of reduced quadrature for the bi-linear shell element considered herein, introduces the possibility of hourglassing. In order to reap the benefits of reduced quadrature (i.e. computational efficiency), a method for controlling the spurious hourglass modes is required.

3.9.2 Hourglass Control

Basically, the idea entails the introduction of an hourglass force which is proportional to the amount of hourglassing into the equilibrium equations. Since the local element internal force vector, F'_{int}, does not include hourglass modes, it is valid to augment it with a local internal hourglass force vector F'_{hg} as;

$$\bar{F}'_{int} = F'_{int} + F'_{hg}$$

In expressing the hourglass force, it is related to displacement or rate of displacement (i.e. velocity). Considering a single degree of freedom system, the equation of motion is given by;

$$m\ddot{x} + c_d\dot{x} + kx = f_{ext}$$

where m, c_d, k are the mass, damping and stiffness coefficients respectively and $\ddot{x}$, $\dot{x}$, x are the acceleration, velocity and displacement respectively. The damping and stiffness coefficients may be written as;

$$c_d = 2\zeta wm$$

$$k = w^2 m$$

where ζ is the damping ratio and w is the undamped natural frequency of the system.

The element developed herein is intended for application to large deformation problems. Since the rate of deformation is used, the viscosity form of hourglass control is desirable.

The pathological oscillations of hourglassing in a system occur at the highest frequencies, w_{max}, of the system. This arises because the hourglass mode is a deformation mode at the element level.

In this work, the highest frequency w_{max} of the system is approximated using the expression in section 3.7.1;

$$w_{max} = \frac{2C}{L_{min}}$$

where C is the speed of sound (dilatational wave) in the material, and L_{min} is the minimum element dimension of the system.

3.9.3 Hourglass γ Operator

As a first step in the development of the hourglass resisting forces, an operator, γ, which relates hourglass strains or strain rates to the displacements or velocities of the hourglass mode is required.

Considering the inplane displacement u' in direction x', the hourglass strain q_1 in the x' direction is defined as;

$$q_1 = \gamma^T u'_x$$

where

$$\gamma = \begin{Bmatrix} \gamma_1 \\ \gamma_2 \\ \gamma_3 \\ \gamma_4 \end{Bmatrix} \quad ; \quad u'_x = \begin{Bmatrix} u'_1 \\ u'_2 \\ u'_3 \\ u'_4 \end{Bmatrix} \quad ; \quad \gamma' = \begin{Bmatrix} \gamma'_1 \\ \gamma'_2 \\ \gamma'_3 \\ \gamma'_4 \end{Bmatrix}$$

Properties desired in the γ operator include:

- orthogonality to the rigid body modes

- orthogonality of hourglass strain with linear strain. In other words, when the displacement mode given by u' is linear $q_1 = 0$ and when it contains an hourglass mode $q_1 \neq 0$.

That is,

$$q_1 = \gamma^T \Sigma_I = 0$$

$$q_1 = \gamma^T \Gamma_I \neq 0$$

The operator γ is defined to consist of four linearly independent vectors/11/ as;

$$\gamma = a_1\Sigma + a_2\Gamma + a_3 b_1 + a_4 b_2$$

where a_1's are constants to be determined.

The operator is developed for the x'-components of displacements and hourglass strain without loss of generality since γ_1 is required to be the same at each coordinate.

A linear field of nodal displacements is expressed as;

$$u'_{lin_x} = C_1\Sigma + C_2 X + C_3 Y$$

where the coefficients C_1 are arbitrary.

The coefficients a_1 are determined using the requirement that hourglass strains vanish for any linear mode. That is,

$$q_1 = \gamma^T u'_{lin_x} = 0$$

Since the coefficients c_i and u'_{lin} are arbitrary, substitution leads to three simultaneous equations in a_i;

$$a_1\Sigma^T\Sigma + a_2\Gamma^T\Sigma + a_3 b_1{}^T\Sigma + a_4 b_2{}^T\Sigma = 0$$

$$a_1\Sigma^T X + a_2\Gamma^T X + a_3 b_1{}^T X + a_4 b_2{}^T X = 0$$

$$a_1\Sigma^T Y + a_2\Gamma^T Y + a_3 b_1{}^T Y + a_4 b_2{}^T Y = 0$$

Using the orthogonality relations given in section 3.9.1;

$$a_1\Sigma^T\Sigma = 0$$

Thus, $a_1 = 0$.

In addition,

$$a_3 = -a_2\Gamma^T X$$

$$a_4 = -a_2\Gamma^T Y$$

Substitution into the expression for γ yields;

$$\gamma = a_2 [\Gamma - (\Gamma^T X)b_1 - (\Gamma^T Y)b_2] = a_2\gamma'$$

where a_2 is an arbitrary constant.

The vector γ is called the hourglass projection operator. When the element is rectangular γ is equal to Γ. In order to ensure that the hourglass strain be zero for linear displacement in an arbitrary quadrilateral element, the γ is used. It will be demonstrated in the following sections that a_2 can be eliminated.

3.9.4 Hourglass Resisting Force

Using the γ operator, the evaluation of hourglass strain q permits the detection of an hourglass mode. Defining an hourglass stress Q, the virtual hourglass energy is equated to the virtual hourglass work done by the internal hourglass force F'_{hg} to yield;

$$\delta u'^T F'_{hg} = \delta q^T Q$$

where $\delta u'$ is a vector of virtual nodal displacements and;

$$q = \begin{Bmatrix} q_1 \\ q_2 \\ q_3 \\ q_4 \\ q_5 \end{Bmatrix} \quad ; \quad Q = \begin{Bmatrix} Q_1 \\ Q_2 \\ Q_3 \\ Q_4 \\ Q_5 \end{Bmatrix}$$

The virtual hourglass strain is given as;

$$\delta q = H \delta u'$$

where;

$$H = [H_1 \quad H_2 \quad H_3 \quad H_4]$$

$$H_I = \begin{bmatrix} \gamma_I & 0 & 0 & 0 & 0 \\ & \gamma_I & 0 & 0 & 0 \\ & & \gamma_I & 0 & 0 \\ & \text{sym.} & & \gamma_I & 0 \\ & & & & \gamma_I \end{bmatrix}$$

The hourglass force can now be expressed as;

$$F'_{hg} = H^T Q$$

This is analogous to the expression for the internal element force vector;

$$F'_{int} = \int_{VOL} B^T \sigma dV$$

Recalling from section 3.9.2, the local hourglass force is added directly to the local internal element force vector;

$$\bar{F}'_{int} = F'_{int} + F'_{hg}$$

As observed above, the matrix H was developed to be linearly independent of the B matrix so that H now makes up for the rank deficiency of B.

3.9.5 Hourglass Stiffness Control

The method of hourglass stiffness control follows from the proportionality of element force to nodal displacements;

$$F'_{hg} = ku' = H^T Q$$

pre-multiplying by H;

$$kHu' = HH^T Q$$

Expanding;

$$HH^T = \gamma^T \gamma I$$

where I is a 5x5 identity matrix.

Expanding $\gamma^T\gamma$ yields;

$$\gamma^T\gamma = a_2^2\, \gamma'^T\gamma'$$

Thus, the hourglass stress Q is given by;

$$Q = \frac{kHu'}{a_2^2\, \gamma'^T\gamma'}$$

And the hourglass force is;

$$F'_{hg} = \frac{kH^THu'}{a_2^2\, \gamma'^T\gamma'}$$

For direction x';

$$F'_{hg_x} = \frac{a_2^2\, k\gamma'\gamma'^T u'_x}{a_2^2\, \gamma'^T\gamma'}$$

Thus, a_2 cancels and F'_{hg} is given as;

$$F'_{hg} = \frac{k\, H^THu'}{\gamma'^T\gamma'}$$

In this context a_2 can be considered an arbitrary constant so that without loss of generality a_2 can be set to unity leading to $\gamma' = \gamma$.

Recalling from section 3.9.2 that $k = w^2 m$ and introducing hourglass control parameter ζ;

$$F'_{hg} = H^T\, Q^{t+\Delta t}$$

where;

$$Q^{t+\Delta t} = Q^t + \Delta t\, \dot{Q}$$

$$\dot{Q} = \frac{\zeta w^2 m\, H\, \dot{x}'}{\gamma' {}^T \gamma'}$$

$\dot{x}'$ is the local nodal velocity vector.

m = nodal mass = $\frac{\rho A h}{4}$

ρ = element material density

h = element thickness

A = element area

3.9.6 Hourglass Viscosity Control

The method of hourglass viscosity control follows from the proportionality of element viscous force to nodal velocities.

$$F'_{hg} = c_d \dot{x}'$$

where (ref. section 3.9.2);

$$c_d = 2\zeta w m$$

Following section 3.9.5, the local element hourglass resisting force vector F'_{hg} using viscosity control is given as;

$$F'_{hg} = \frac{2\zeta w m\, H^T H\, \dot{x}'}{\gamma' {}^T \gamma'}$$

This form of control is particularly attractive in the explicit scheme adopted since it precludes the time integration of hourglass stress.

The form used in the implementation of F'_{hg} in the computer code H3DMAP is described in section 4.2.

3.10 Pressure Boundary

The element consistent load vector $F_p{}^t$ at time 't' for traction forces was given in section 2.2 as;

$$F_p{}^t = \int_{b_p} N^T p^t dS$$

where N^T is the transpose of the interpolation function matrix

P^t is the time varying uniform boundary traction at time t

b_p is the surface upon which P^t acts

Referring to figure 3.1, the global coordinates at a sampling point (r,s,0) on the mid-plane are given as;

$$X(r,s,0) = \begin{Bmatrix} x(r,s,0) \\ y(r,s,0) \\ z(r,s,0) \end{Bmatrix}$$

A unit vector normal $\vec{v}_z$ to the surface defined at the mid plane is obtained as;

$$\vec{v}_z(r,s,0) = \frac{\frac{\partial \vec{x}}{\partial r}(r,s,0) \times \frac{\partial \vec{x}}{\partial s}(r,s,0)}{\left| \frac{\partial \vec{x}}{\partial r} \times \frac{\partial \vec{x}}{\partial s} \right|} = \frac{V_{z1}\vec{i} + V_{z2}\vec{j} + V_{z3}\vec{k}}{\left| \frac{\partial \vec{x}}{\partial r} \times \frac{\partial \vec{x}}{\partial s} \right|}$$

The pressure P^t acts in the positive t direction over the element surface as shown in figure 3.1.

In section 3.2.1, the bi-linear interpolation functions are given as;

$$N_i = 0.25(1 + r_i r)(1+s_i s)$$

From which;

$$\frac{\partial x}{\partial r}(r,s) = \sum_{i=1}^{4} \frac{\partial N_i}{\partial r} \cdot X_i = \sum_{i=1}^{4} 0.25 r_i (1+s_i s) \begin{Bmatrix} x_i \\ y_i \\ z_i \end{Bmatrix}$$

$$\frac{\partial x}{\partial s}(r,s) = \sum_{i=1}^{4} \frac{\partial N_i}{\partial s} \cdot X_i = \sum_{i=1}^{4} 0.25 s_i (1+r_i r) \begin{Bmatrix} x_i \\ y_i \\ z_i \end{Bmatrix}$$

The differential surface area $ds = \left| \frac{\partial \vec{x}}{\partial r} \times \frac{\partial \vec{x}}{\partial s} \right| drds$

The global components of the pressure loading are written for node 'i' as;

$$F_{pi}^{t} = P^{t} \int_{-1}^{+1} \int_{-1}^{+1} N_i \begin{Bmatrix} V_{z1}(r,s) \\ V_{z2}(r,s) \\ V_{z3}(r,s) \end{Bmatrix} \left| \frac{\partial \vec{x}}{\partial r} \times \frac{\partial \vec{x}}{\partial s} \right| drds \left[\left| \frac{\partial \vec{x}}{\partial r} \times \frac{\partial \vec{x}}{\partial s} \right| \right]^{-1}$$

$$F_{pi}^{t} = P^{t} \int_{-1}^{+1} \int_{-1}^{+1} N_i \begin{Bmatrix} V_{z1}(r,s) \\ V_{z2}(r,s) \\ V_{z3}(r,s) \end{Bmatrix} drds$$

Numerical integration is applied with one point Gauss quadrature similar to that used for the volume integrals evaluated in the previous sections.

$$F_{pi}^{t} = 4.0\ P^{t} \left[N_i(0,0) \begin{Bmatrix} V_{z1}(0,0) \\ V_{z2}(0,0) \\ V_{z3}(0,0) \end{Bmatrix} \right]$$

Where the element area is approximated by:

$$4 \left| \frac{\partial \vec{x}}{\partial r}(0,0) \times \frac{\partial \vec{x}}{\partial s}(0,0) \right|$$

4.0 COMPUTER IMPLEMENTATION

The shell element developed in this report has been implemented into the explicit module EXTRA of the three dimensional structural analysis code H3DMAP/1/. This module covers analysis option (LTYP=8), which performs explicit geometric and material non-linear, finite deformation, transient dynamic analysis. Version 4 of H3DMAP includes a number of new features which are described in /1/.

In addition to shell elements, the code includes linear isoparametric two and three dimensional (solid) continuum elements, isoparametric axisymmetric continuum elements, both three-dimensional Euler-Bernoulli (cubic) and Timoshenko (linear isoparametric) beam elements and analog elements which can be used to model interfaces, gaps, and elements whose force-deflection relationships are known.

In the explicit module EXTRA, the high degree of non-linearity considered has necessitated the use of efficient element formulations such as the one described in this report.

The shell element is compatible with the beam and continuum elements used in H3DMAP and as such, permit complex simulation models which are comprised of these different element types.

In H3DMAP, the explicit analysis option is based on the hydrodynamic finite element formulation which is suitable for finite deformation problems. The material types currently available include elastic, elastic-plastic with isotropic hardening, general elastic-plastic hydrodynamic, and hydrodynamic models which are used in conjunction with equations of state to provide material models for fluids, soil and foams.

Loading conditions include time dependent follower traction forces, concentrated nodal forces/moments, and initial conditions such as velocities in impulsive problems.

This type of approach makes it possible to accurately model fluid-structure interaction problems. Examples of applications and verification cases are given in section 5 and reference /1/.

The explicit module is intended for problems involving impact, wave propagation and shock. However, a dynamic relaxation procedure has been included in H3DMAP which makes it possible to solve large static problems as a dynamic problem. The advantage here, is that the explicit technique requires very little memory compared to implicit methods, since the storage and solution of large sets of equations are avoided. Problems involving tens of thousands of degrees of freedom are feasible. Although the explicit central difference operator used is conditionally stable, the small time steps required for operator stability are also needed to accurately track the response of highly nonlinear problems. This would to some degree be necessary in the implicit method as well when the non-linearity is high.

The H3DMAP code architecture uses a form of dynamic storage allocation so that a single array controls the capacity. The address locations of the various arrays required for a specific problem is calculated so that only the necessary memory is utilized. The code is set to exploit the memory limits of the particular computer in which H3DMAP is installed. All coding is written in standard FORTRAN 77 and avoids use of compiler extensions in order to remain device independent and portable.

H3DMAP has been successfully ported to a number of computer facilities and work stations which run under both DEC VMS and UNIX operating systems.

4.1 Shell Element Implementation

The implementation of the shell element as described in this report has been achieved using a module (SHEX) containing eight routines. The module tree is shown in figure 4.1. It is placed in the explicit analysis solution driver (EXPRES) at the branch where the global internal element force vectors, F^t_{int}, are evaluated for all the elements in the element library.

The function of the various routines are as follows:

- SHEX: This routine is the root of the shell element routines. All the routine calls are made from here. Loops over all shell elements and minimum stable time step calculations are performed here.

- XTRANS: This routine evaluates the transformation matrix, T, relating the local to global element or material axes, the local x', y' coordinates and the minimum effective element length for use in the stable time step calculation.

- XBMTRX: In this routine the constant terms of the local strain rate - velocity matrix B, are obtained for the mid-surface of the shell.

- SHINS: The numerical integration through the thickness direction is performed in this routine. Calls to the material model routines are made using the velocity strains calculated. The local element internal force vector is obtained and the thickness modified if required.

- MAT1SH: The material model for an elastic constitutive law is computed in this routine and is called by SHINS.

- MAT2SH: The material model for a plane stress elastic-plastic constitutive law with a failure criterion is computed in this routine.

- HRGS: This routine contains the computation of the local hourglass resisting force vector for the shell element using either viscous (default) or stiffness hourglass control. The hourglass force vector is computed and added to the local element internal force vector.

Basically the computation of the local shell element internal force vector is summarized in the following steps:

- Loop over the number of shell elements.

- Compute transformation matrix T and local coordinates x', y', and minimum effective element length (section 3.1).

- Obtain local velocity $\dot{x}'$ at the mid-step $t+\Delta t/2$.

- Compute the constant terms of matrix B (section 3.4).

- Loop over the number of integration points in the thickness direction (section 3.5).

- Compute velocity strains, $\dot{\varepsilon}_{ij}^{t+\Delta t/2}$ (section 3.4).

- Compute stress rates (section 3.6), and update stresses;

$$\sigma_{ij}^{t+\Delta t} = \sigma_{ij}^{t} + C_{ijkl}\,\dot{\epsilon}_{kl}^{t+\Delta t/2}\,\Delta t$$

- Calculate internal force vector $F'_{int}{}^{t+\Delta t}$ (section 3.5);

$$F'_{int}{}^{t+\Delta t} = \int_{Vol} B^{T}\sigma^{t+\Delta t}\,dV$$

- Compute thickness modification (section 3.6.4) and complete integration.

- Compute hourglass resisting force vector F'_{hg} and add to F'_{int} (section 3.9);

$$F'_{int} + F'_{hg}$$

- Transform internal element force vector to the global axes and assemble contribution to global system internal force vector F_{int}.

- Calculate minimum element stable time step Δt_{cr}, for the next time increment (section 3.8).

The H3DMAP user manual/1/, outlines the user input data required along with numerous verification cases.

4.2 Hourglass Control Implementation

In the computer code H3DMAP, both the hourglass stiffness and viscous control of section 3.9 are available in the explicit analysis module EXTRA. However, emphasis is placed on the viscous form of hourglass control since it is more compatible with the rate of deformation formulation used in the explicit module. It leads to a more efficient implementation since it uses the nodal velocity variables directly and avoids the additional operations and array storage associated with the time integration of hourglass stress which are mandatory with the stiffness form of control. In fact, the default is now viscous control in H3DMAP.

In section 3.9.6, the form of viscous control gave the local element hourglass resisting force vector F'_{hg} as:

$$F'_{hg} = \frac{2\zeta w m\, H^{T} H\, \dot{x}'}{\gamma'^{T}\gamma'}$$

Recalling from 3.9.2 that the maximum mesh frequency, w, is based at the element level results in the following equality;

$$2\zeta w_m = \zeta \frac{4C}{L_{min}} \frac{\rho A h}{4} = \zeta C \rho h \frac{4|J|}{L_{min}}$$

where ρ, A, h, C, $|J|$ are defined in section 3.9.

When the geometry of the element is rectangular $\gamma' = \Gamma$.

In H3DMAP, the form used to obtain the hourglass resisting force vector F'_{hg} is given at node i as;

$$F'_{hgi} = \begin{Bmatrix} C_1 \gamma'_i \dot{q}_1 \\ C_2 \gamma'_i \dot{q}_2 \\ C_3 \gamma'_i \dot{q}_3 \\ C_4 \gamma'_i \dot{q}_4 \\ C_5 \gamma'_i \dot{q}_5 \end{Bmatrix}$$

where the hourglass strain-rates $\dot{q}$ are given by;

$$\dot{q} = \begin{Bmatrix} \dot{q}_1 \\ \dot{q}_2 \\ \dot{q}_3 \\ \dot{q}_4 \\ \dot{q}_5 \end{Bmatrix} = \sum_{i=1}^{4} \begin{Bmatrix} \gamma'_i \dot{x}'_i \\ \gamma'_i \dot{y}'_i \\ \gamma'_i \dot{z}'_i \\ \gamma'_i R\dot{x}'_i \\ \gamma'_i R\dot{y}'_i \end{Bmatrix}$$

$$C_1 = C_2 = C_3 = \frac{4\zeta C \rho h |J|}{L_{min}\, \gamma'^T \gamma'}$$

For the rotational terms, the hourglass control constants C_4, C_5 are scaled by the element thickness h leading to:

$$C_4 = C_5 = \frac{4\zeta_r C \rho h^2 |J|}{L_{min}\, \gamma'^T \gamma'}$$

Since the rotational hourglass modes are not associated with a locking mode (e.g. shear) the values of the rotational hourglass stabilization coefficient ζ_r have a wider range.

Excellent results have been obtained with H3DMAP using the following range of values;

$$0.01 < \zeta < 0.20$$

$$0.0001 < \zeta_r < 1.0$$

In the computer code default values of ζ=0.1 and ζ_r=0.005 are used. All the verification cases presented in this report use the default values unless otherwise specified.

5.0 VERIFICATION CASES

The test cases described in this section serve to demonstrate the variety of problems to which the element described herein may be applied. The problems presented were solved with H3DMAP on both the MicroVax II using the VMS operating system and the DECstation 3100 (RISC processor) with the UNIX operating system.

5.1 Uniformly Loaded Cantilever Plate

A cantilever beam shown in Figure 5.1.1 is used to test the linear and geometric non-linear response of the shell element. A uniform pressure is applied as a step function on the beam in the positive y-direction.

The linear response is obtained by applying a pressure of P=0.01 psi. Theoretically the maximum deflection should be twice the value of the static deflection.

$$\delta_{max} = 2 \cdot \delta_{static} = 2 \cdot \left(\frac{wL^4}{8EI} \right)$$

The first period is found using the following relationship:

$$T_1 = \frac{2\pi}{3.515} \sqrt{\frac{\rho\, AL^4}{EI}}$$

The computed and theoretical results compare very well as shown in the following table.

	THEORY	H3DMAP
Maximum deflection δ_{max} (in)	0.0250	0.246
Period T (sec)	0.00572	0.0058

A pressure of P=2.85 psi is used to verify the geometric non-linear response. This pressure amplitude results in large displacement response which is captured by the non-linear geometric shell formulation. Figure 5.1.1 shows

the response of Node 6 and 12 in the y-direction and Figure 5.1.2 shows the deformed geometry at 4 ms. The deflections of Node 6 and 12 are in close agreement with Belytschko et al. results/12/.

5.2 Moment-Loaded Cantilever Plate (Non-Linear Geometric)

The purpose of this test case was to verify the capacity of the shell element formulation to handle geometric non-linear deformation. This test consists of bending an initial straight beam into a circular shape. The moment, M, required to bend the beam of length, L, into a circular shape is given by the curvature formula;

$$\frac{M}{EI} = \frac{\dfrac{d^2w}{dx^2}}{\left[1 + \left(\dfrac{dw}{dx}\right)^2\right]^{\frac{3}{2}}} = \frac{1}{R}$$

Thus, $$M = \frac{EI}{R} = \frac{2\pi EI}{L}$$

An accurate solution will lead to a fully circular shape when M is applied. Since the static solution is sought, the moment M required to bend the beam into a circular shape is applied as a ramp function (Figure 5.2.1) and solved using dynamic relaxation.

The model is shown in Figure 5.2.1 along with the material properties and the applied load. Fig. 5.2.2 shows the displacement time history of node 13 in both x and y direction while Figures 5.2.3 and 5.2.4 depict the response of the metal strip during and at the end of loading, respectively. From this example, it can be seen that the shell element formulation easily handles this type of large deformation problem.

5.3 Corner Supported Plate

The purpose of this test was to verify the hourglass control algorithm. A quarter mesh model was used as shown in Figure 5.3.1. Boundary node 9 is constrained in the translational degrees of freedom. The corner point loading of the plate in this case provides an excitation mechanism for the w-hourglass mode described in section 3.9. Inadequate control of the hourglass mode leads to unacceptable mesh distortion as shown in Figures 5.3.3, 5.3.4 and 5.3.5. Hourglass control is obtained using the viscous form of control described in section 3.9 using an hourglass stabilization coefficient of 0.1. This results in the proper response as seen in Figure 5.3.2. The results obtained in this case are in good agreement with the classical solution (Figures 5.3.1 and 5.3.6).

5.4 Uniformly Loaded Elastic Plastic Square Plate

A simply supported square plate is loaded with a constant downward pressure of 300 psi which is applied as a step function. One quarter of the plate was modelled as shown on Figure 5.4.1. Two material types were studied: elastic and elastic-perfectly plastic. H3DMAP results are shown on Figures 5.4.2 and 5.4.3 and compare very well with the results obtained by Belytschko et al/12/. A plot of the plate's response at time=0.7 ms is shown in Figure 5.4.4.

5.5 Impulsively Loaded Circular Plate

One of the verification cases used to validate H3DMAP Version 4 was taken from ref. 13. This case involved the experimental evaluation of the response of impulsively loaded clamp circular plates. It is similar to the type of analysis being performed on the transportation cask designs where an initial velocity is applied to a structure. The model geometry used for both the experiment and analysis is shown in Figure 5.5.1. The results reported herein correspond to test P-8 in ref. 13 for an initial velocity of 4410.0 in/sec. The material is Aluminum 6061-T6 and the properties are given in Figure 5.5.1. The analysis was carried out using shell elements in order to verify the validity of the element explicit formulation. The shell model is shown in Figures 5.5.2 and 5.5.3.

The comparison of the predicted vertical central deflection (node 1) time history with the experimental value is shown in Figure 5.5.4. Some error is observed but as indicated in ref. 13, slippage occurred between the clamping surface and the plate after detonation and the effective radius increased slightly, leading to somewhat higher responses. The correlation is excellent for this class of problem. A typical plot of the deformed structure is shown in Figure 5.5.5.

5.6 Impulsively Loaded Cylindrical Shell

As part of the shell element verification, H3DMAP predictions were compared against the experimental results obtained by Morino, Leech and Witmer/14/.

In this case a cylindrical panel is impulsively loaded with explosive as shown on Figure 5.6.1. The panel is clamped along the side edges and simply supported at both ends. The explosion is simulated by an initial velocity which yields the same impulse obtained by the explosive.

In the experiment/14/, the boundary of the panel in contact with the explosive is partially constrained against rotation. This requires special attention since this condition lies between the ideal boundary constraints of simply supported and fully fixed. To circumvent this problem, the simple support was modelled using a plastic hinge, i.e. using a softer material in the boundary region, and that hinge is fully restrained as far as the computer code is concerned. Consequently, the first layer of elements rotate more easily than the rest of the panel, but at the same time, it offers a certain resistance to rotation, which is not provided with normal simple supports. This approach provides a more realistic representation of the boundaries present in the experiment.

Figures 5.6.2 to 5.6.4 compare experimental data and H3DMAP results while Figure 5.6.5 shows the deformed structure after 0.8 ms. Fig. 5.6.6 and 5.6.7 show the plastic strain in the structure.

The differences observed between the experimental and computed results can be attributed to the difficulty in accurately modelling the boundary conditions of the experiment and discretization error. As observed, the agreement in results is very good for this class of problem.

5.7 Punch Verification Test

Mathematical Model

In order to demonstrate the validity of the analytical models used for shell and solid modelling in H3DMAP, and provide some insight into the error bounds which can be expected, a benchmark with an experimental model was performed. Details are given in /15,17/. The comparison serves to test the polyurethane foam and stainless steel material models and demonstrate the use of the shell elements in combination with solid elements representing hydrodynamic materials. The model used an outer shell thickness of 0.2920 inches in order to provide for a failure of the outer shell in punching shear. This would enable a benchmark of the failure limits used in /15/ in order to confirm that they were both conservative and realistic.

The case considered, was the accident scenario involving a 4 ft drop (impact velocity: 192.6 in/sec) of the package analyzed in /15/ onto a mild steel pin. The material properties used are given in /15,17/. Due to the localized nature of this drop, only the lower portion of the overpack was modelled as shown in Figure 5.7.1. It consisted of polyurethane foam sandwiched between a 0.2920 inch thick outer plate and a 0.2692 inch thick inner plate.

The model topology is shown in Figures 5.7.1, 5.7.2 and 5.7.3. There are a total of 1574 nodes, 1140 solid elements representing the foam and 416 shell elements for the plate. The pin was modelled using the partial rigid wall option in H3DMAP.

Since the model only partially represents the package weight, the remaining weight of package plus contents was included as a non-structural mass. The total weight of the package is 31,550 lbs. This includes the inner container with payload and the overpack. Since the experimental model was ballasted in such fashion that the remaining package weight was uniformly distributed across the 0.2692 in inner liner plate, the same approach was adopted here by increasing the density of the inner liner plate.

Experimental Model - 1/4 Scale

The experimental model is described in detail in /17/. It is a 1/4 scale model of the bottom portion of the overpack. The model was instrumented to obtain impact force and displacement time histories. The drop height was 4 ft and the experimental model was ballasted to simulate the total package weight.

Scaling Laws

In order to compare the results of analysis and experiment the following relationships between scale model (m) and full scale prototype (p) were used:

Deflection	Y_m	-	Y_p/n
Stress	S_m	-	S_p
Force	F_m	-	F_p/n^2
Energy	E_m	-	E_p/n^3
Mass	M_m	-	M_p/n^3
Time	T_m	-	T_p/n
Acceleration	A_m	-	nA_p

where n = 4 for 1/4 scale model.

These relations were applied to the experimental results and the comparison with analysis presented with reference to full scale.

Analytical Results and Comparisons

The impact simulation was run to 36 ms. In the experiment, failure of the outer shell occurred at approximately 28 ms in the form of a punch through. A deformed plot at that time is shown in Figure 5.7.6. The comparisons with experimental results are shown, in terms of the full scale quantities of displacement and impact force time histories in Figures 5.7.7 and 5.7.8. The details of the experimental results are given in /17/. As demonstrated in the plots, excellent agreement is obtained for impact forces and displacements. At the time of failure (28 ms), a total peak impact force in the analytical model of 460,000 lbs. is observed.

Figure 5.7.9 shows the plastic strain as a function of time in the shell element underneath the edge of the pin, while Figure 5.7.10 describes the hydrostatic stress evaluation in the foam element directly below the center of the pin (refer to Figure 5.7.3 for the position of these elements).

This benchmark serves to demonstrate the accuracy of the mathematical modelling through the excellent correlation obtained between the experimental and analytical results.

Plastic strains in the shell elements at the time of failure are shown in Figures 5.7.11 and 5.7.12. Von Mises stresses and hydrodynamic stresses in the foam elements at the same time can be found on Figures 5.7.13 and 5.7.14.

5.8 Pipe Impact on Rigid Surface

The following test case was designed to show the capacity of H3DMAP to handle pipe whip problems. The pipe shown on Figure 5.8.1 was rotated around a pivot in such a way that the free end of the pipe would hit a rigid wall at an angle

of 30° and a velocity of 1250 in/sec. The deformed structure at time = 3.5 ms is shown in Figure 5.8.2. The corresponding effective plastic strains and von Mises stresses are shown on Figures 5.8.3 to 5.8.6, and the X-displacement time history of node 1 is shown in Figure 5.8.7.

ACKNOWLEDGMENTS

The author would like to express appreciation to Ms. C. Robshaw for her patience and skill in typing this report. Special thanks to Dr. T. Byrne for his useful comments and his continual support.

Approved by:

G.J. Clarke
Manager
Mechanical Research Dept.

Submitted by:

R.G. Sauvé
Engineer
Applied Mechanics Section

Reviewed by:

T.P. Byrne
Unit Head-Stress Analysis & Heat Transfer
Applied Mechanics Section

RGS:cr

REFERENCES

1. Sauvé, R.G., *H3DMAP Version 4, A General Three Dimensional Finite Element Computer Code for Linear and Non-Linear Analysis of Structures: User Manual and Verification Cases*, Ontario Hydro Research Report No. 89-221-K, October 1989.

2. Sauvé, R.G., *H3DMAP Three Dimensional Matrix Analysis Program for Structures, Theoretical Manual Volume 1, User and Verification Case Manual Volume 2*, Ontario Hydro Design and Development Report Nos. 86035 (Version 2), February 1986, 87419 (Version 3), October 1987.

3. Cook, R., *Concepts and Applications of Finite Element Analysis*, 2nd Edition, John Wiley and Sons, Toronto, 1981.

4. Malvern, L.E., *Introduction to the Mechanics of a Continuous Medium*, Prentice Hall, 1969.

5. Hughes, T.J.R., Taylor, R.L., Kanoknukulchai, W., *A Simple and Efficient Finite Element for Plate Bending*, International Journal of Numerical Methods in Engineering, Vol. II, pps. 1529-1547, 1977.

6. Hughes, T.J.R., Cohen, M., Haroun, M., *Reduced and Selective Integration Techniques in the Finite Element Analysis of Plates*, Nuclear Engineering and Design, Vol. 46, pps. 203-222, 1978.

7. Wylie, R.C., *Advanced Engineering Mathematics*, 4th Edition, McGraw-Hill, 1975.

8. Dodds, R.H., *Numerical Techniques for Plasticity Computations in Finite Element Analysis, Computers and Structures*, Vol. 26, pps. 767-779, 1987.

9. Krieg, R.D., Key, S.W., *Implementation of a Time Independent Plasticity Theory Into Structural Computer Programs, Constitutive Equations in Viscoplasticity: Computational and Engineering Aspects*, ASME Vol. 20, pps. 125-137, 1976.

10. Belytschko, T., Tsay, C., *A Stabilization Procedure for the Quadrilateral Plate Element with One Point Quadrature*, International Journal for Numerical Methods in Engineering, Vol. 19, pps. 405-419, 1983.

11. Flanagan, D.P., Belytschko, T., *A Uniform Strain Hexahedron and Quadrilateral with Orthogonal Hourglass Control*, International Journal for Numerical Methods in Engineering, Vol. 17, pps. 674-706, 1981.

12. Belytschko, T., Lin, J., Tsay, C., *Explicit Algorithms for the Non-Linear Dynamics of Shells*, Computer Methods in Applied Mechanics and Engineering, Vol. 42, pps. 225-251, 1984.

13. Duffey, T., Key, S., *Experimental-Theoretical Correlations of Impulsively Loaded Clamped Circular Plates*, Experimental Mechanics, pps. 241-249, June 1969.

14. Morino. L., et al., *An Improved Numerical Calculation Technique for Large Elastic-Plastic Transient Deformations of Thin Shells: Part 2 - Evaluation and Applications*, Journal of Applied Mechanics, 1971.

15. Sauvé, R.G., et al., *Material Modelling and Impact Analysis of Polyurethane Foam Filled D_2O Transportation Packages Proceedings of the International Symposium on the Packaging and Transportation of Radioactive Materials (PATRAM 1986)*, Vol. 2., Paper SM-286/10P, IAEA, June 1986.

16. Metzger, D.R., Dubey, R.N., *Corotational Rates in Constitutive Modelling of Elastic-Plastic Deformation*, International Journal of Plasticity, Vol. 4, pps. 341-368, 1987.

17. Russell, J.H., *Tritiated D_2O Transport Container Computer Model Verification Punch Test No. 2*, Ontario Hydro Research Division Report No. 85-83-K, April 1985.

18. Nadeau, E., Sauvé, R.G., *Analytical Simulation of Bruce Unit 2 Pressure Tube Response to SLAR Tool Loading*, Ontario Hydro Research Report No. 89-220-K, September 1989.

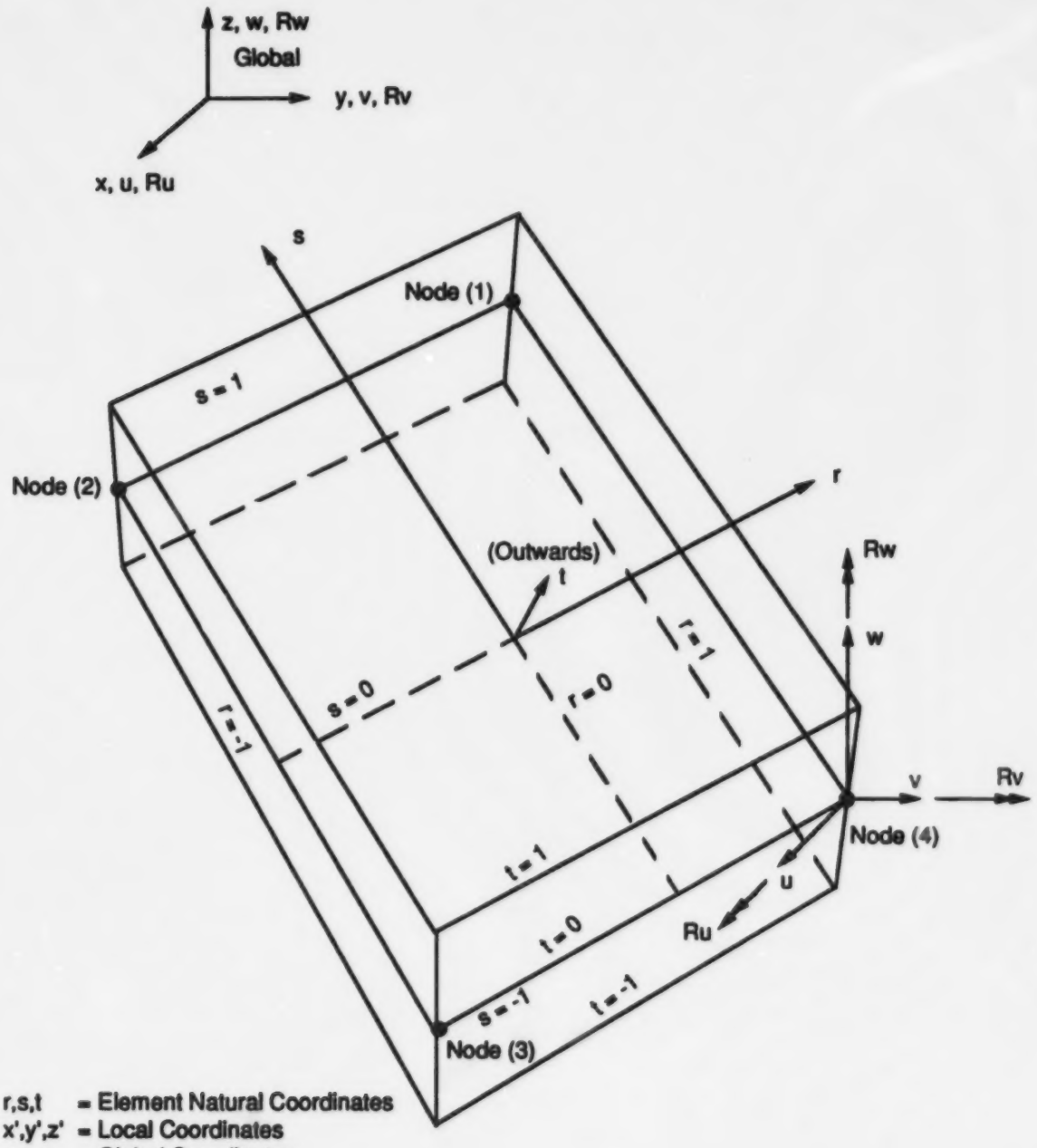

FIGURE 3.1

BI-LINEAR DEGENERATED ISOPARAMETRIC THIN/THICK SHELL ELEMENT

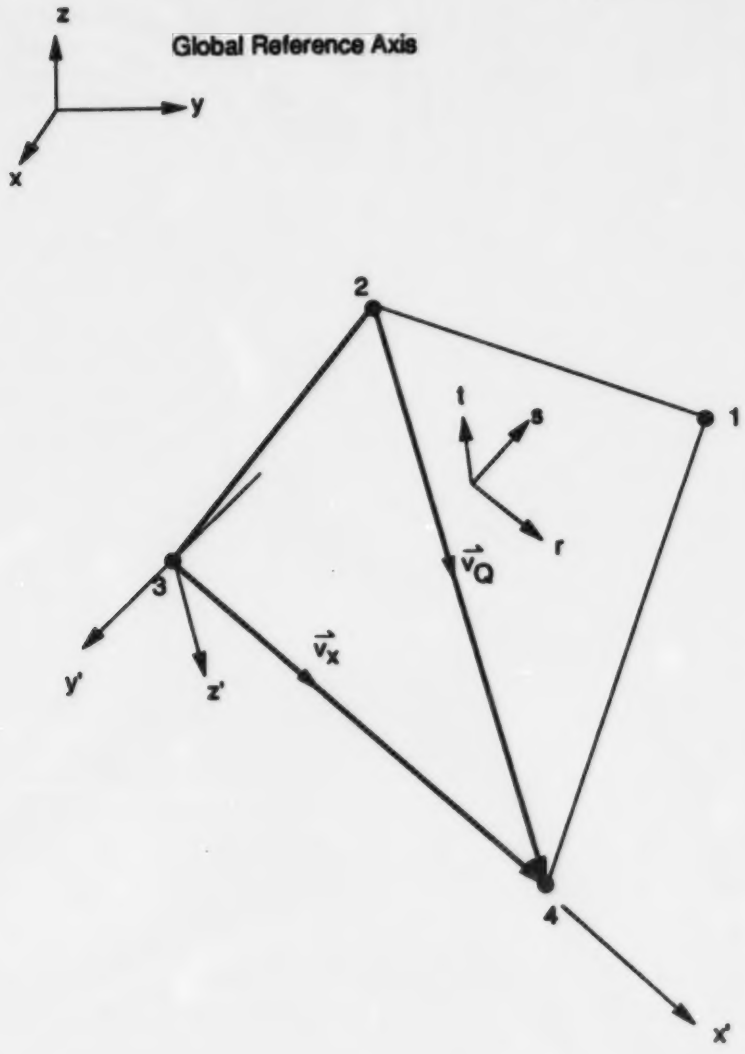

r,s,t = Element Natural Coordinates
x'y'z' = Local Coordinate System (Material Axes)
x,y,z = Global Coordinate System

FIGURE 3.2

SHELL ELEMENT CO-ROTATIONAL COORDINATE SYSTEM

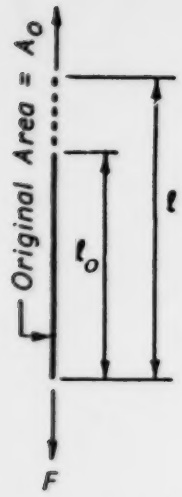

ℓ_o = Original Length
ℓ = Final Length

True Stress/Strain

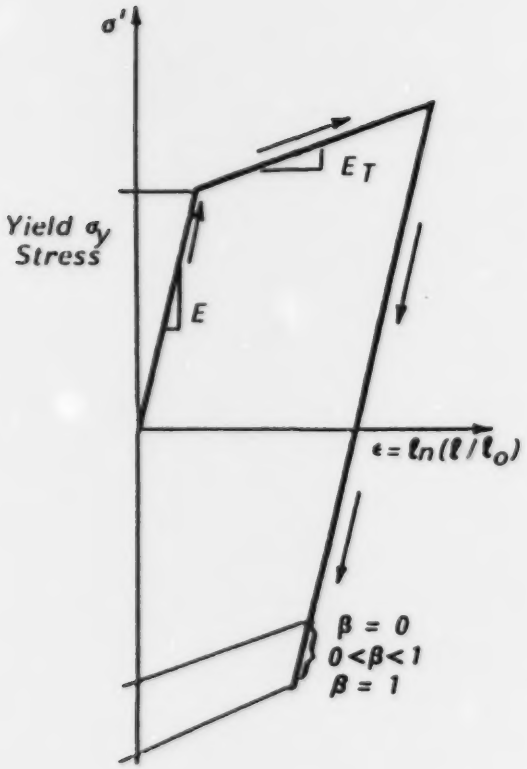

FIGURE 3.3

STRESS/STRAIN MEASURES
ELASTO-PLASTIC MATERIAL MODEL

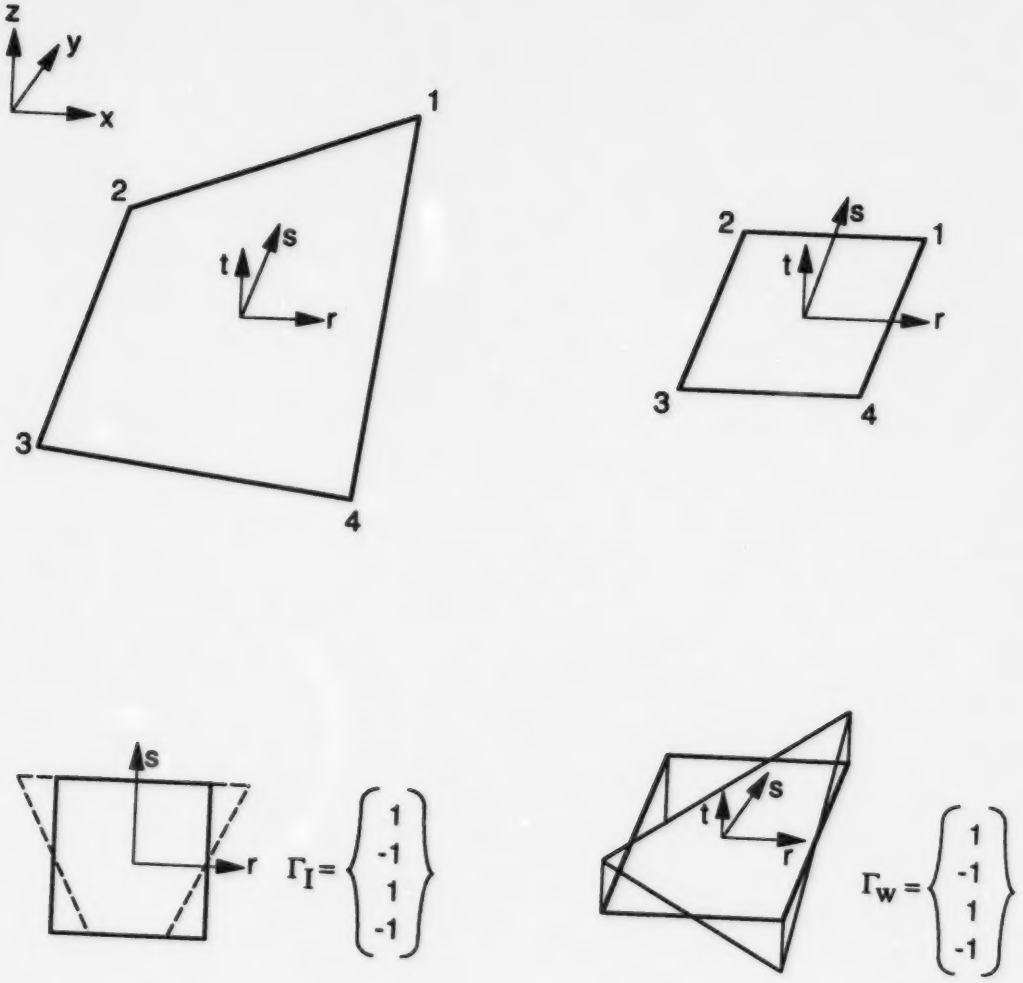

Membrane Hourglass Mode

Bending w - Hourglass Mode

FIGURE 3.4

TYPICAL HOURGLASS MODES FOR MEMBRANE AND BENDING DEFORMATIONS

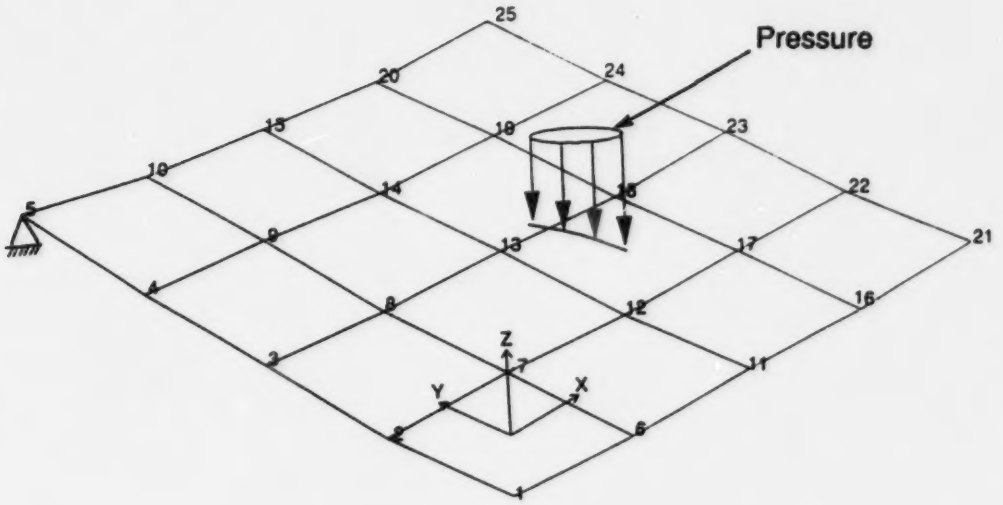

FULLY CONTROLLED HOURGLASSING

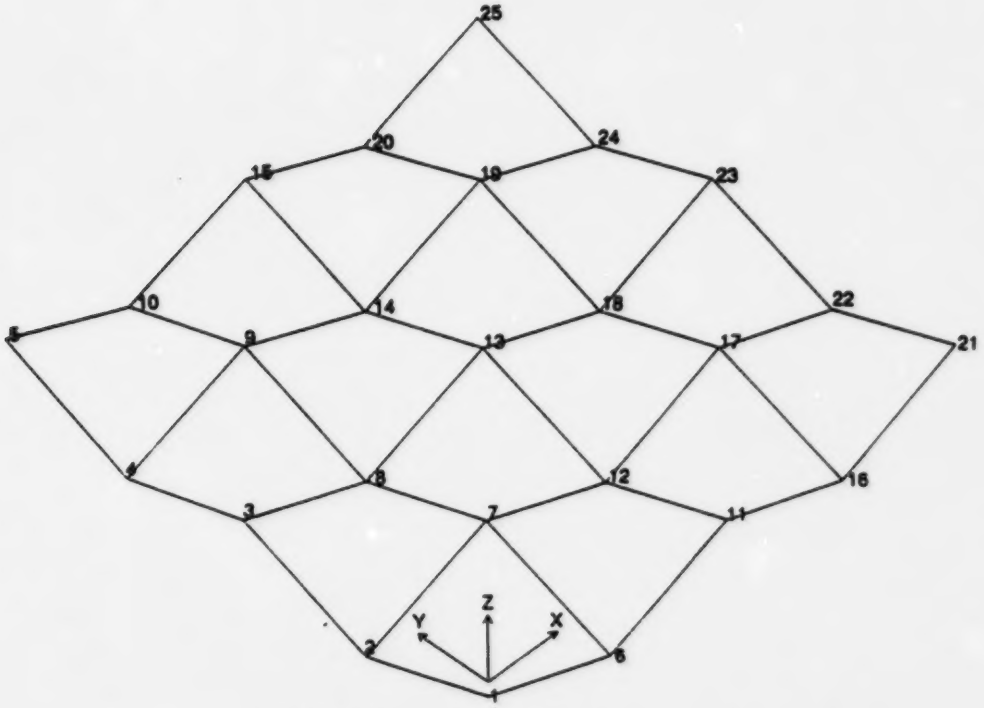

UNCONTROLLED HOURGLASSING

FIGURE 3.5

EXAMPLE OF HOURGLASS MODES IN PLATE BENDING OF CORNER SUPPORTED PLATE UNDER UNIFORM LOADING

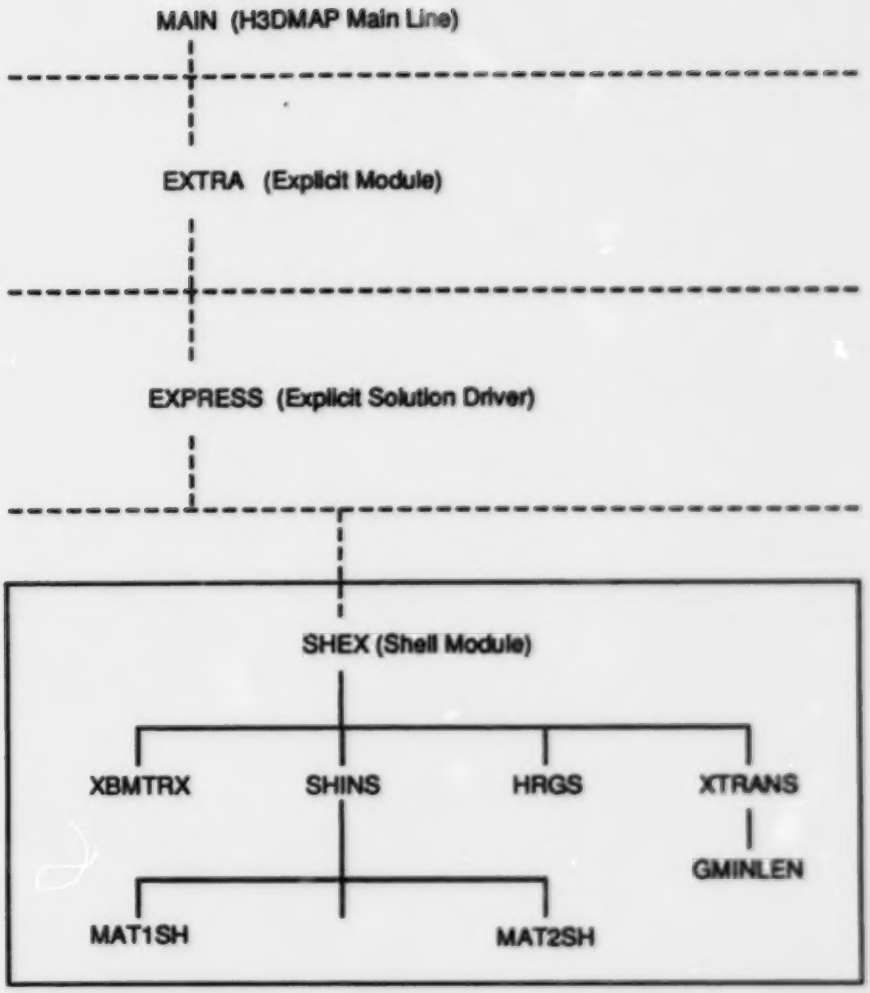

FIGURE 4.1

SHELL ELEMENT ROUTINES FOR EXPLICIT ANALYSIS (H3DMAP MODULE SHEX)

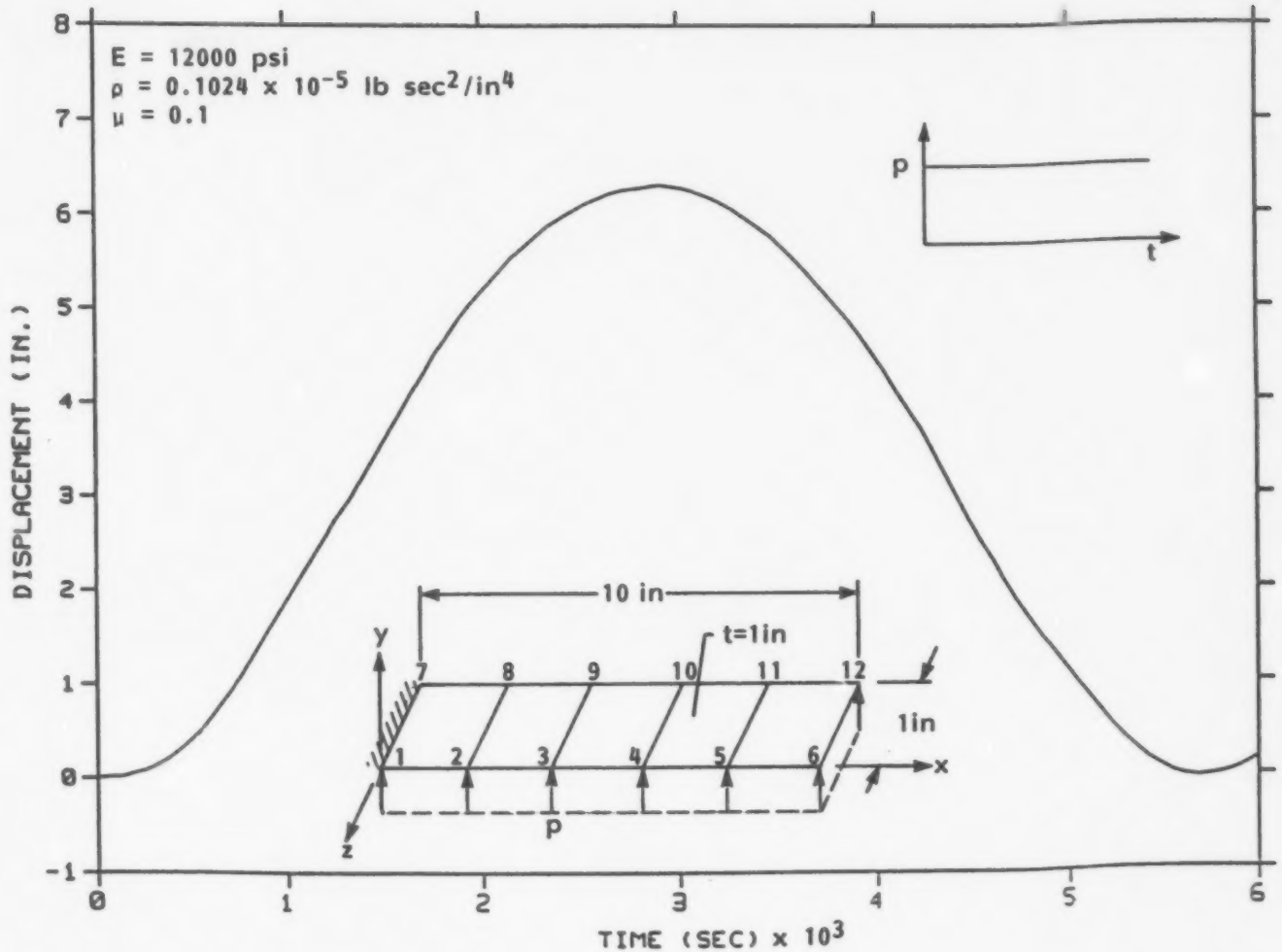

FIGURE 5.1.1

GEOMETRIC NON-LINEAR CANTILEVER SHELL TEST - P = 2.85 psi
DISPLACEMENT RESPONSE OF NODE 6 AND 12 IN THE Y-DIRECTION

89-222
181768-RD

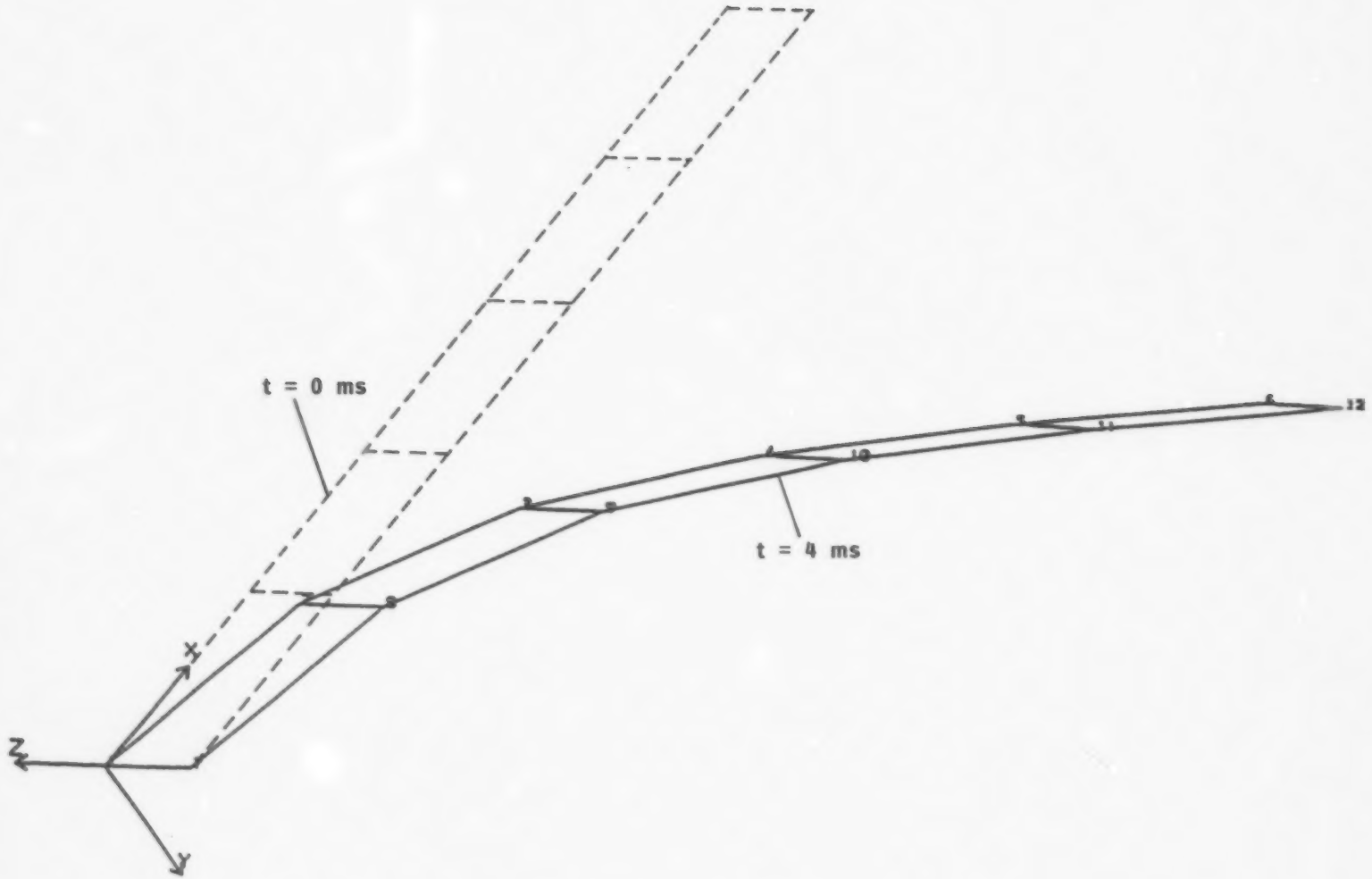

FIGURE 5.1.2
GEOMETRIC NON-LINEAR CANTILEVER SHELL TEST - P = 2.85 psi
RESPONSE AT TIME = 4 ms

181769-RD
89-222

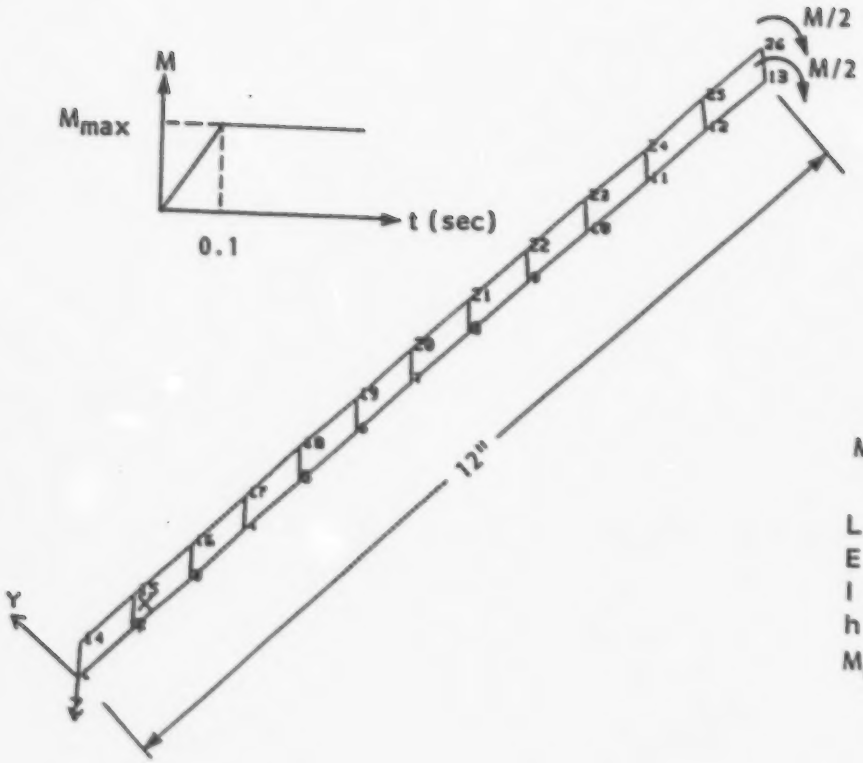

$$M_{max} = \frac{2\pi EI}{L}$$

L = 12"
E = 30×10^6 psi
I = 1/12
h = 1."
$M_{max} = 1.308 \times 10^6$ lb - in

FIGURE 5.2.1
MOMENT LOAD TEST FOR NON-LINEAR SHELL (DYNAMIC RELAXATION)
MODEL AND LOAD

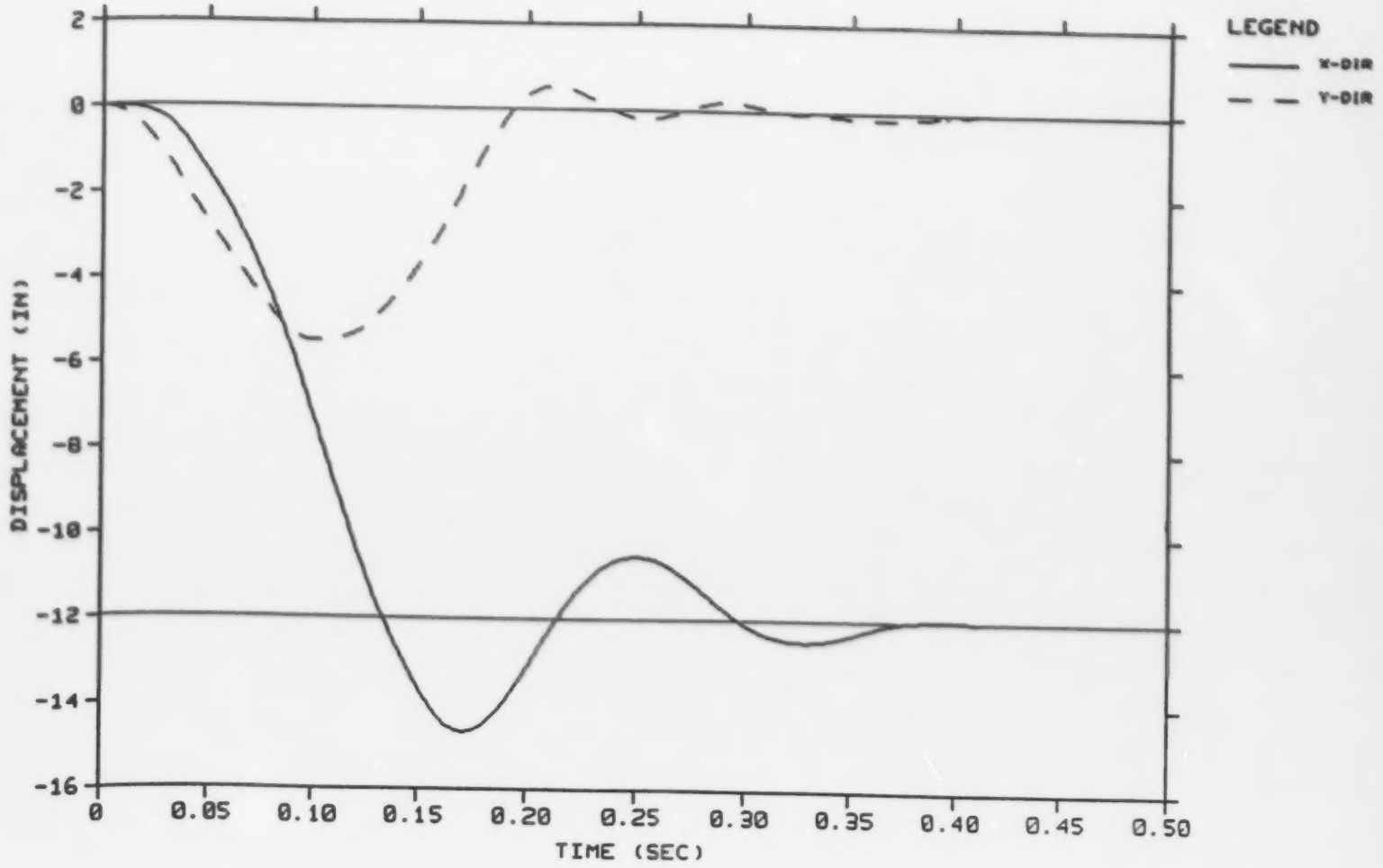

FIGURE 5.2.2
DISPLACEMENT OF NODE 13 IN BOTH X AND Y DIRECTIONS

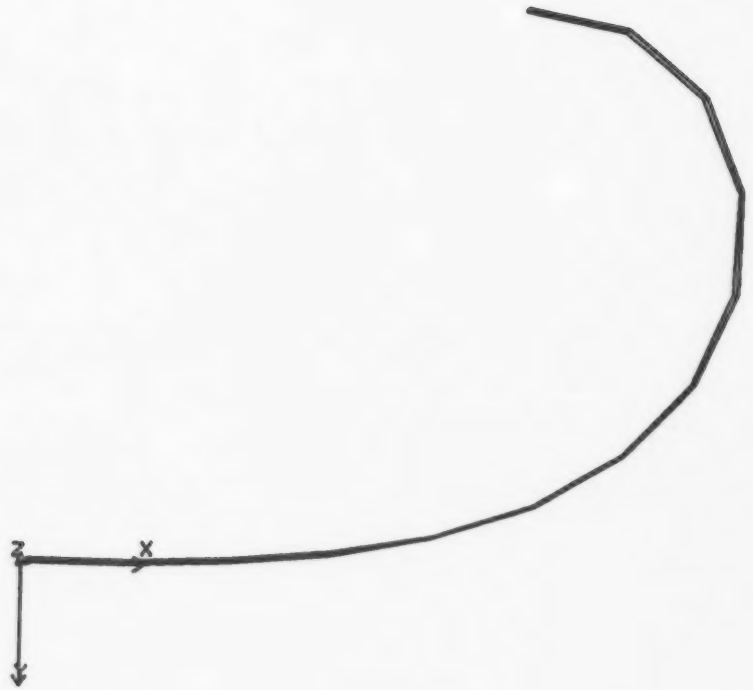

FIGURE 5.2.3
RESPONSE AT TIME = 0.1 sec

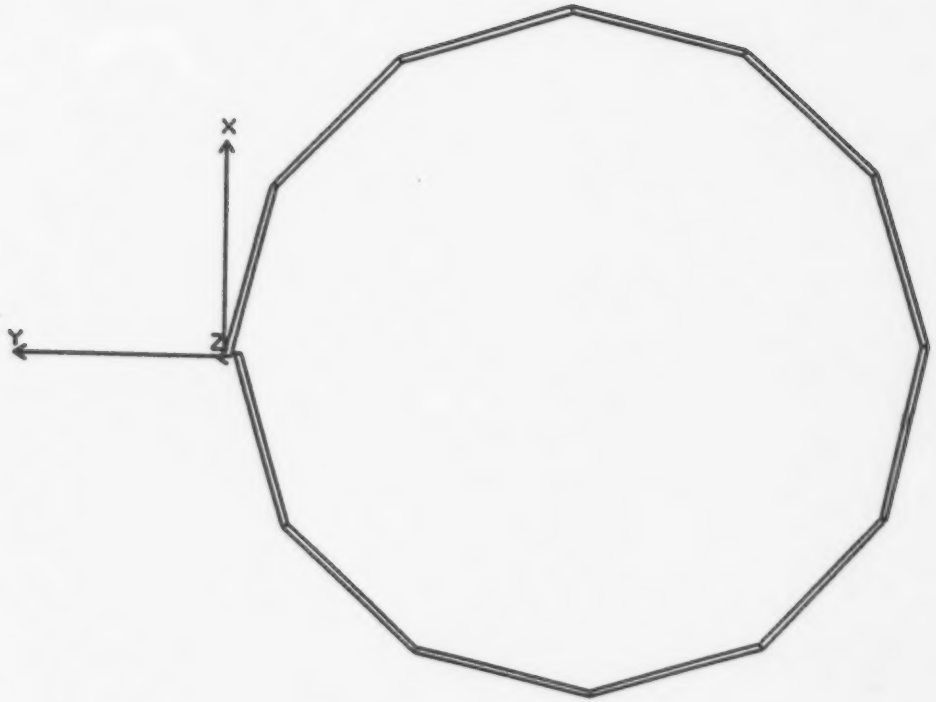

FIGURE 5.2.4
RESPONSE AT TIME = 0.4 sec

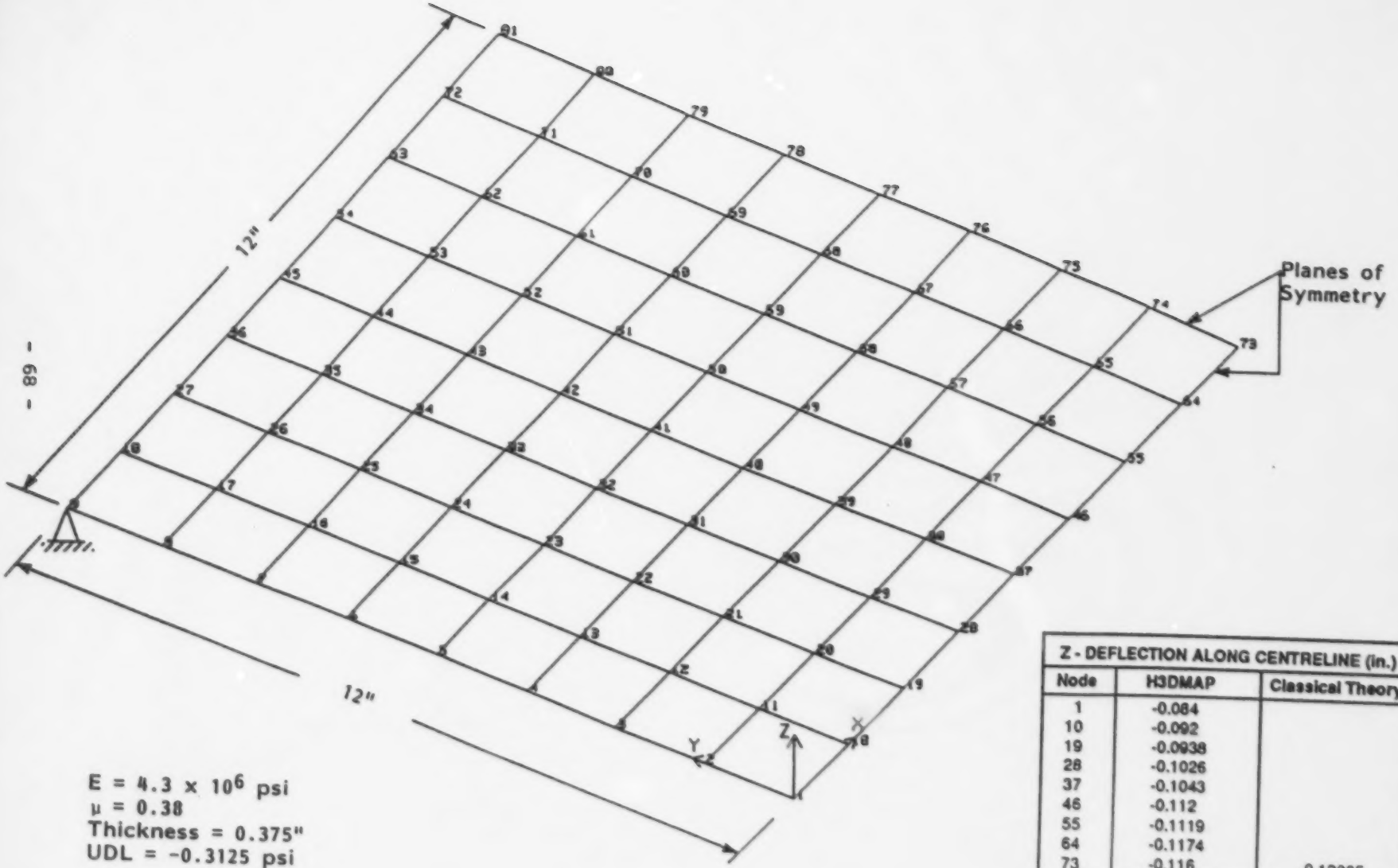

$E = 4.3 \times 10^6$ psi
$\mu = 0.38$
Thickness = 0.375"
UDL = -0.3125 psi

Z - DEFLECTION ALONG CENTRELINE (in.)		
Node	H3DMAP	Classical Theory
1	-0.084	
10	-0.092	
19	-0.0938	
28	-0.1026	
37	-0.1043	
46	-0.112	
55	-0.1119	
64	-0.1174	
73	-0.116	-0.12065

FIGURE 5.3.1
CORNER SUPPORTED FLAT PLATE UNDER PRESSURE LOAD
H3DMAP MODEL

181774-RD
89-222

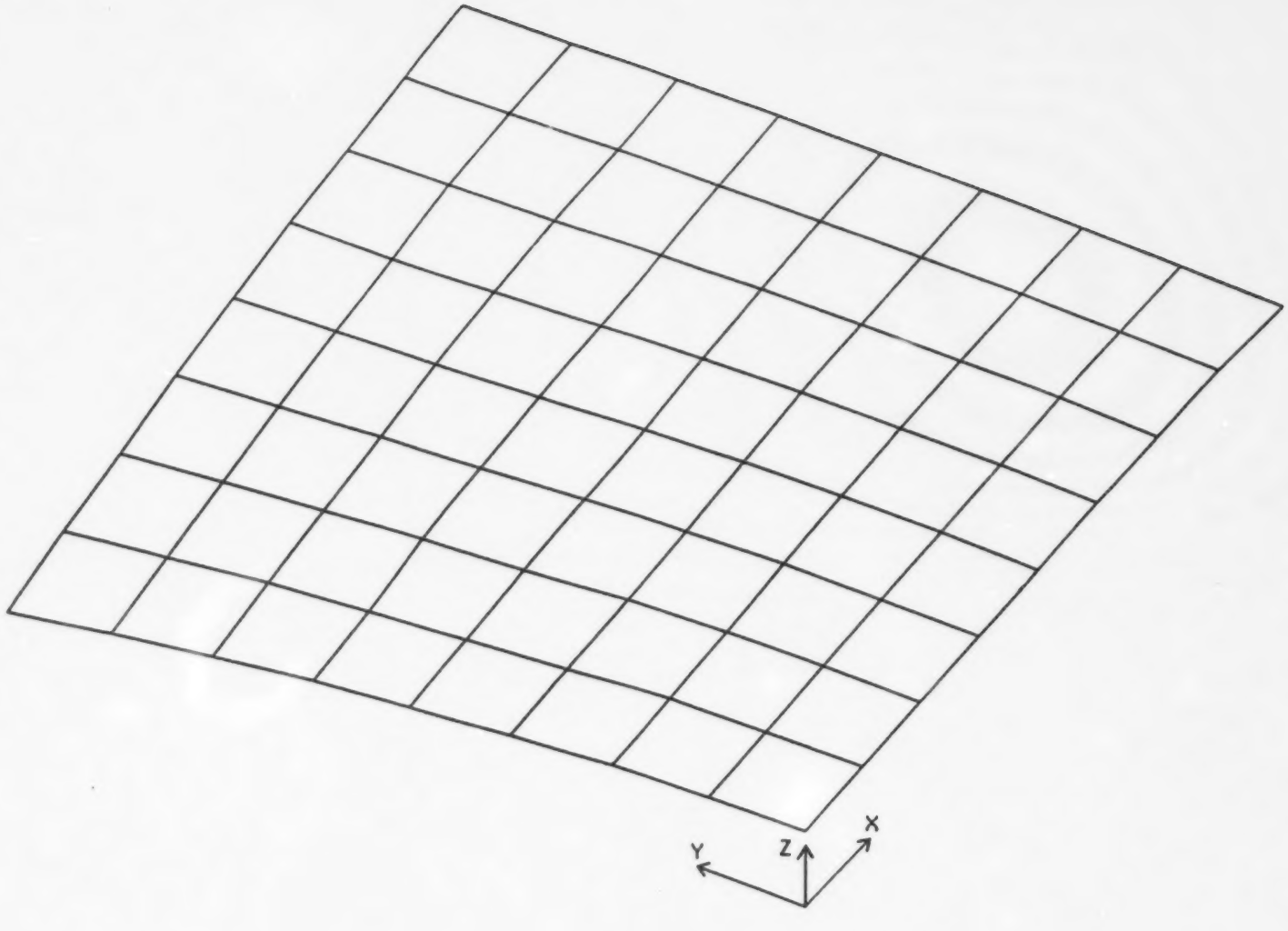

FIGURE 5.3.2
RESPONSE AT TIME = 0.02 sec

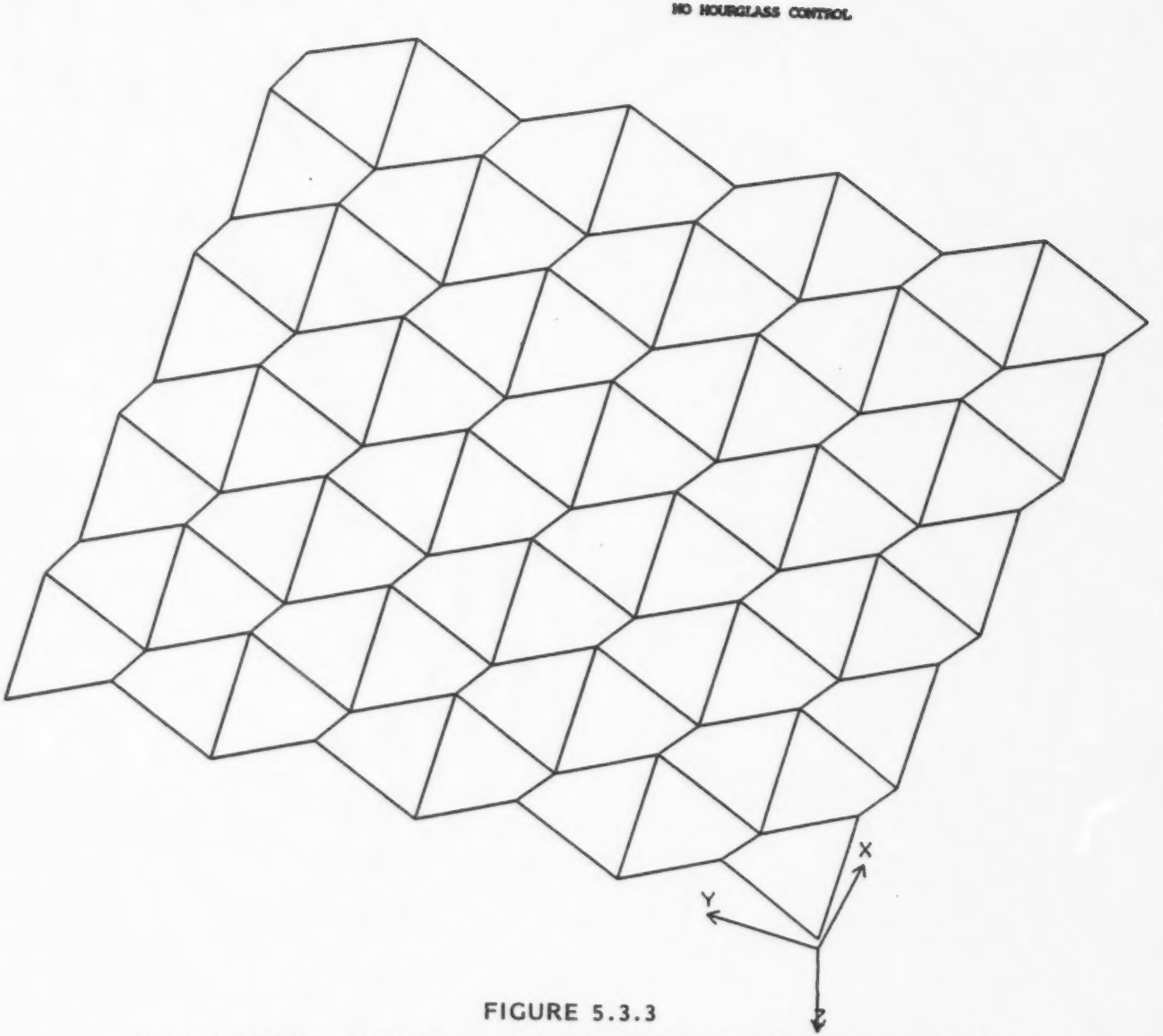

FIGURE 5.3.3
UNCONTROLLED HOURGLASSING FOR CORNER SUPPORTED PLATE
VIEW A

89-222
181653-RD

FIGURE 5.3.4
UNCONTROLLED HOURGLASSING FOR CORNER SUPPORTED PLATE
VIEW B

89-222
181654-RD

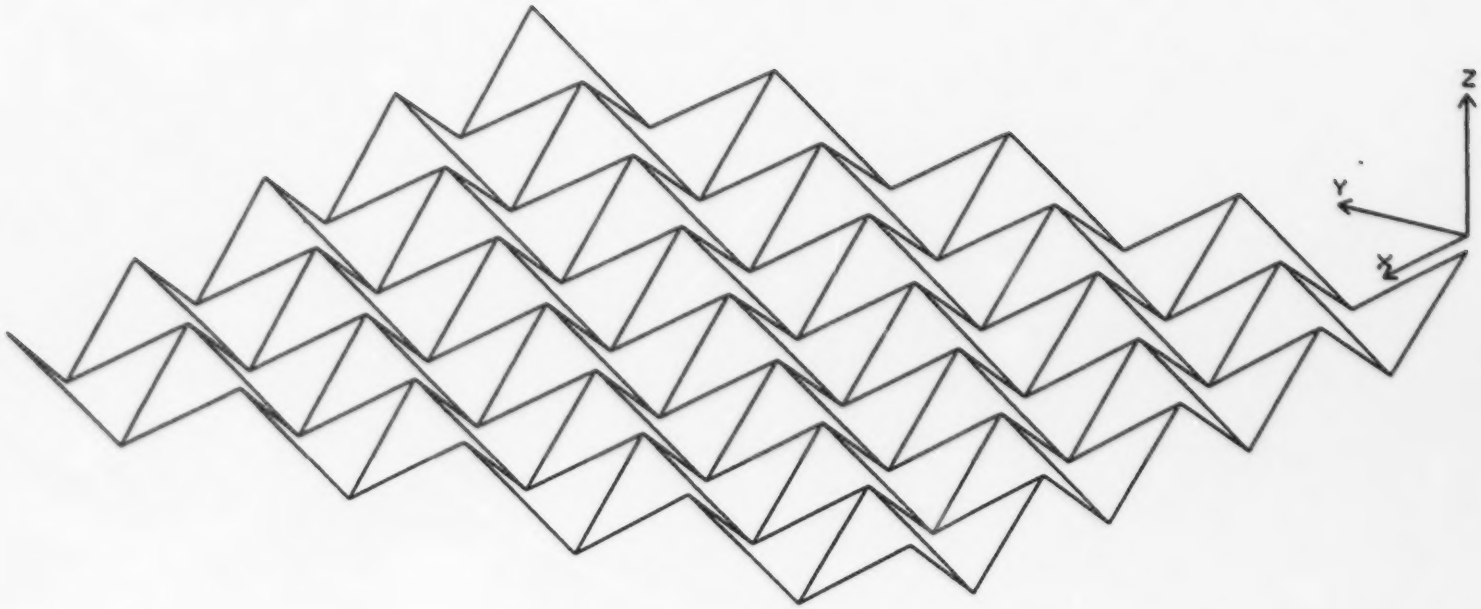

FIGURE 5.3.5
UNCONTROLLED HOURGLASSING FOR CORNER SUPPORTED PLATE
VIEW C

89-222
181655-RD

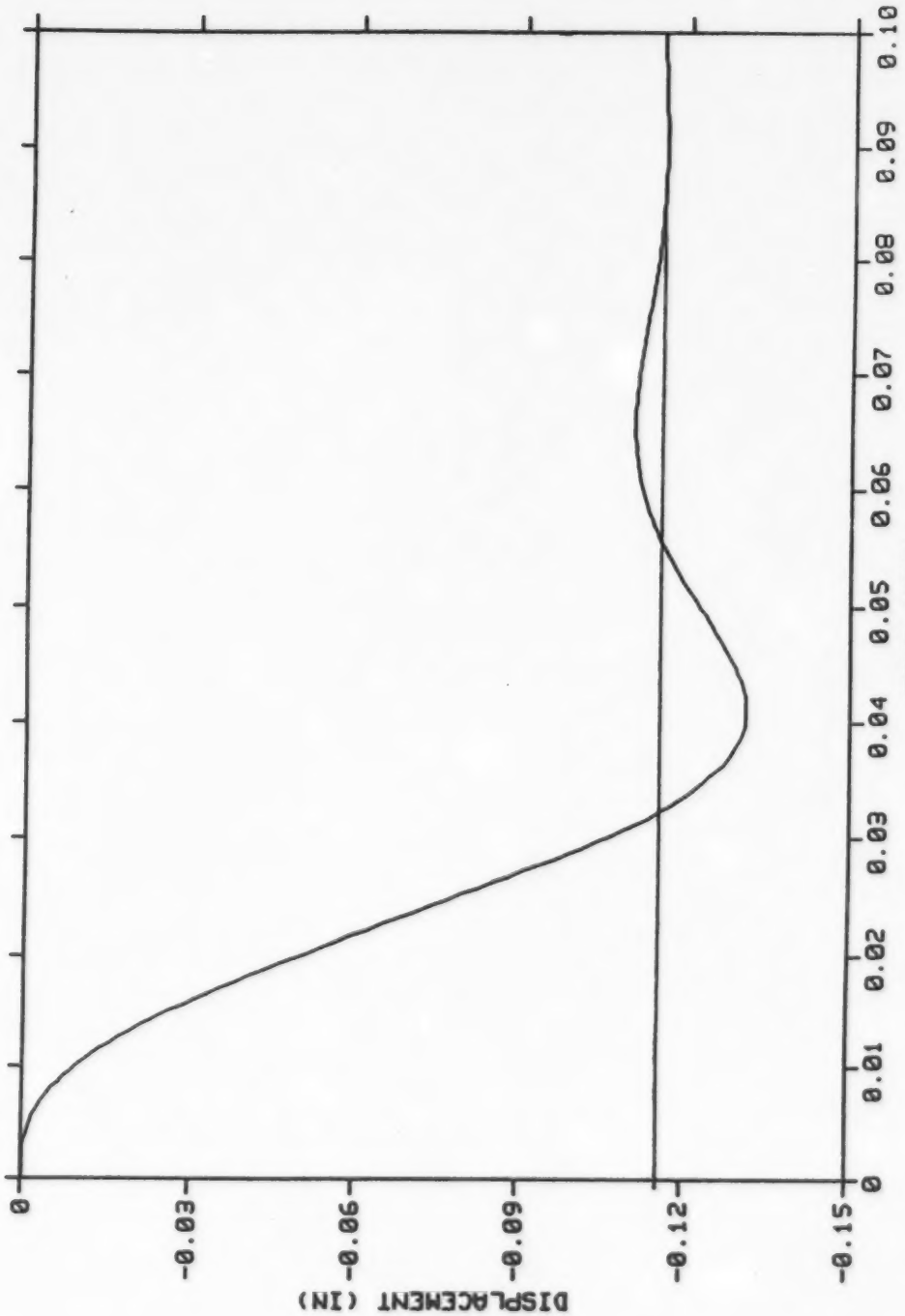

FIGURE 5.3.6
VERTICAL DEFLECTION OF NODE 73

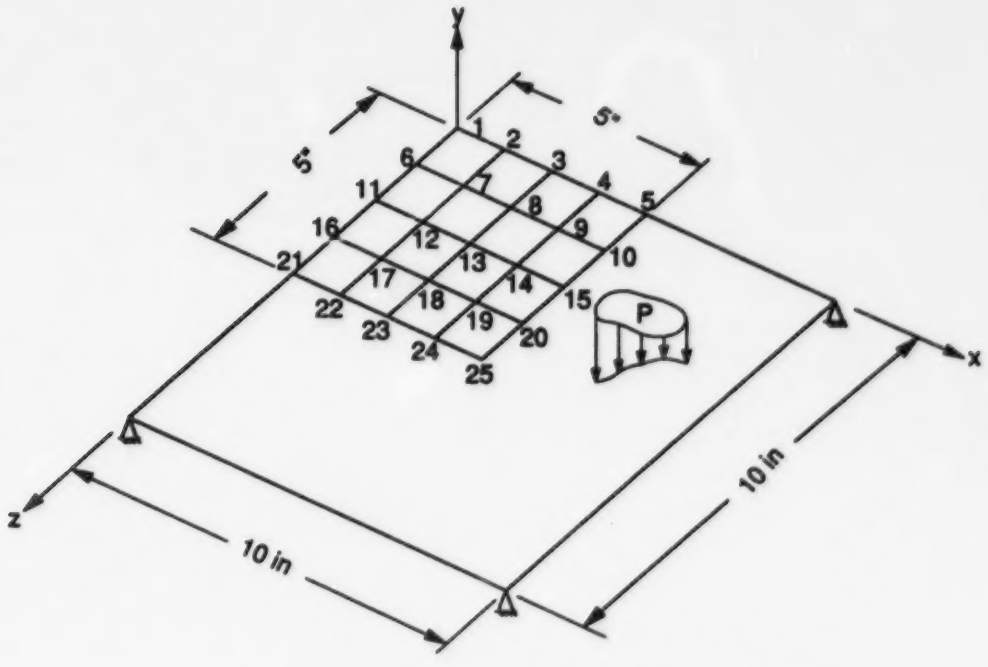

Thickness = 0.5 in
$\rho = 2.588 \times 10^{-4}$
$E = 10^7$
$\mu = 0.3$

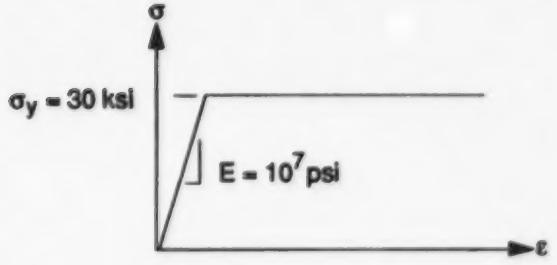

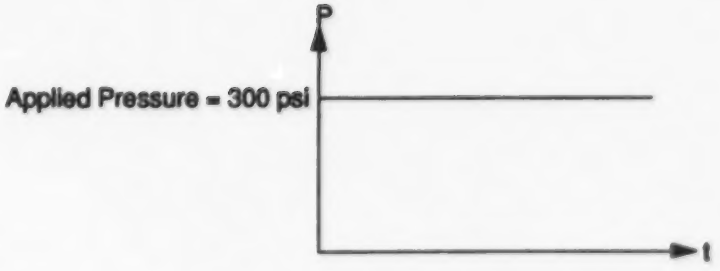

FIGURE 5.4.1

SIMPLY SUPPORTED SQUARE PLATE TEST MODEL, MATERIAL PROPERTIES AND APPLIED LOAD

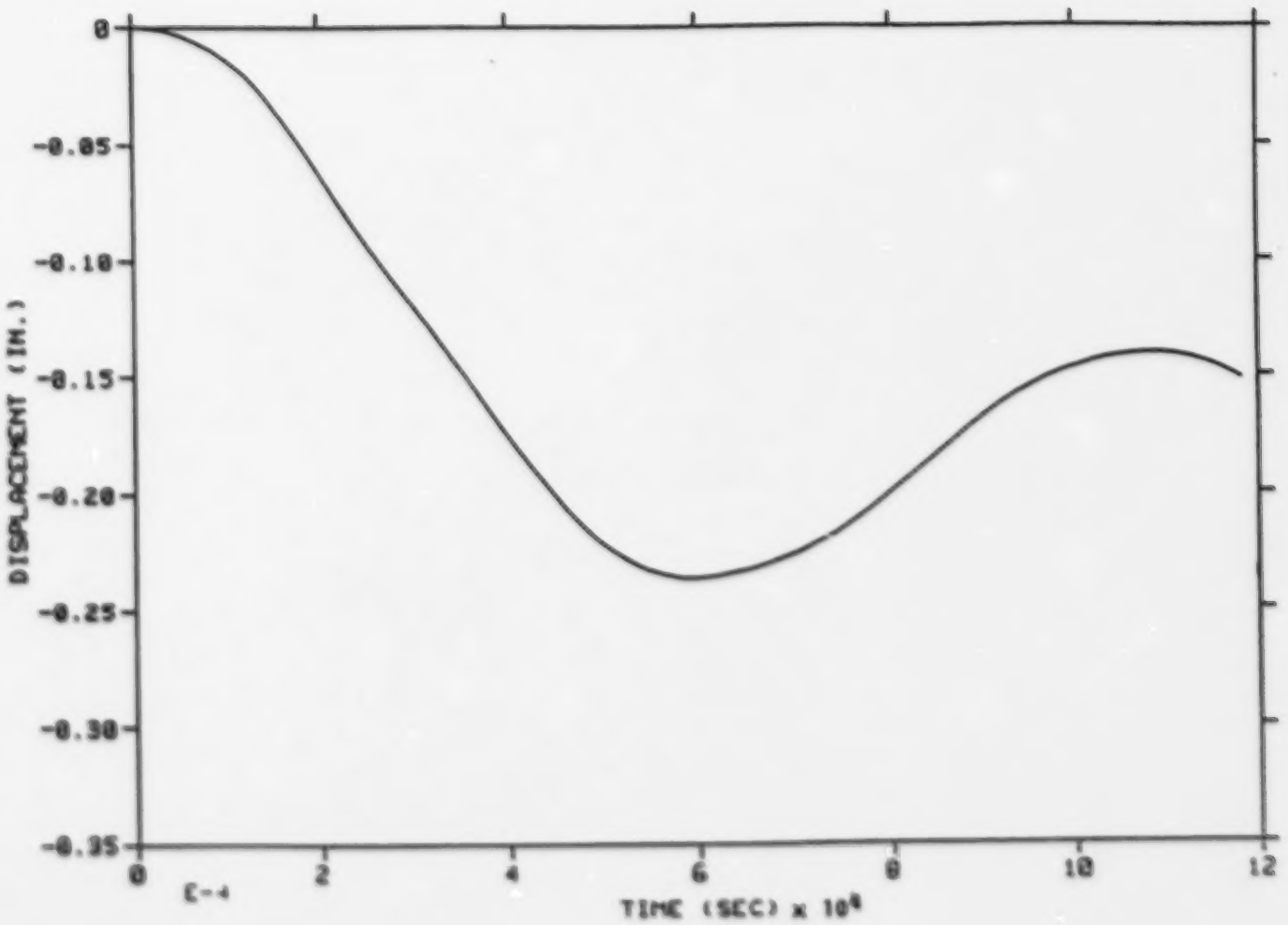

FIGURE 5.4.2

DISPLACEMENT AT NODE 25 IN THE Y-DIRECTION
ELASTIC-PLASTIC MATERIAL

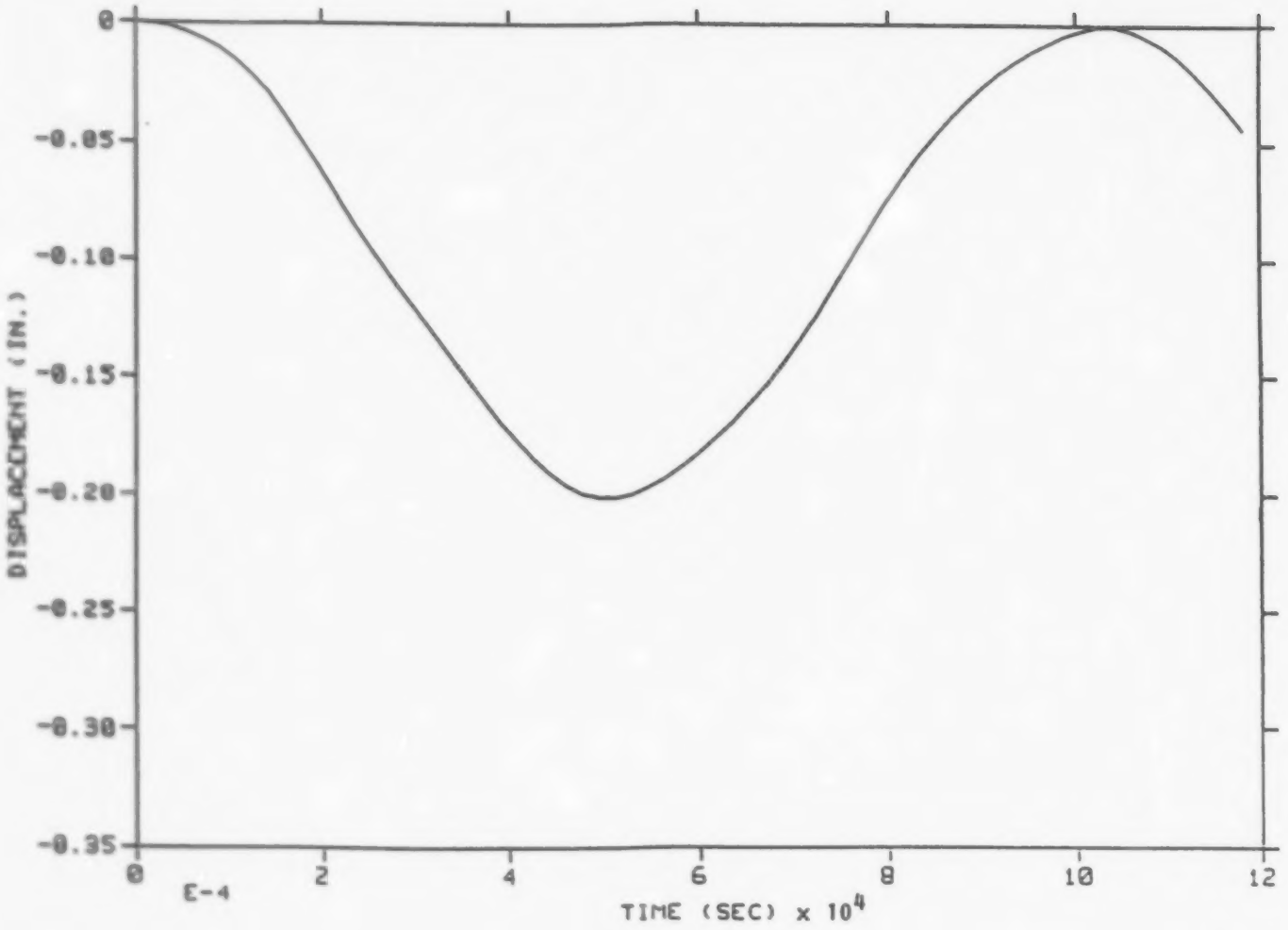

FIGURE 5.4.3

DISPLACEMENT AT NODE 25 IN THE Y-DIRECTION
ELASTIC MATERIAL

89-222
181778-RD

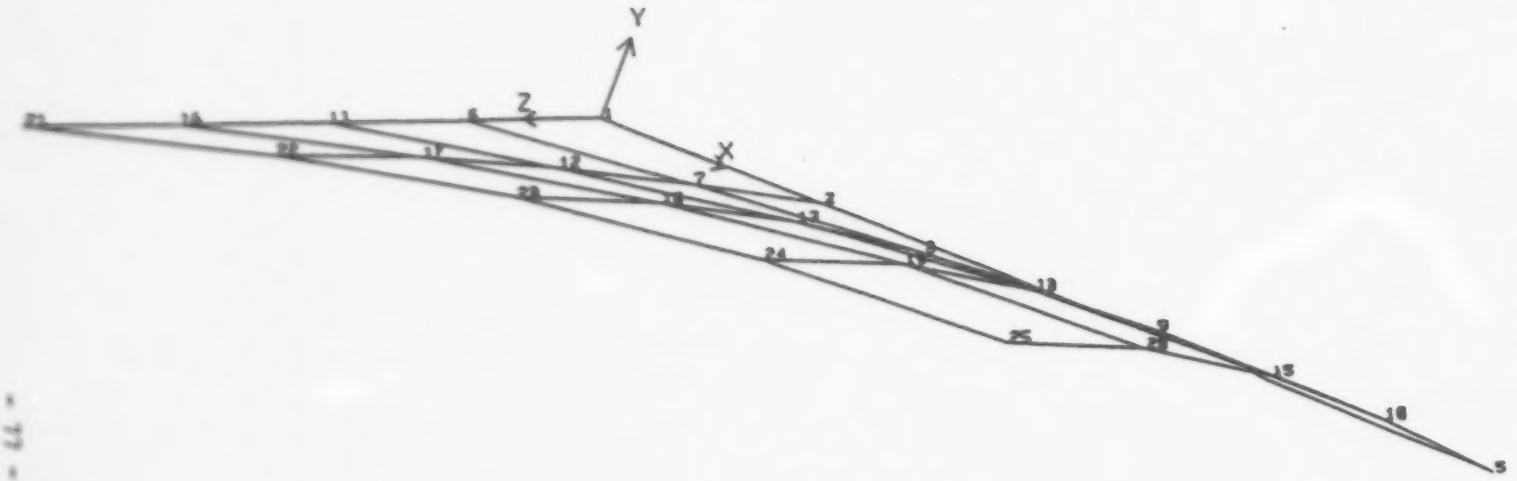

FIGURE 5.4.4
RESPONSE AT TIME = 0.7 ms

09-222
181766-RD

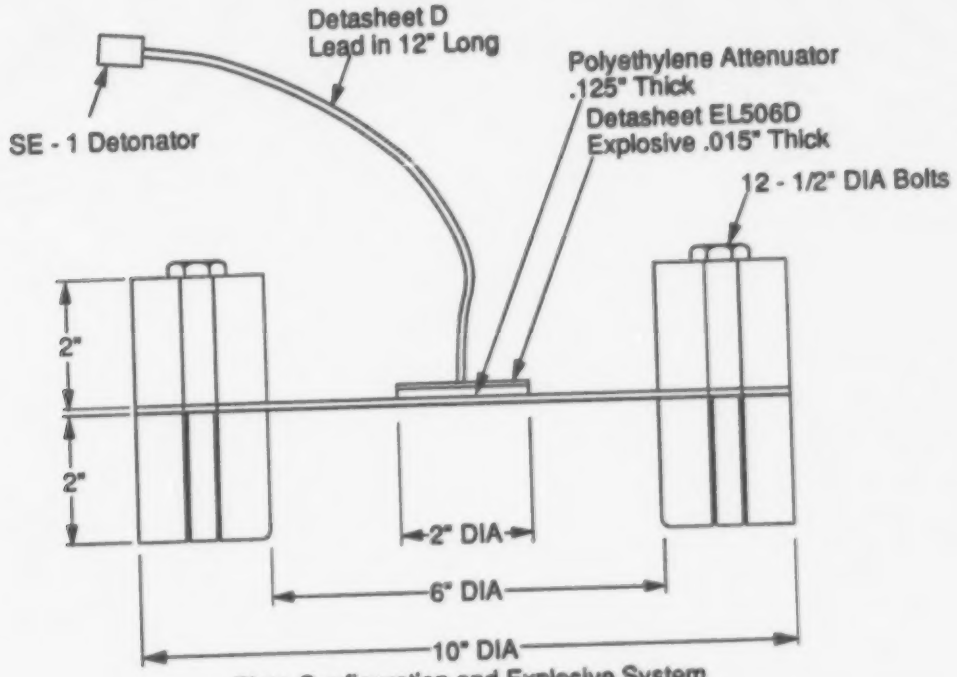

Plate Configuration and Explosive System

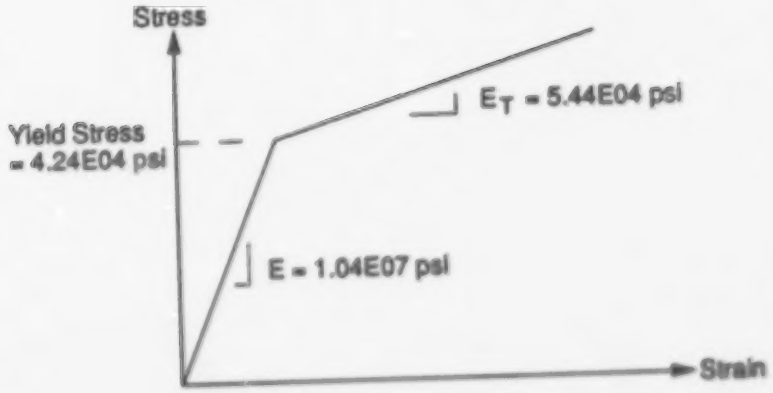

Material: Aluminum 6061-T6
Poisson's Ratio = 0.30
Density = 0.0002508 $\frac{lb \cdot sec^2}{in^4}$

FIGURE 5.5.1

IMPULSIVELY LOADED CIRCULAR PLATE
EXPERIMENTAL TEST RIG AND
MATERIAL PROPERTIES

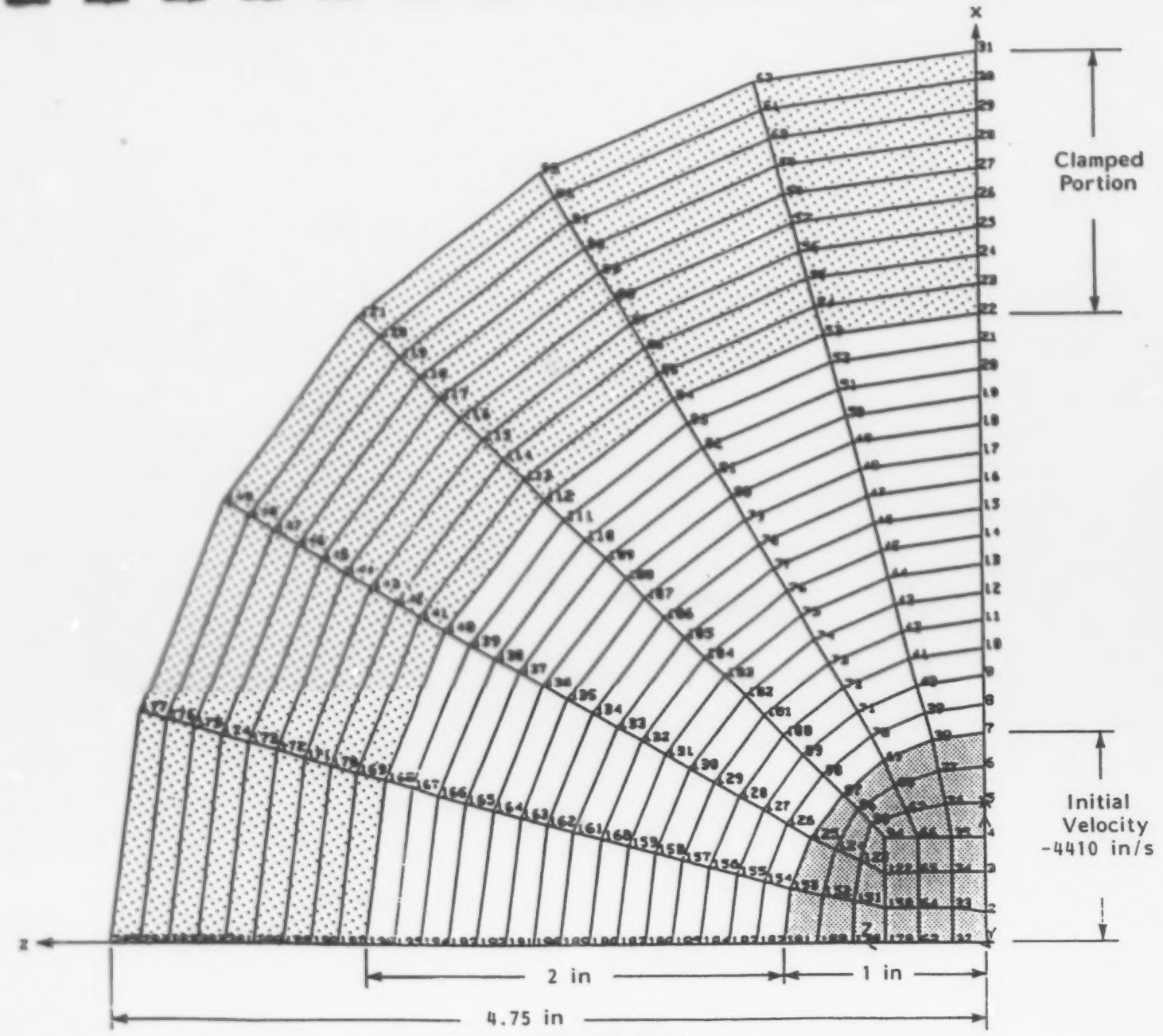

FIGURE 5.5.2
IMPULSIVELY LOADED CIRCULAR PLATE - NODE NUMBERS

89-222
181779-RD

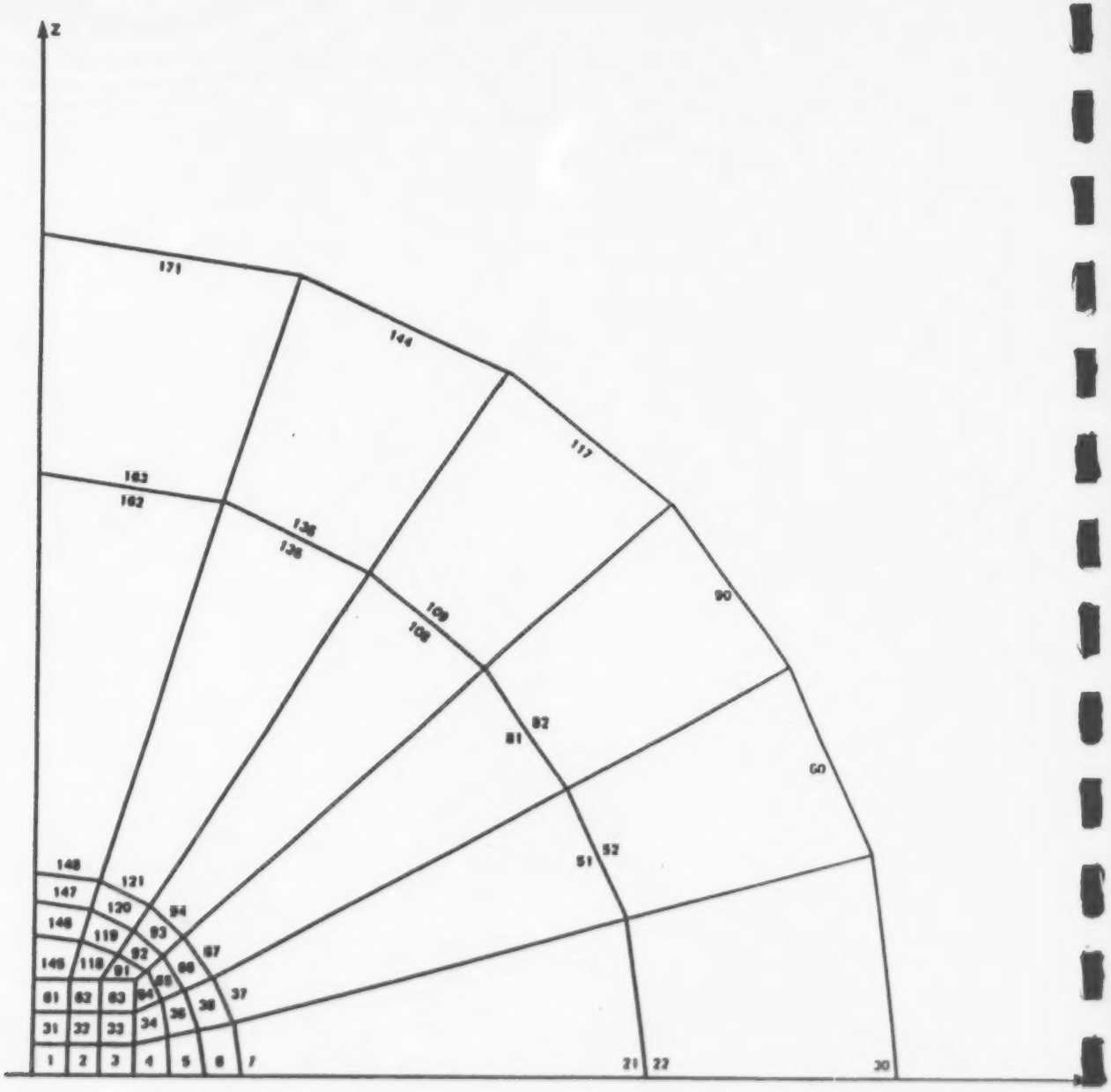

FIGURE 5.5.3

IMPULSIVELY LOADED CIRCULAR PLATE
ELEMENT NUMBERS

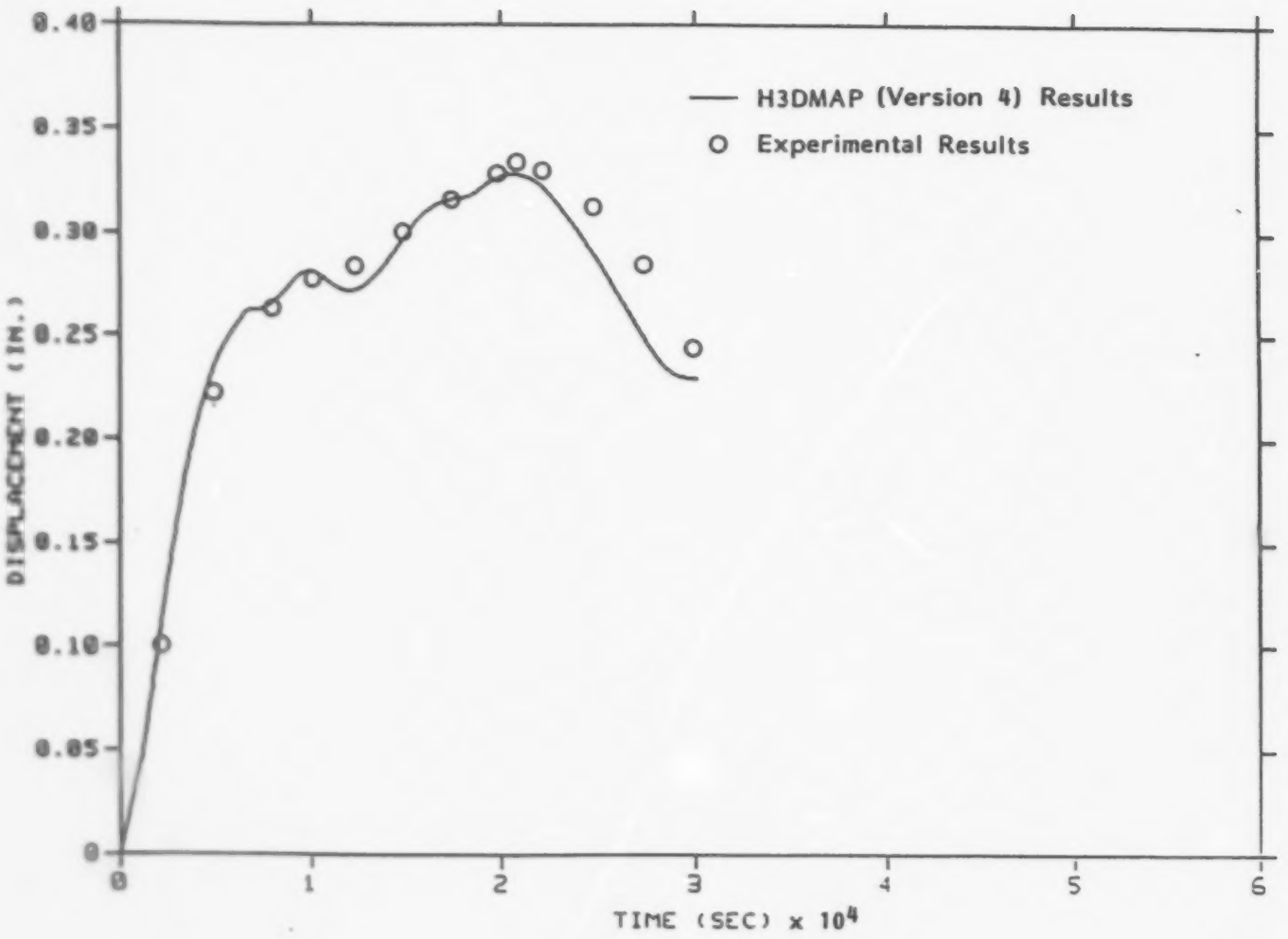

FIGURE 5.5.4

IMPULSIVELY LOADED CIRCULAR PLATE
DISPLACEMENT IN Y-DIRECTION AT NODE 1
COMPARISON OF THEORETICAL AND EXPERIMENTAL RESULTS

CM-192181-MD
09-223

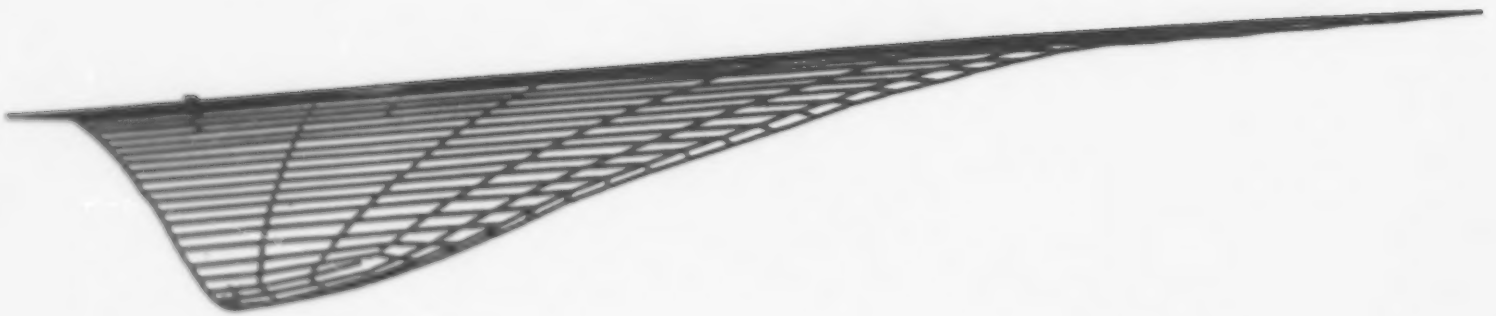

FIGURE 5.5.5

IMPULSIVELY LOADED CIRCULAR PLATE
RESPONSE AT TIME = 0.2 ms

69-222
IBITR3-RD

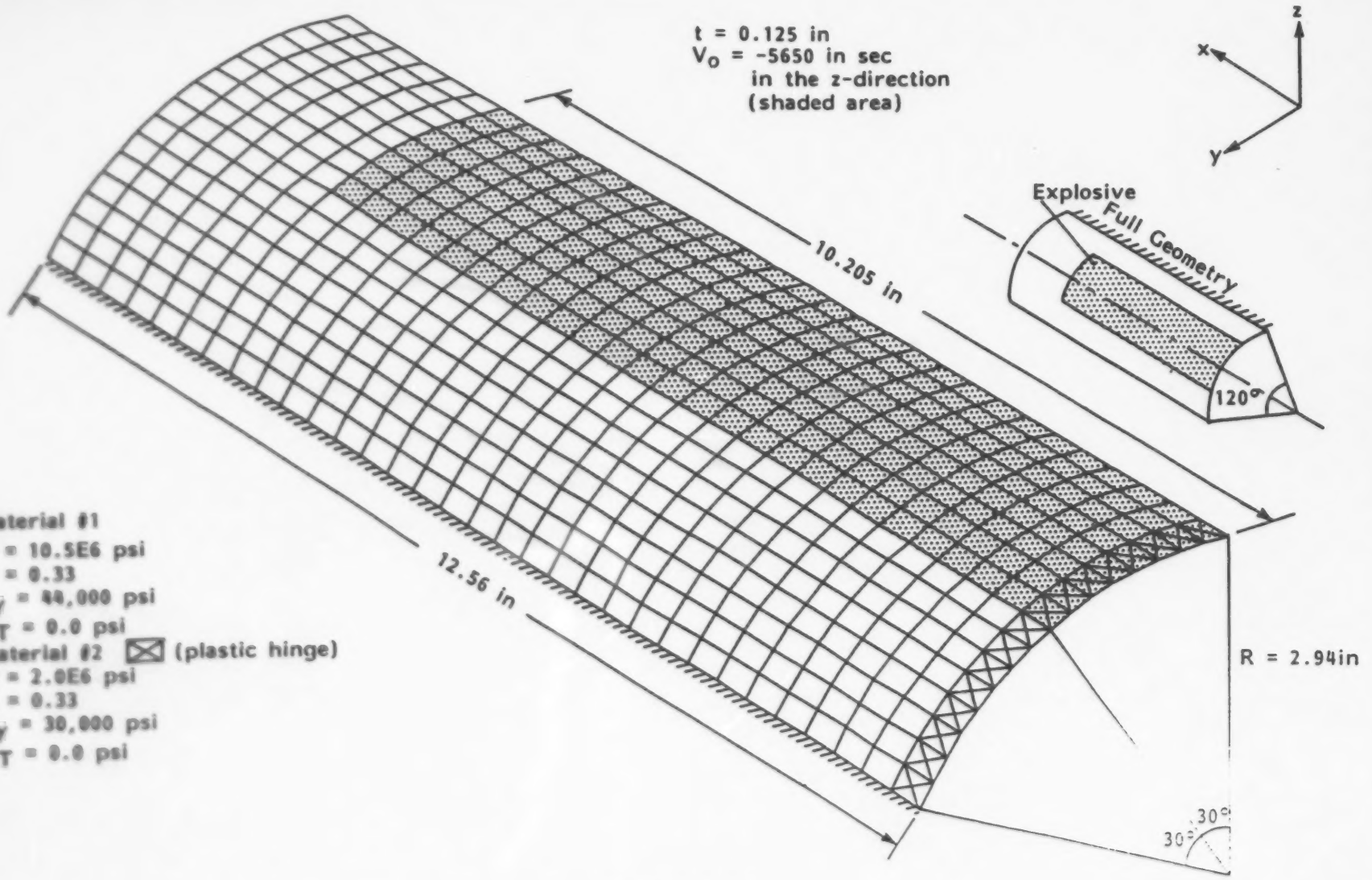

FIGURE 5.6.1

IMPULSIVELY LOADED CYLINDRICAL SHELL
MODEL AND MATERIAL PROPERTIES

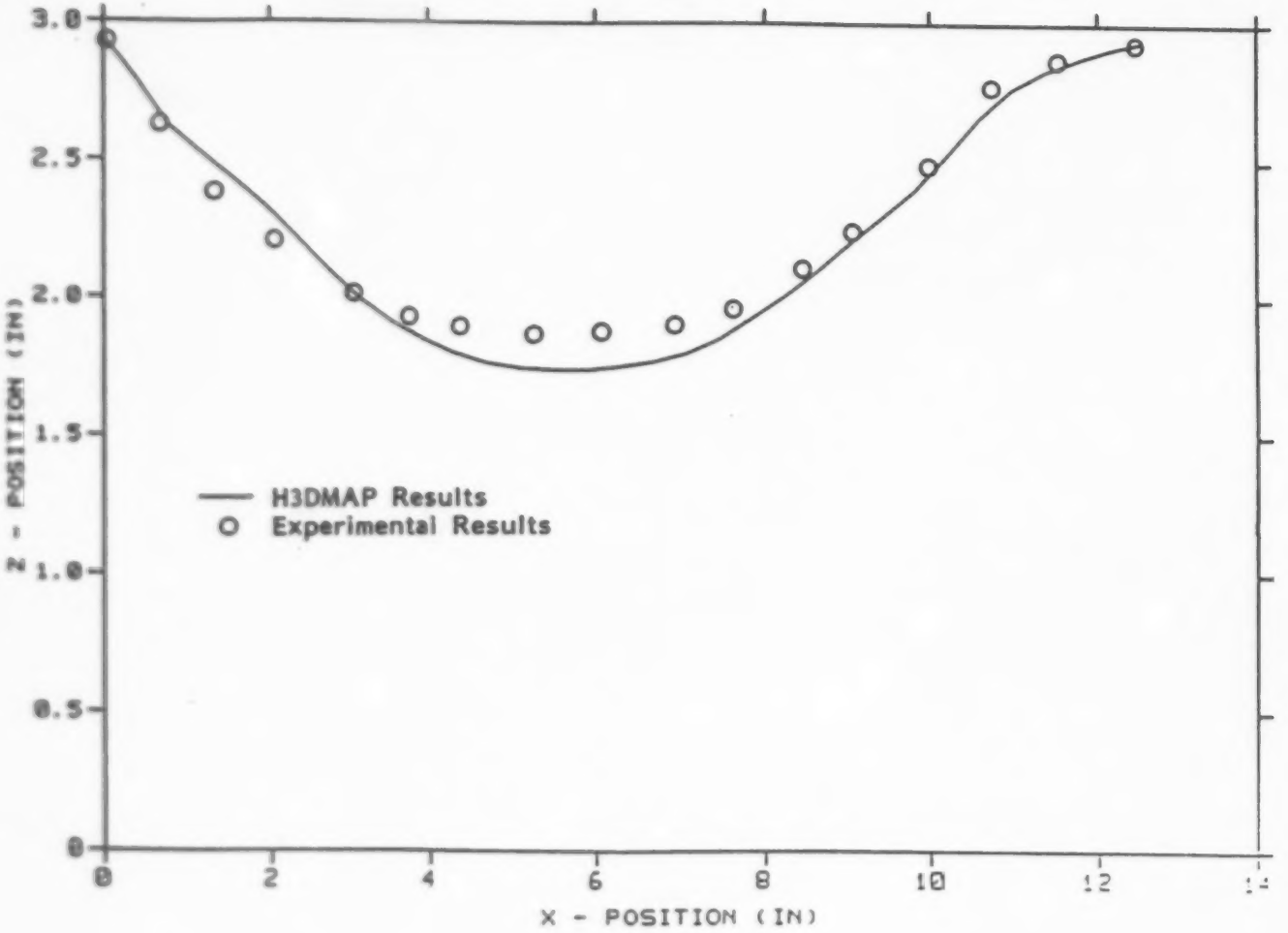

FIGURE 5.6.2

IMPULSIVELY LOADED CYLINDRICAL SHELL
DEFORMED SHAPE OF CROWN LINE

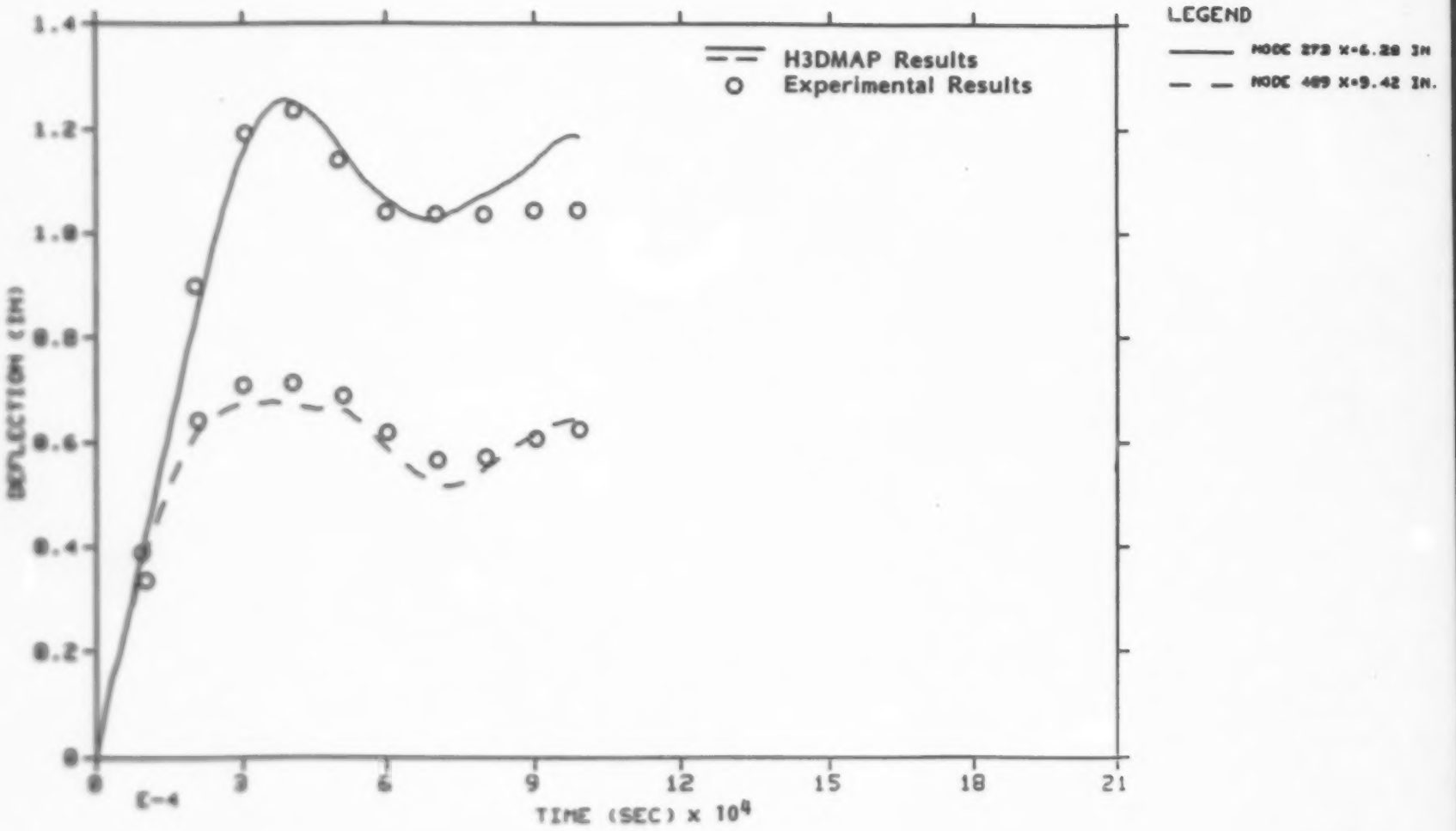

FIGURE 5.6.3

IMPULSIVELY LOADED CYLINDRICAL SHELL
VERTICAL DEFLECTION OF NODE 273 AND 409

FZZ-69
GB-881181

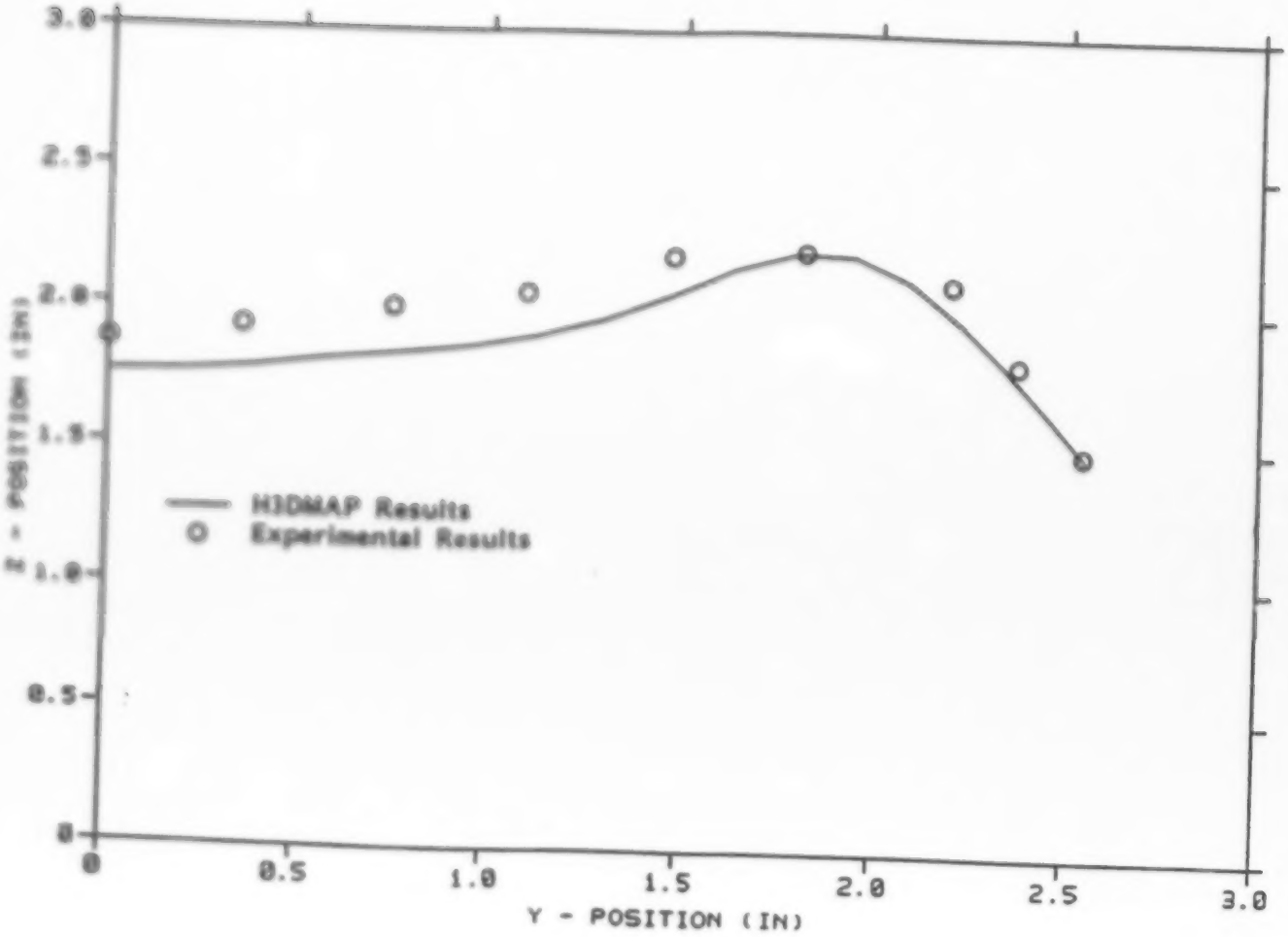

FIGURE 5.6.4
IMPULSIVELY LOADED CYLINDRICAL SHELL
DEFORMED SHAPE AT X = 6.28

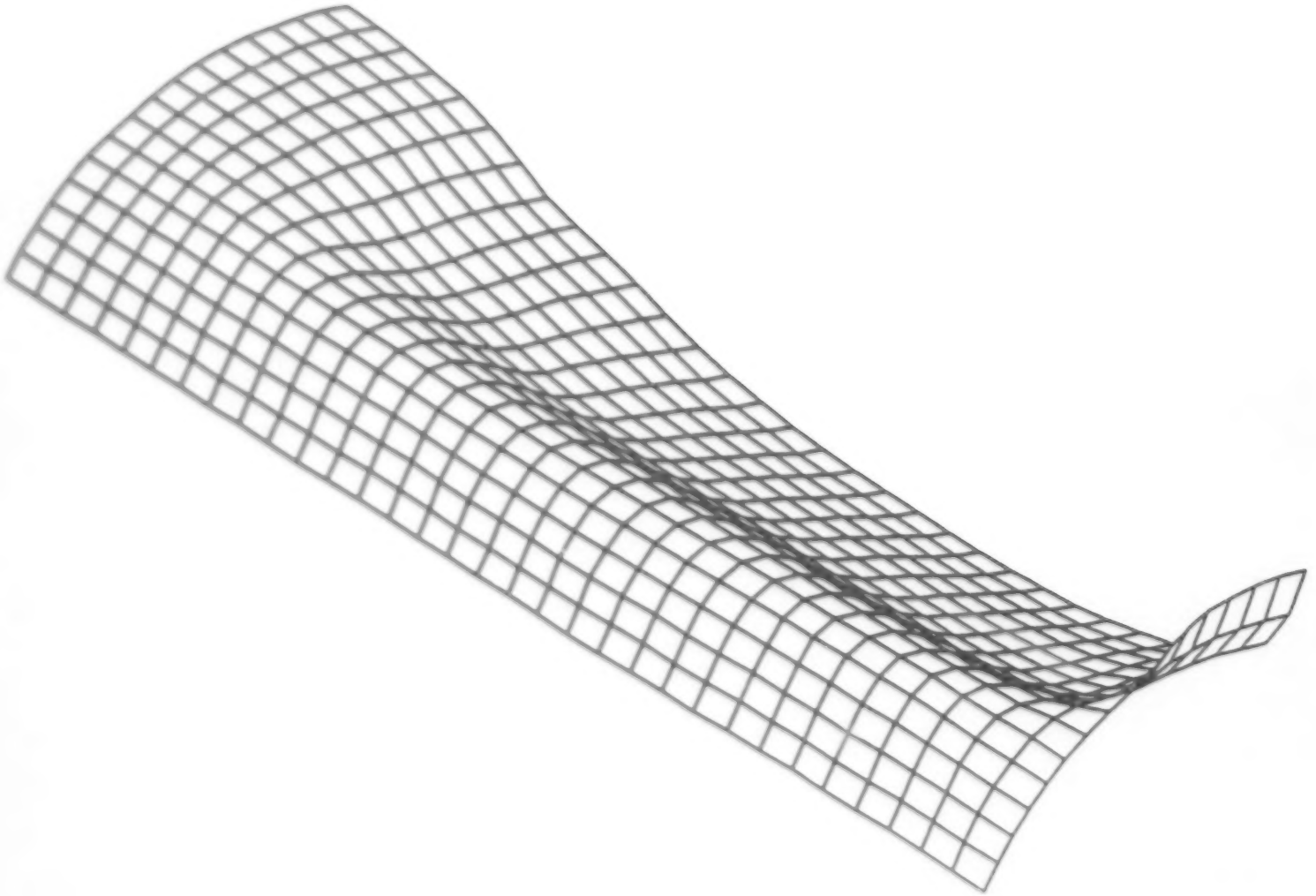

FIGURE 5.6.5

IMPULSIVELY LOADED CYLINDRICAL SHELL
RESPONSE AT TIME = 0.8 ms

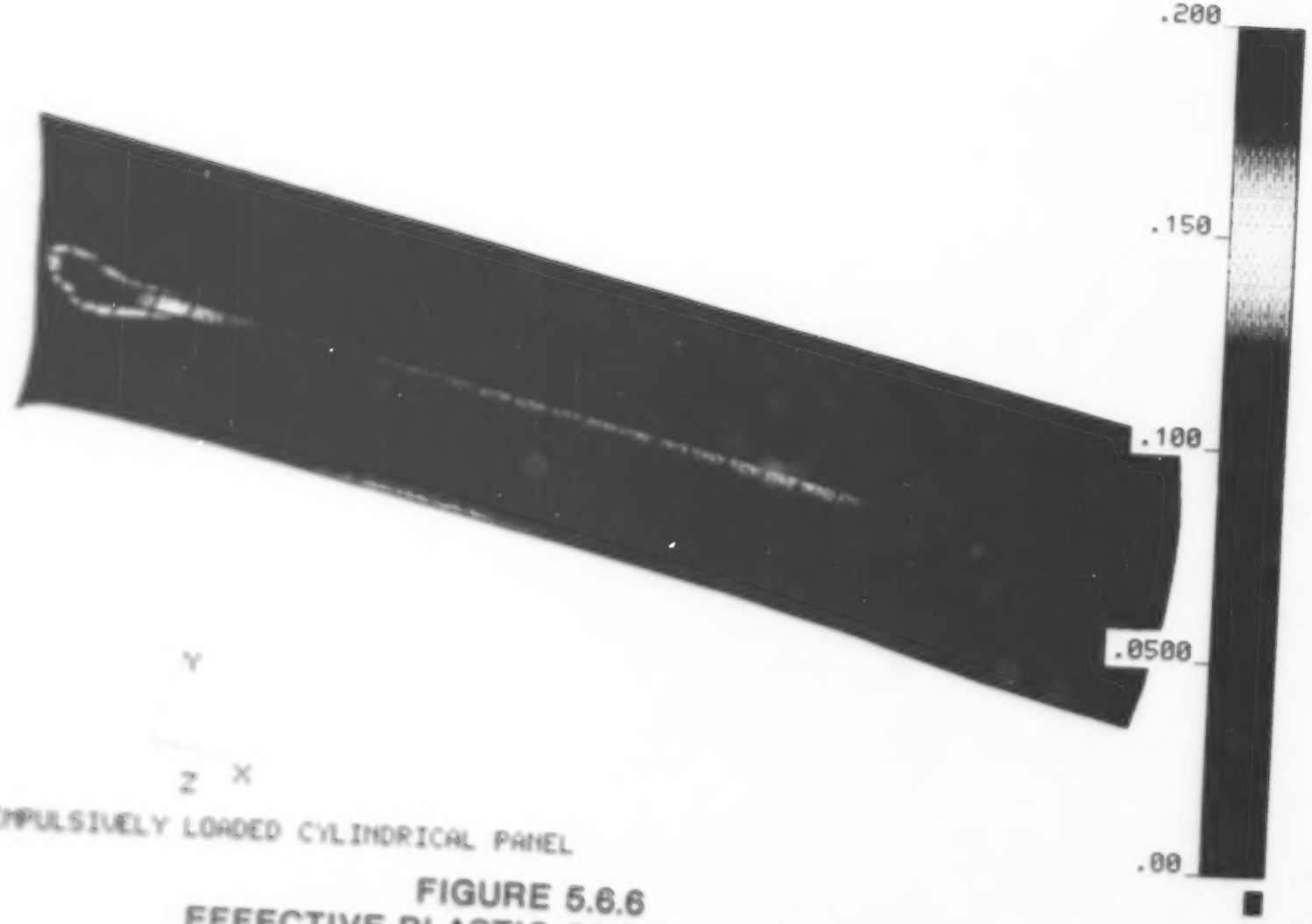

FIGURE 5.6.6
EFFECTIVE PLASTIC STRAIN - VIEW A

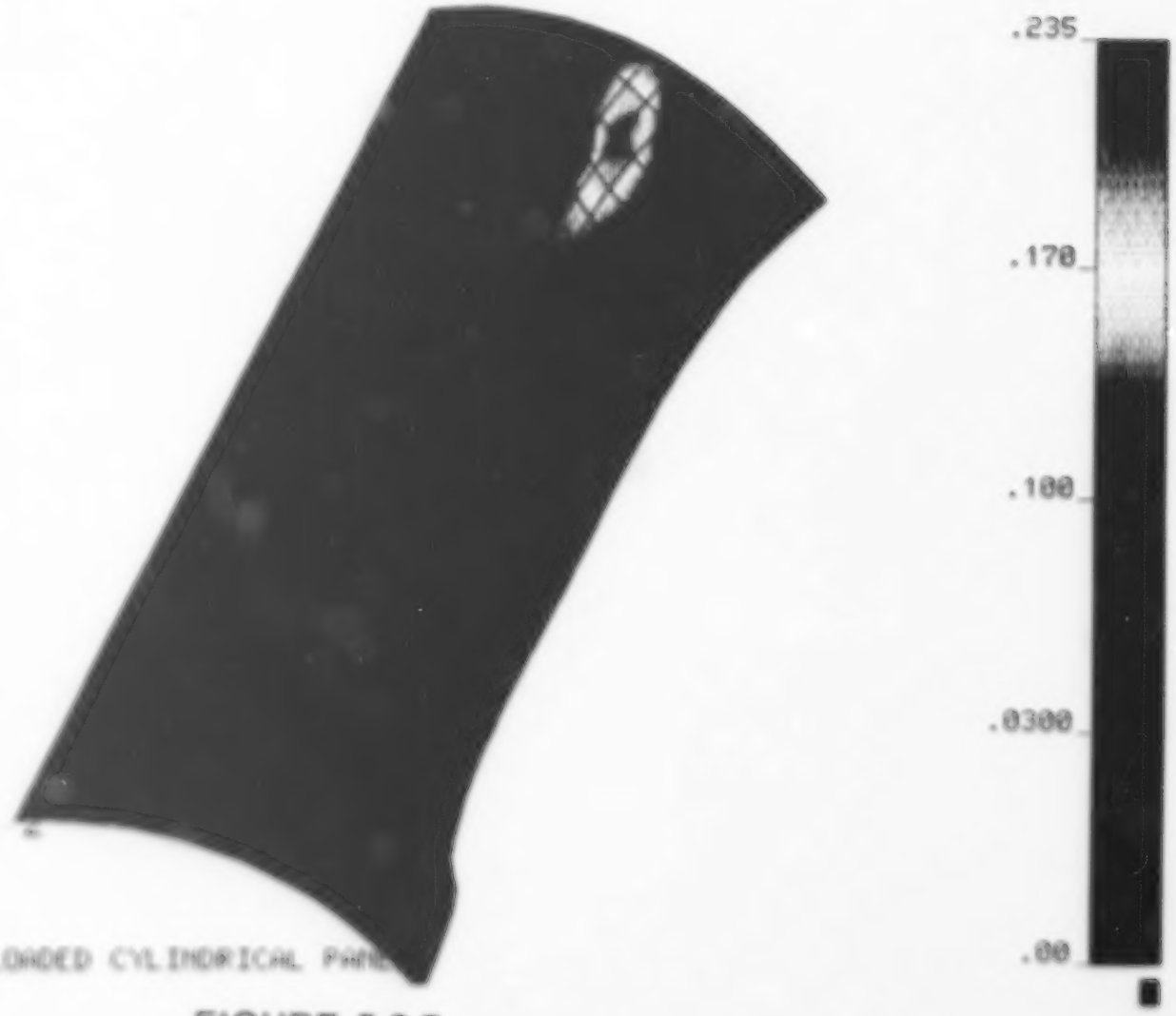

FIGURE 5.6.7
EFFECTIVE PLASTIC STRAIN - VIEW B

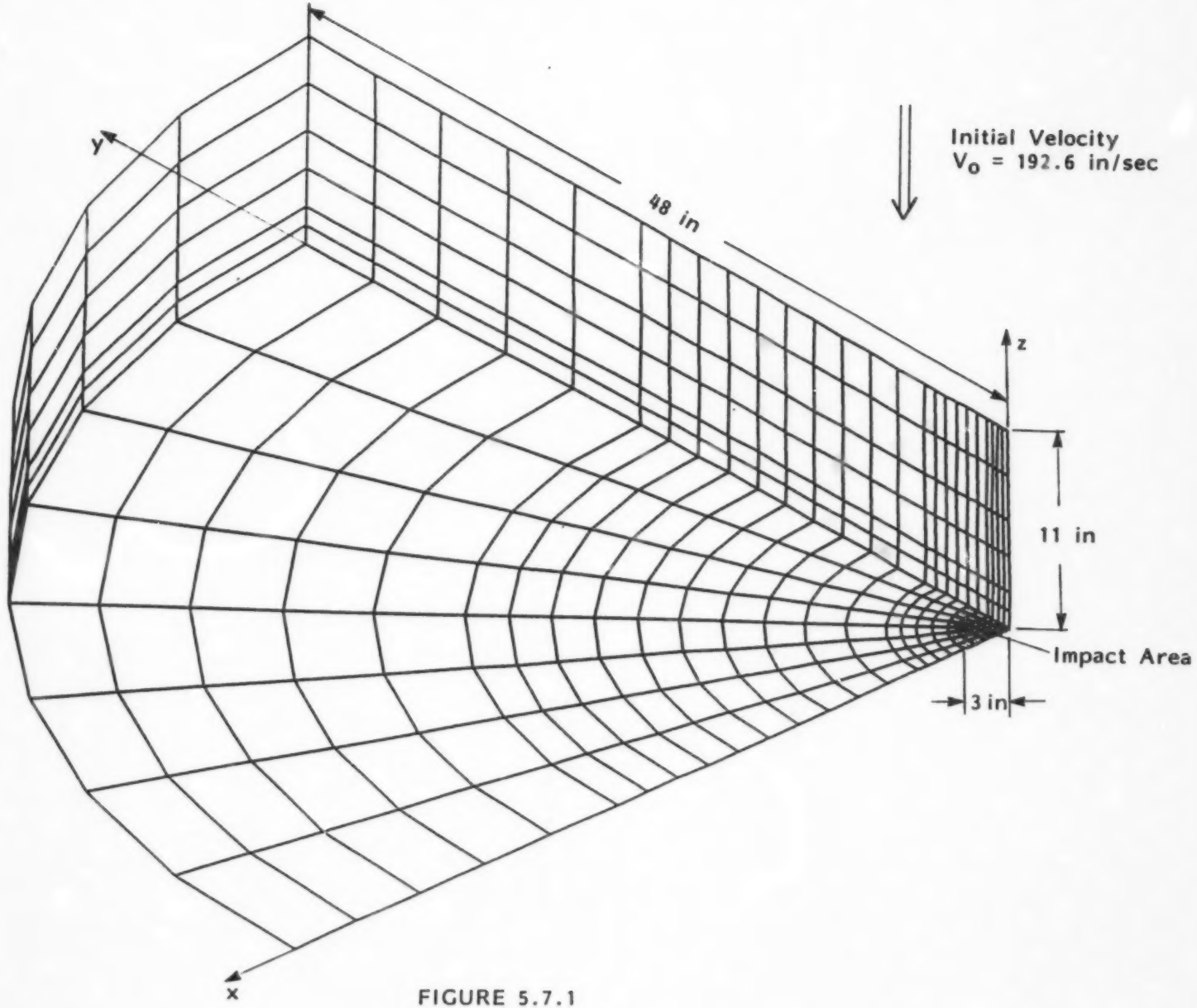

FIGURE 5.7.1
PUNCH VERIFICATION TEST

89-222
181788-RD

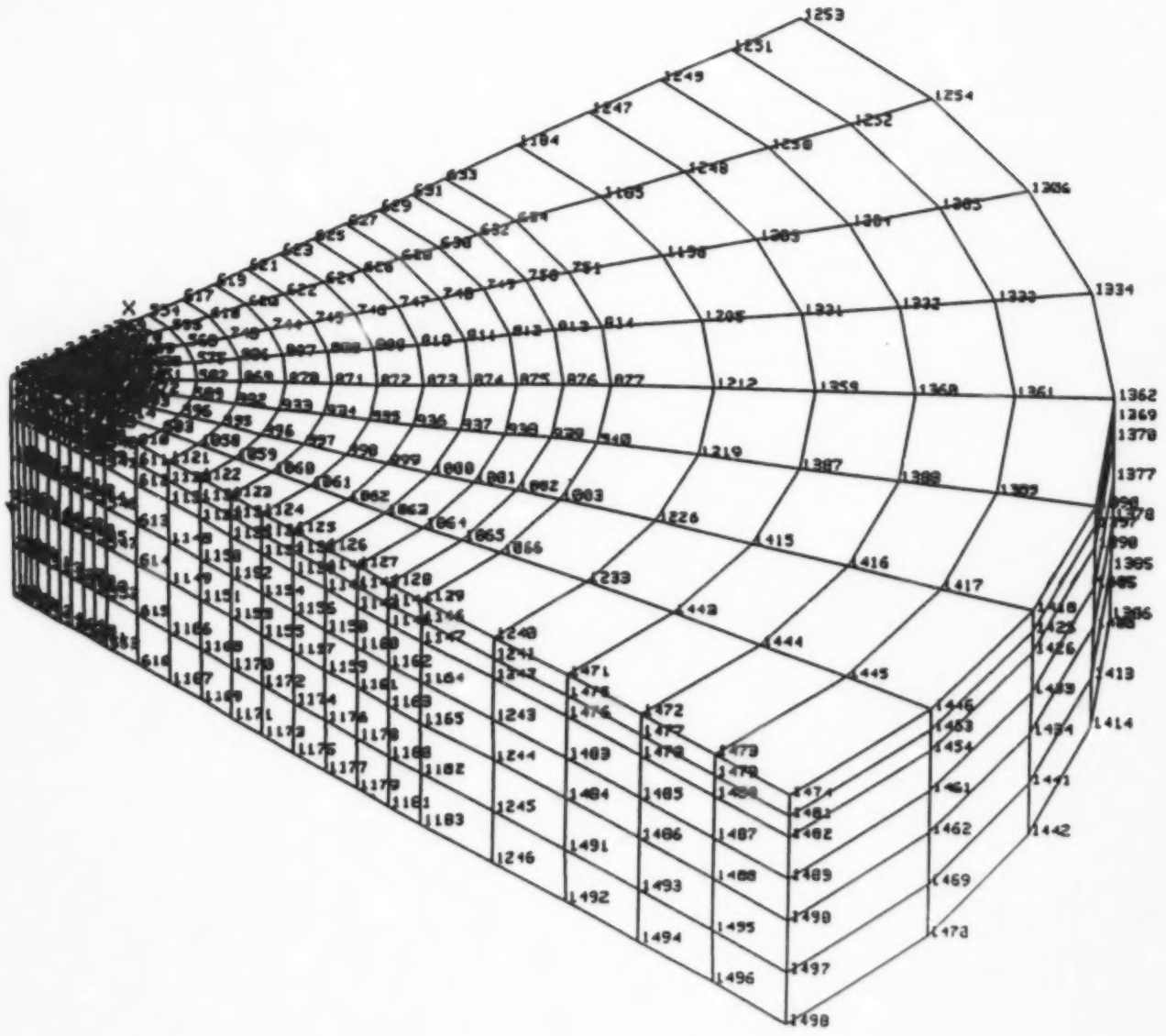

FIGURE 5.7.2

PUNCH VERIFICATION TEST
NODE NUMBERING

89-222
181789-RD

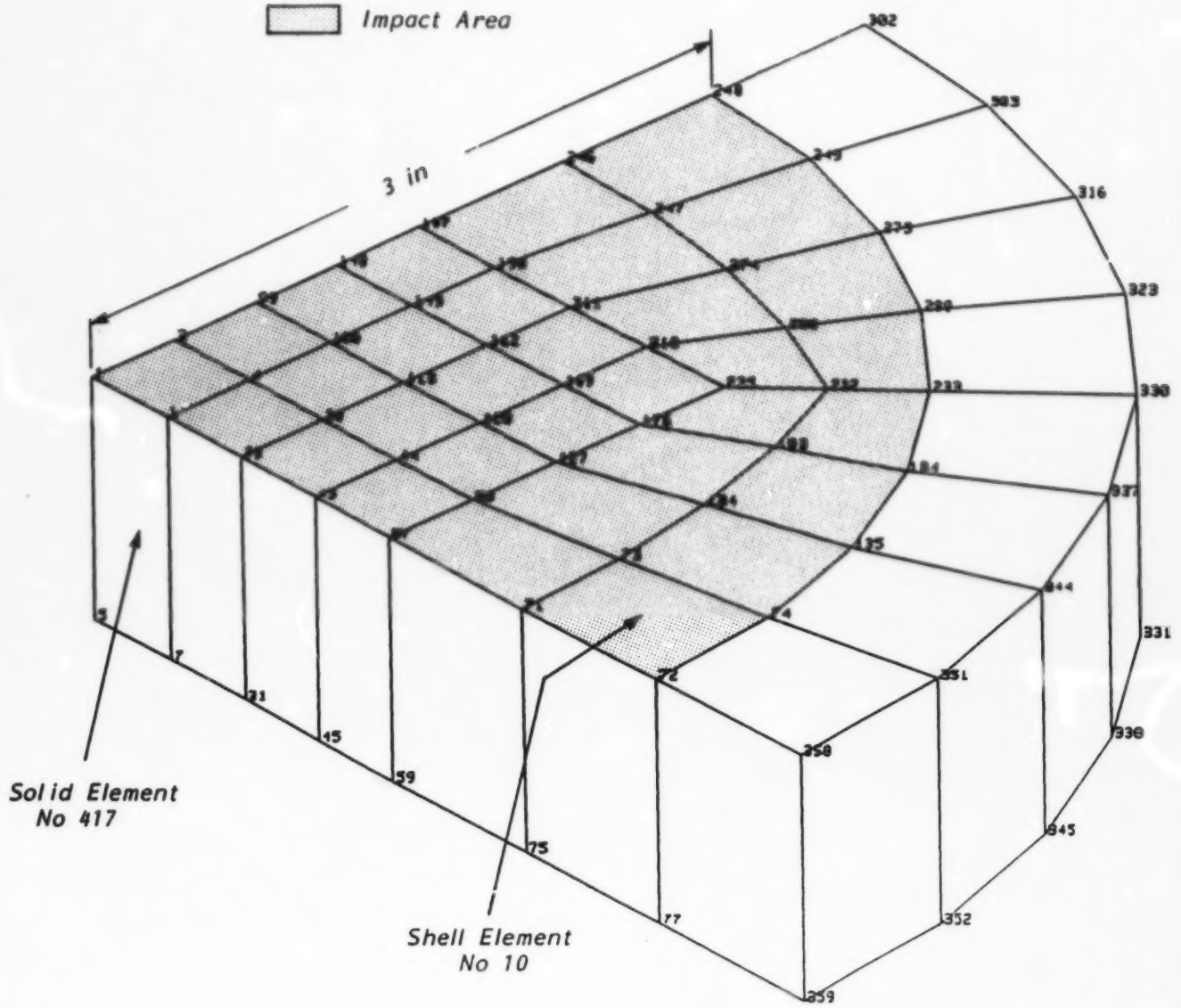

FIGURE 5.7.3

PUNCH VERIFICATION TEST
NODE NUMBERING - CLOSE-UP OF IMPACT AREA

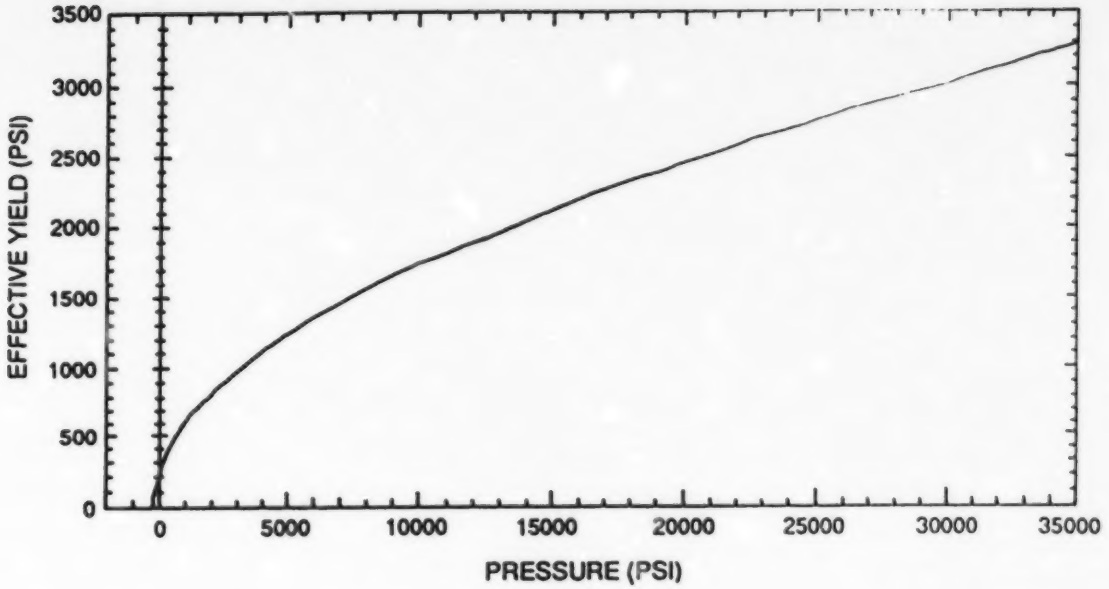

FIGURE 5.7.4

YIELD VS PRESSURE CURVE FOR
POLYURETHANE FOAM MODEL

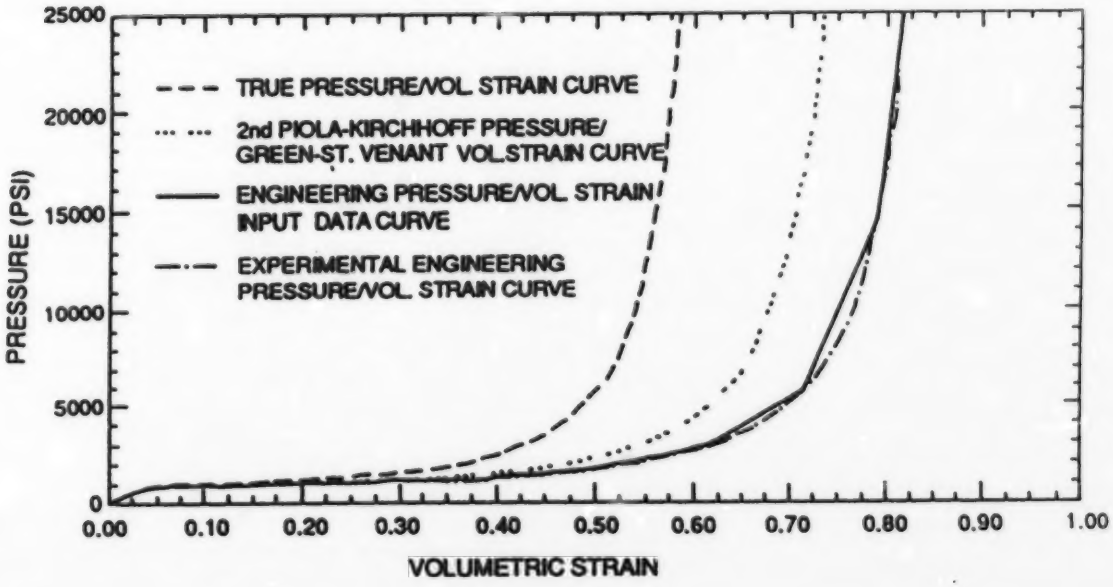

FIGURE 5.7.5

PRESSURE/VOLUMETRIC STRAIN CURVE FOR
POLYURETHANE FOAM MODEL

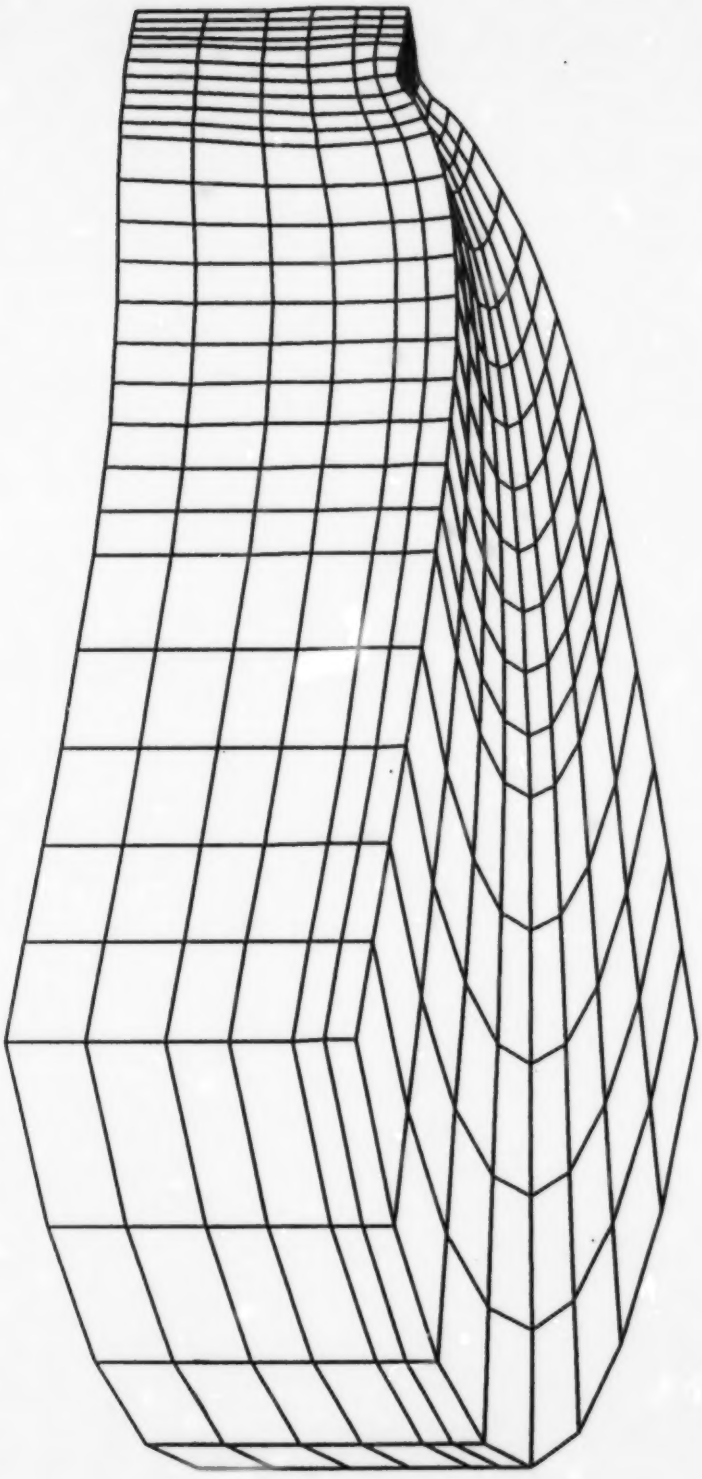

FIGURE 5.7.6
PUNCH VERIFICATION TEST
DEFORMED GEOMETRY - RESPONSE AT TIME = 0.028 SECOND

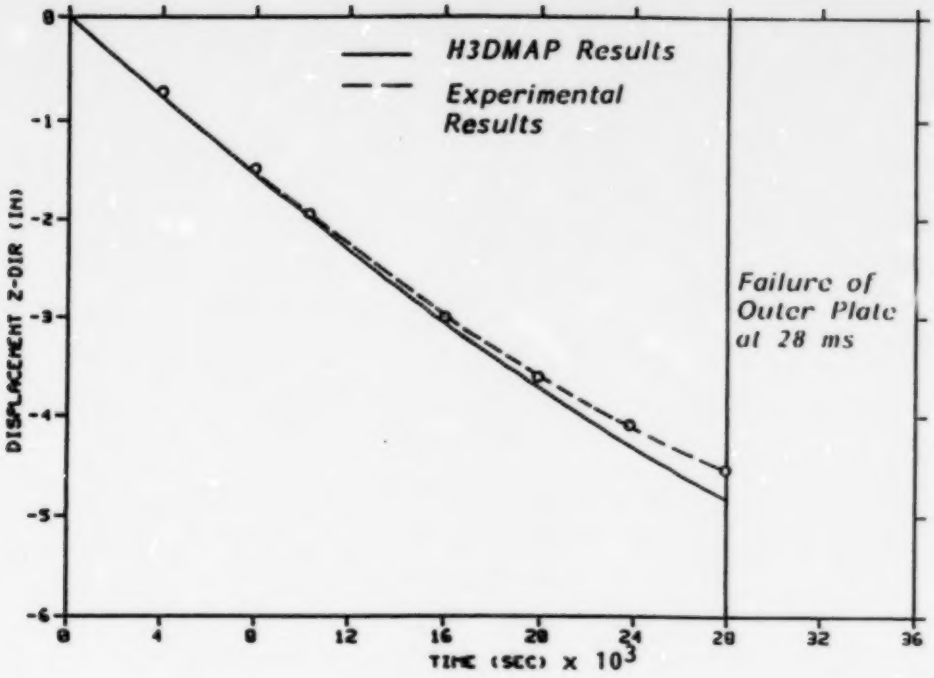

FIGURE 5.7.7

PUNCH VERIFICATION TEST
VERTICAL DISPLACEMENT AT THE PERIPHERY (NODE 1474)

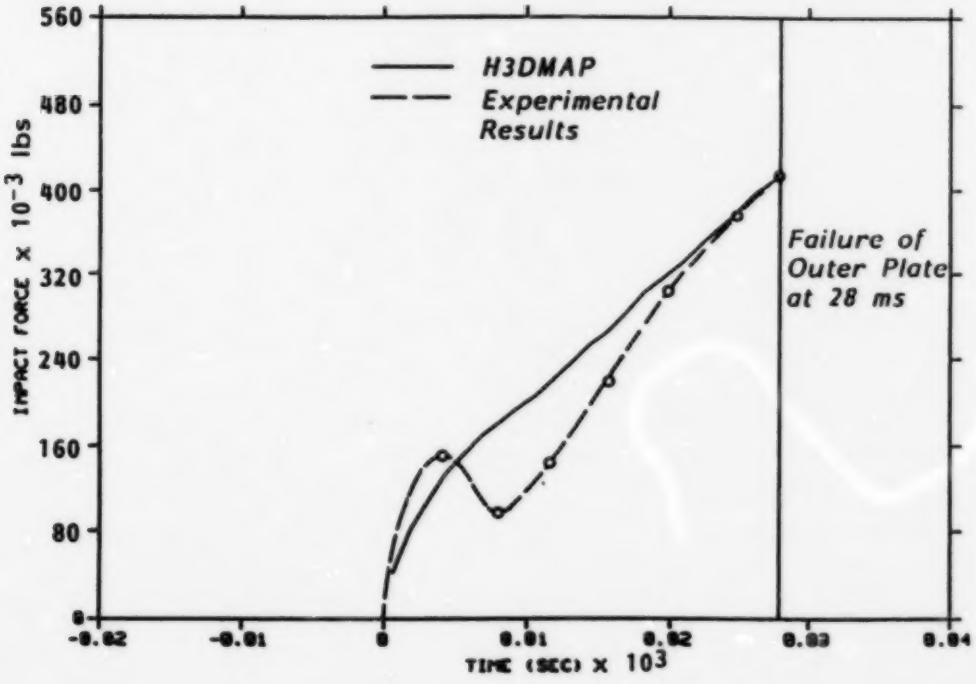

FIGURE 5.7.8

PUNCH VERIFICATION TEST
IMPACT FORCE TIME HISTORY

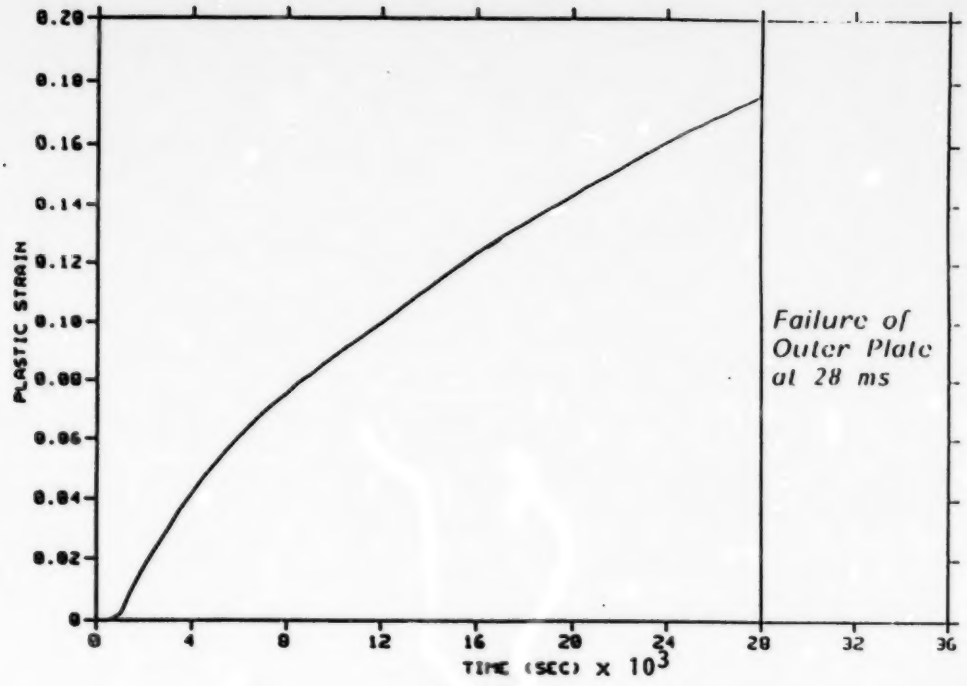

FIGURE 5.7.9

PLASTIC STRAIN IN SHELL ELEMENT
NO 10 SAMPLING PT NO. 3

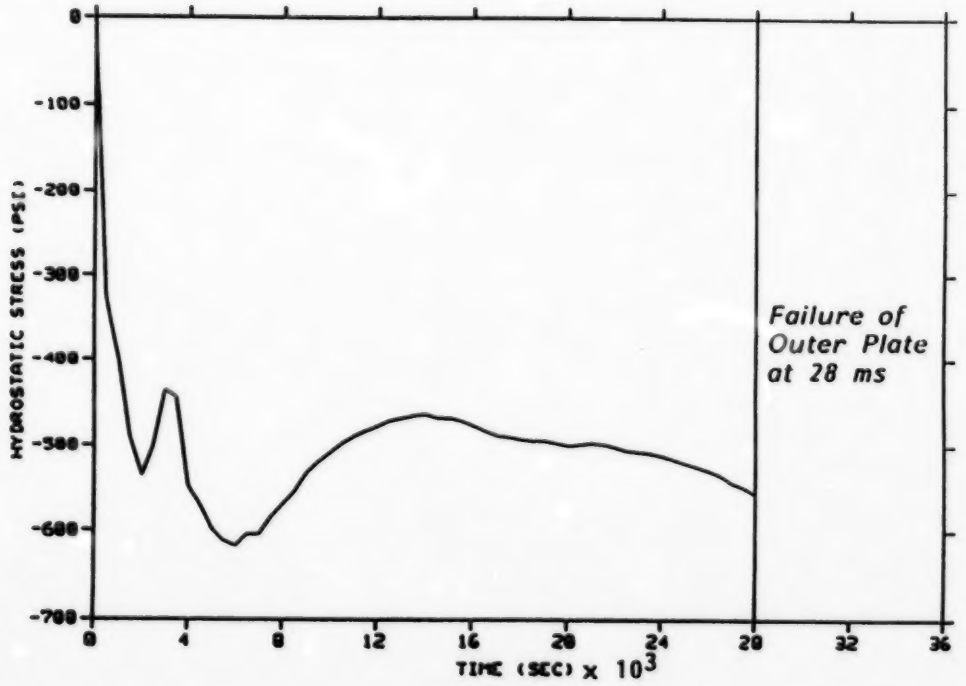

FIGURE 5.7.10

HYDROSTATIC STRESS IN SOLID ELEMENT NO 417

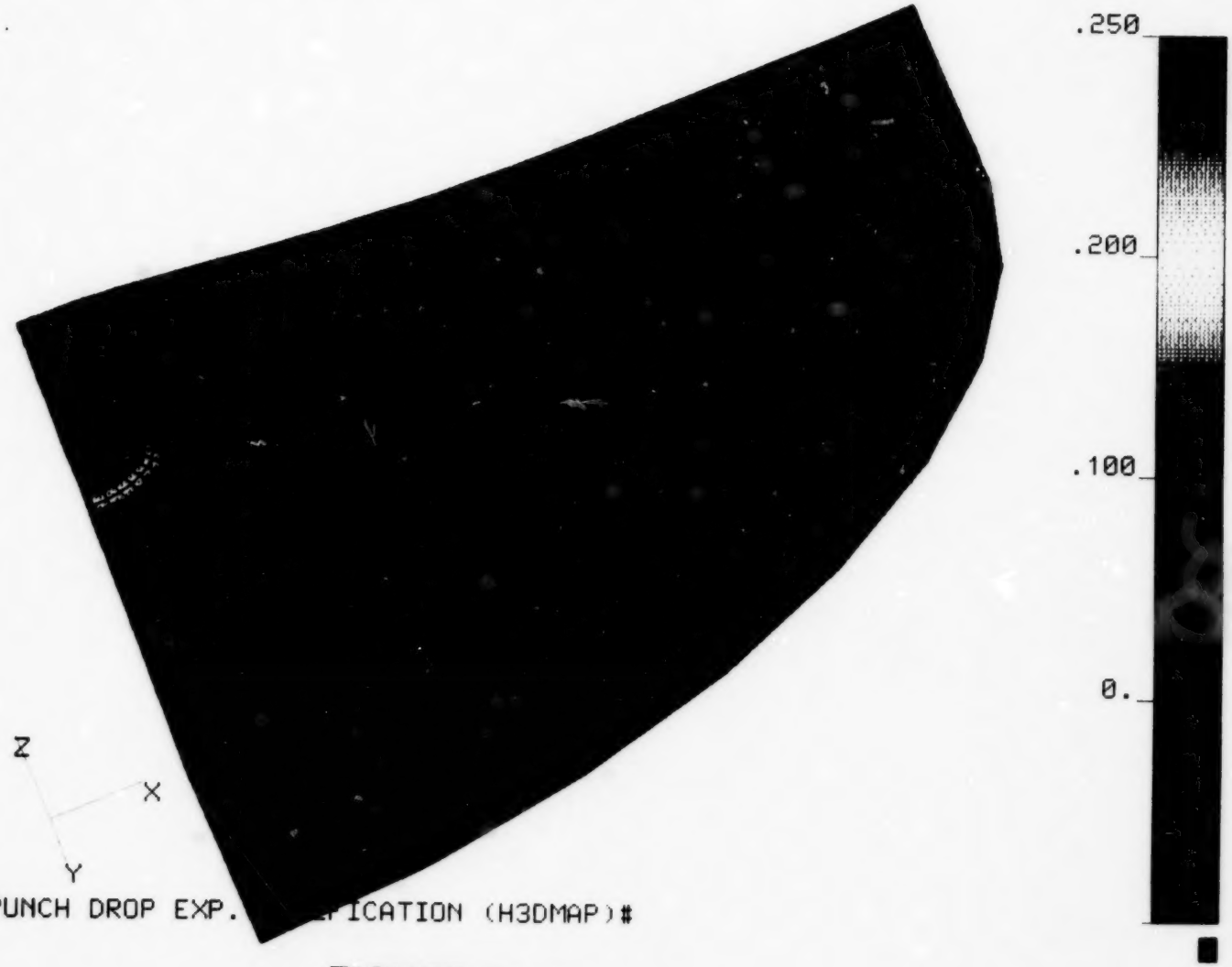

FIGURE 5.7.11
PLASTIC STRAIN IN METAL SHEET
OUTER SHELL - TIME: 28 ms

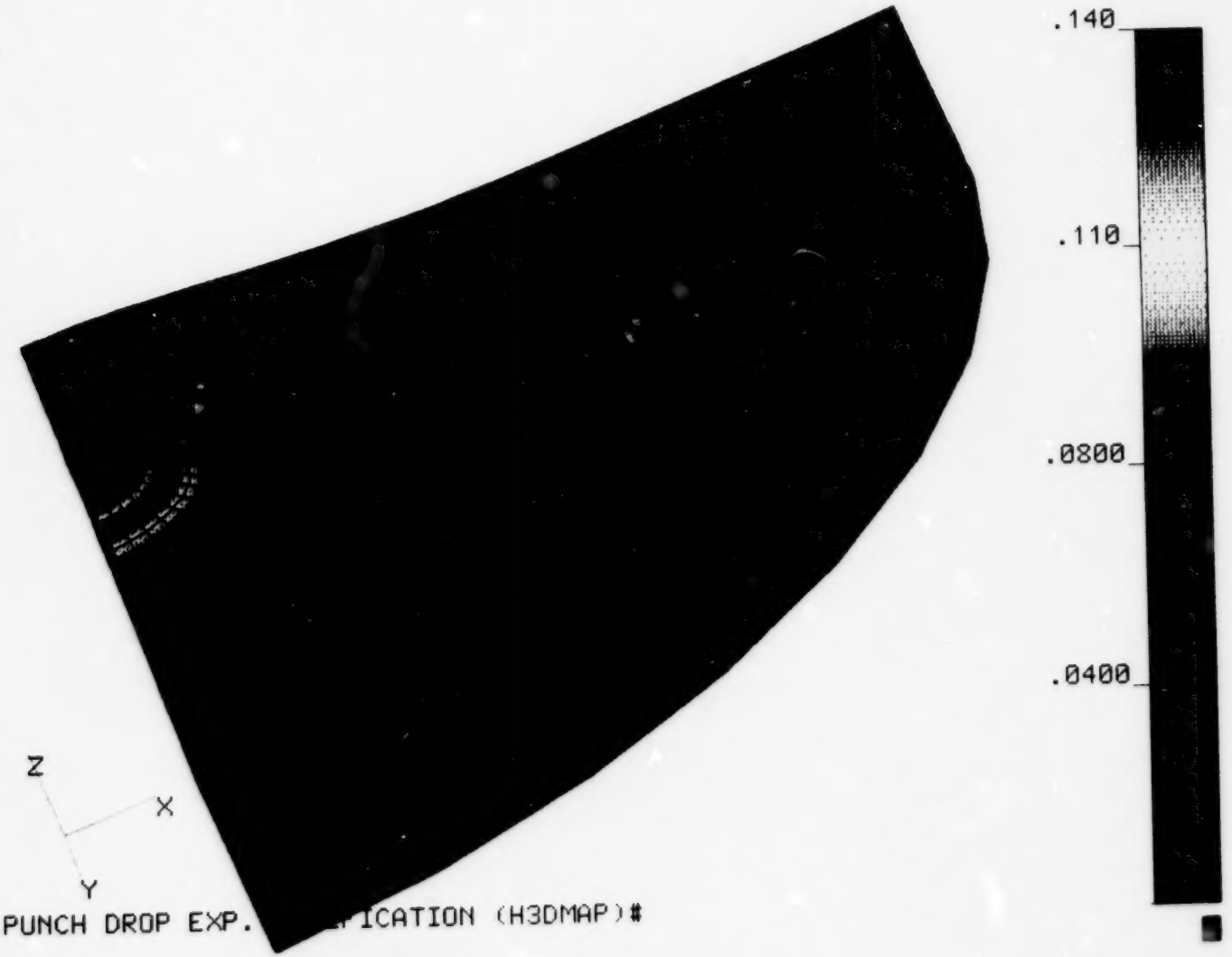

FIGURE 5.7.12
PLASTIC STRAIN IN METAL SHEET
INNER SHELL - TIME: 28 ms

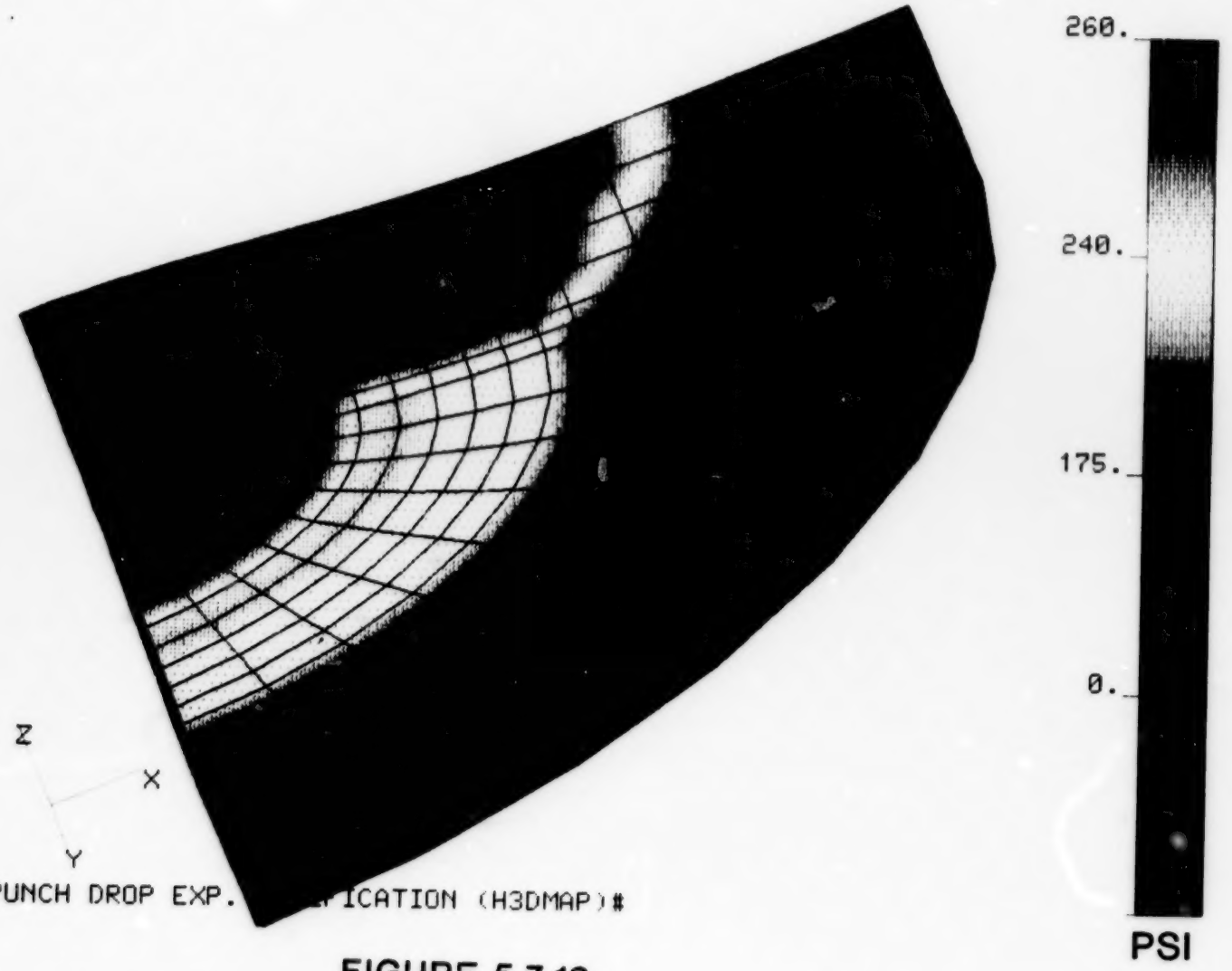

FIGURE 5.7.13
VON MISES STRESS IN FOAM AT TIME: 28 ms

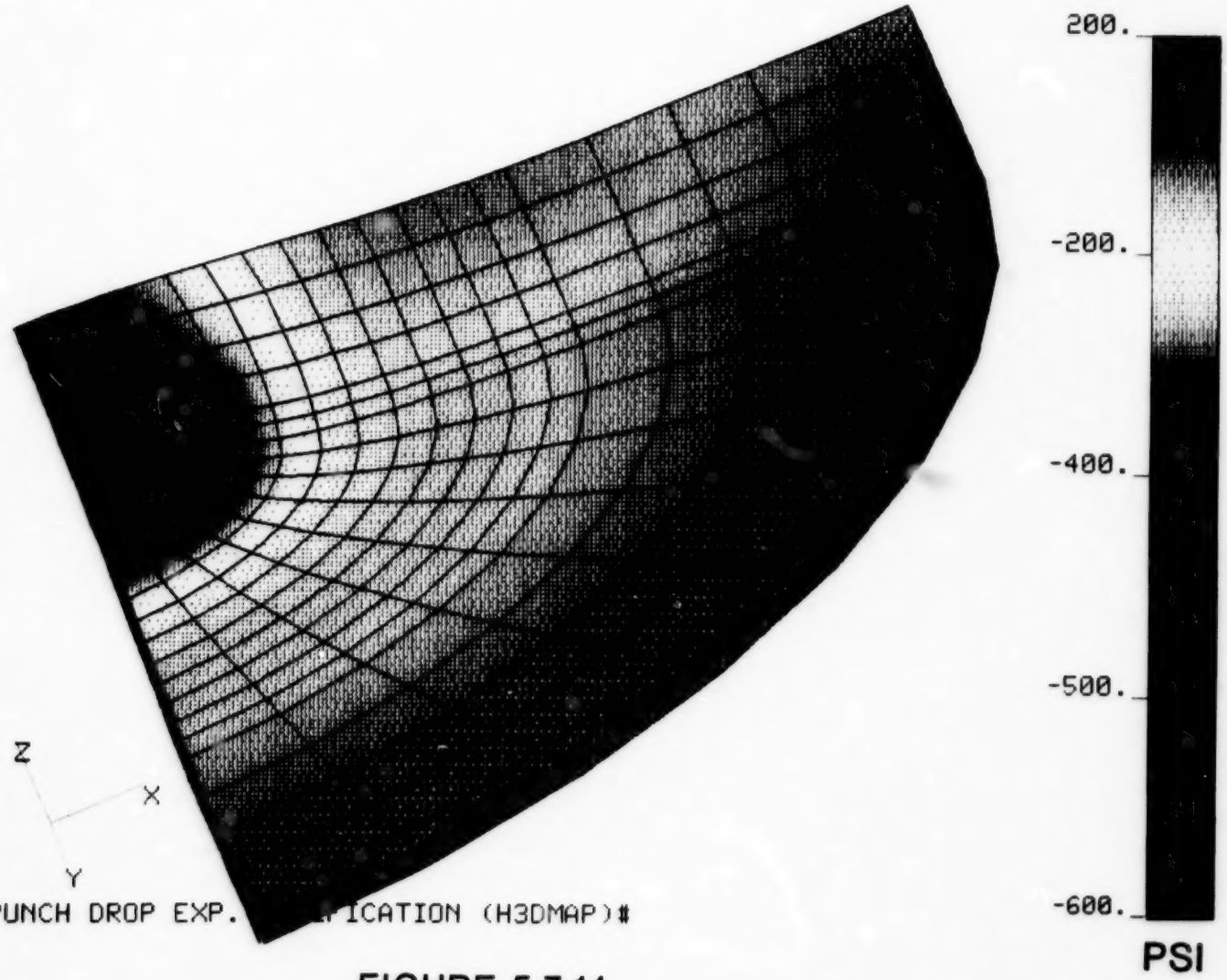

FIGURE 5.7.14
HYDROSTATIC STRESS IN FOAM AT TIME: 28 ms

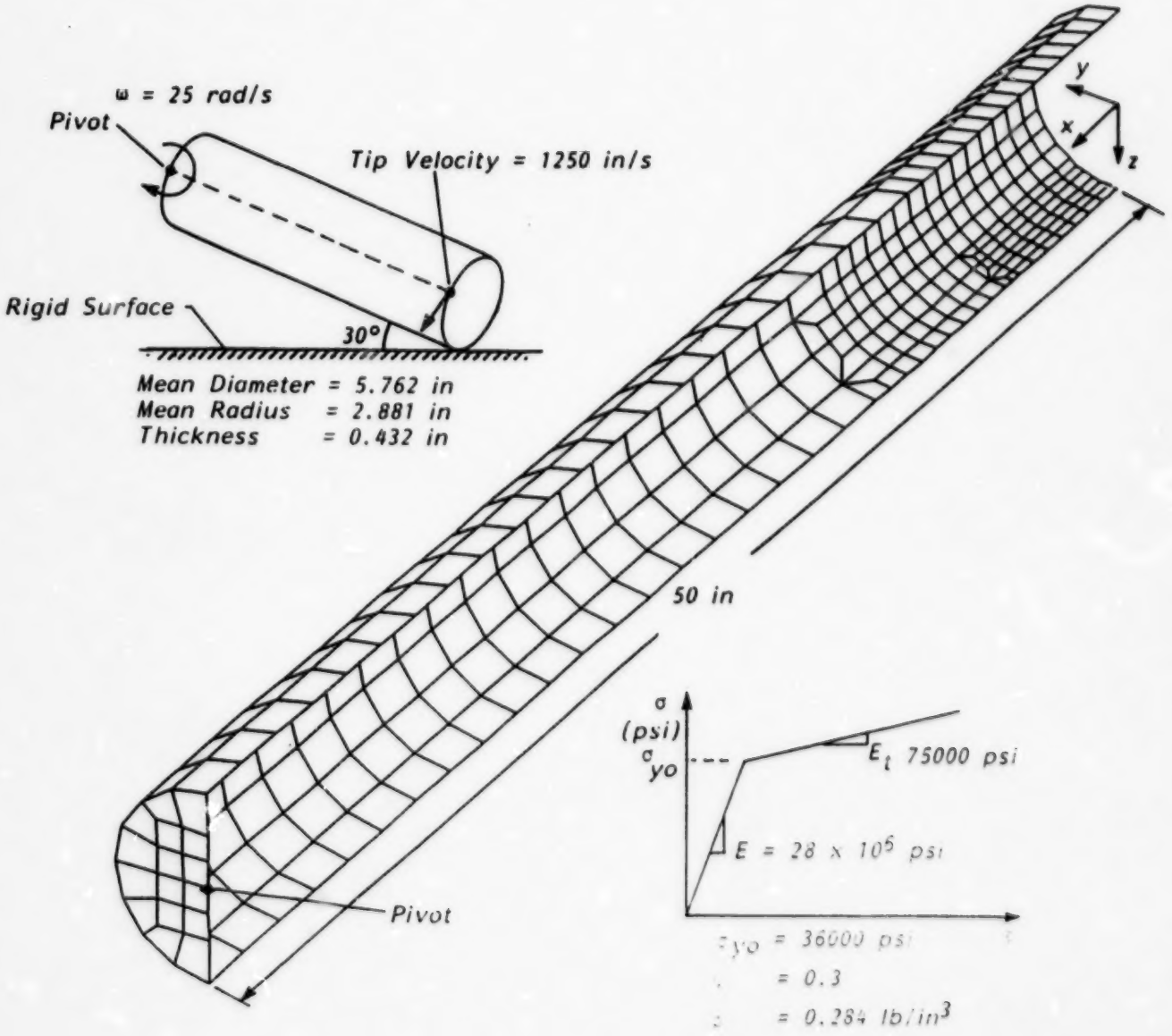

FIGURE 5.8.1

PIPE WHIP TEST - MODEL AND MATERIAL PROPERTIES

89-222
181794-RD

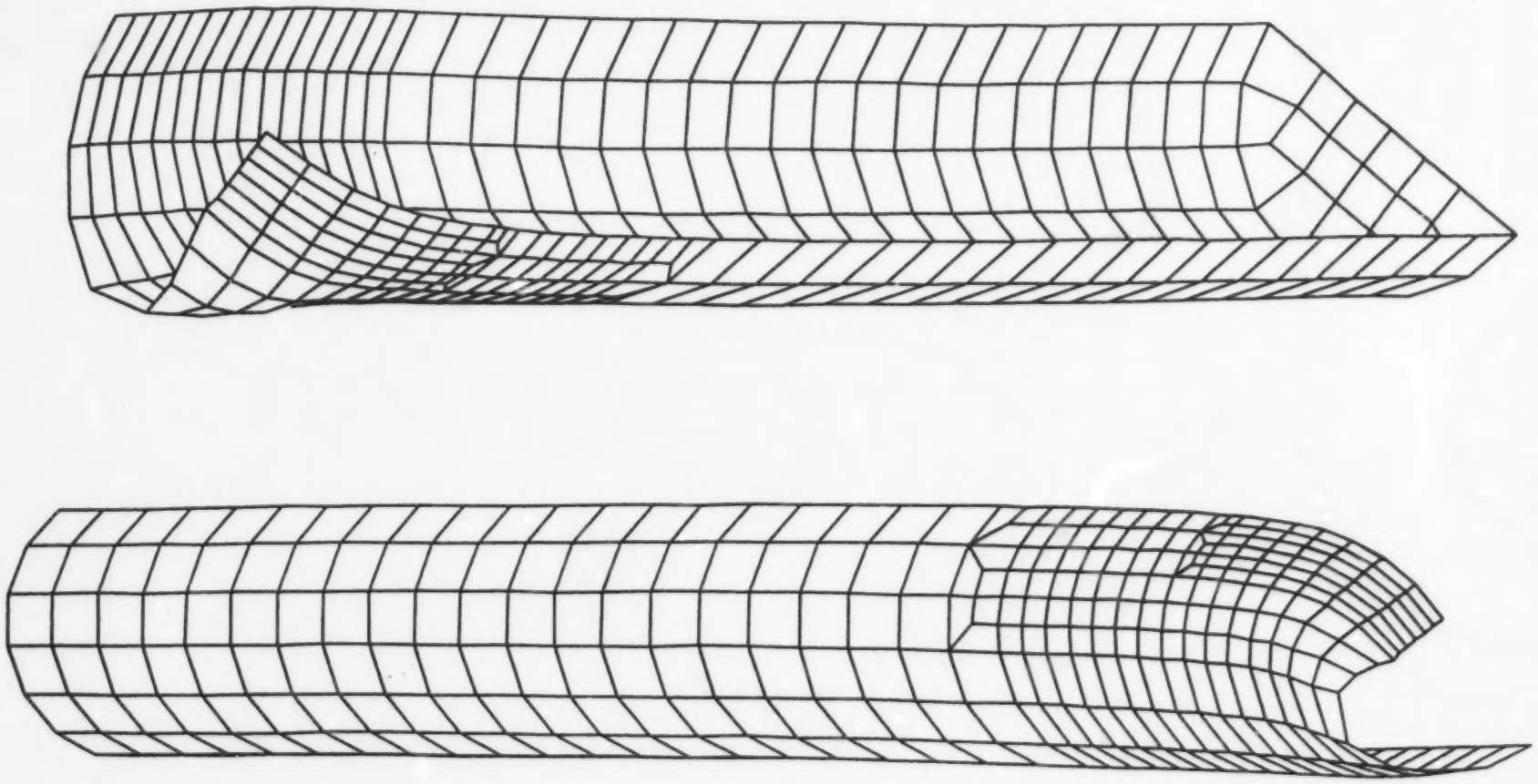

FIGURE 5.8.2

PIPE WHIP TEST
DEFORMED STRUCTURE - RESPONSE AT TIME 0.0035 SECOND

181795-RD
89-222

FIGURE 5.8.3
EFFECTIVE PLASTIC STRAIN - OUTER SHELL
TIME: 3.5 ms

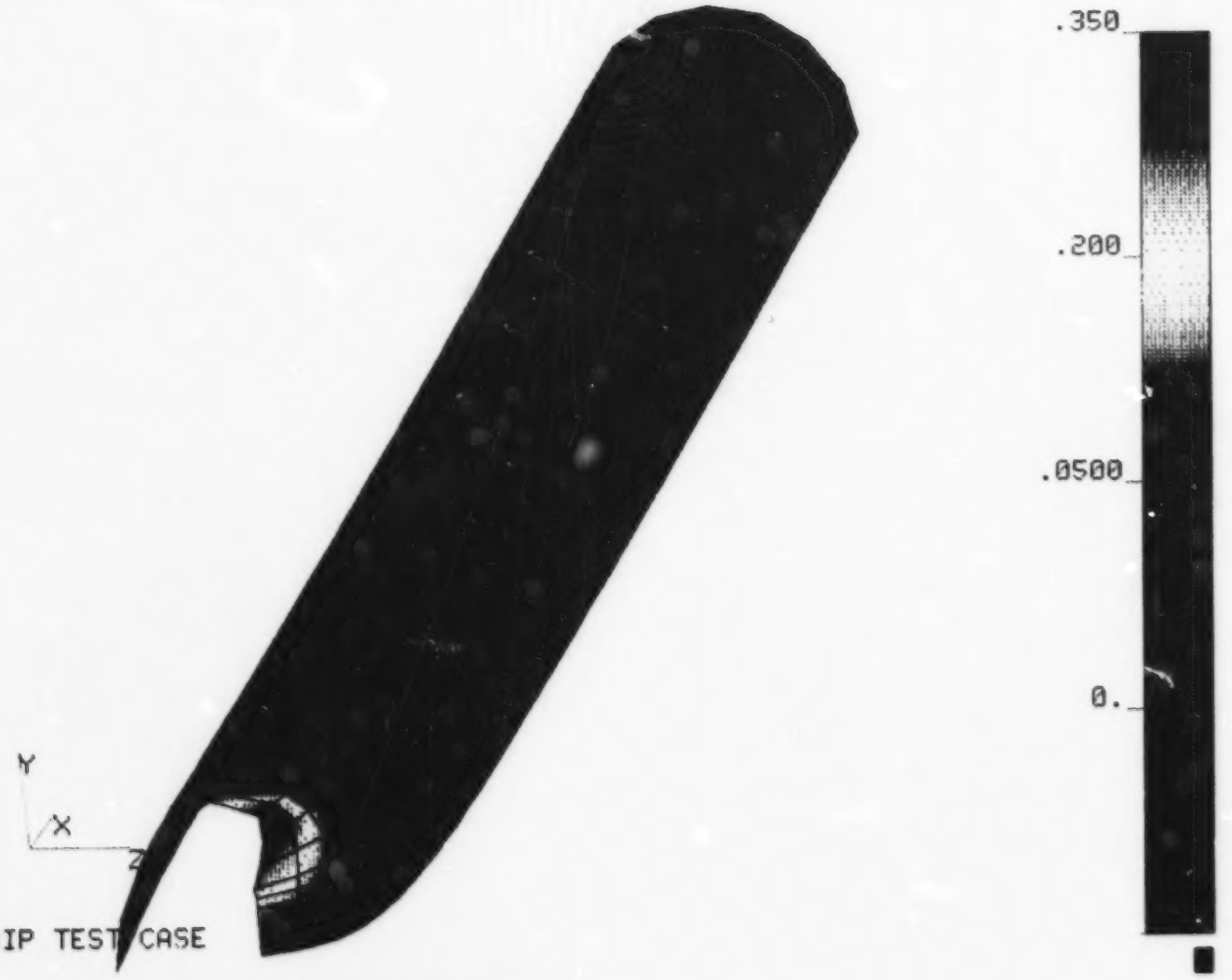

FIGURE 5.8.4
EFFECTIVE PLASTIC STRAIN - INNER SHELL
TIME: 3.5 ms

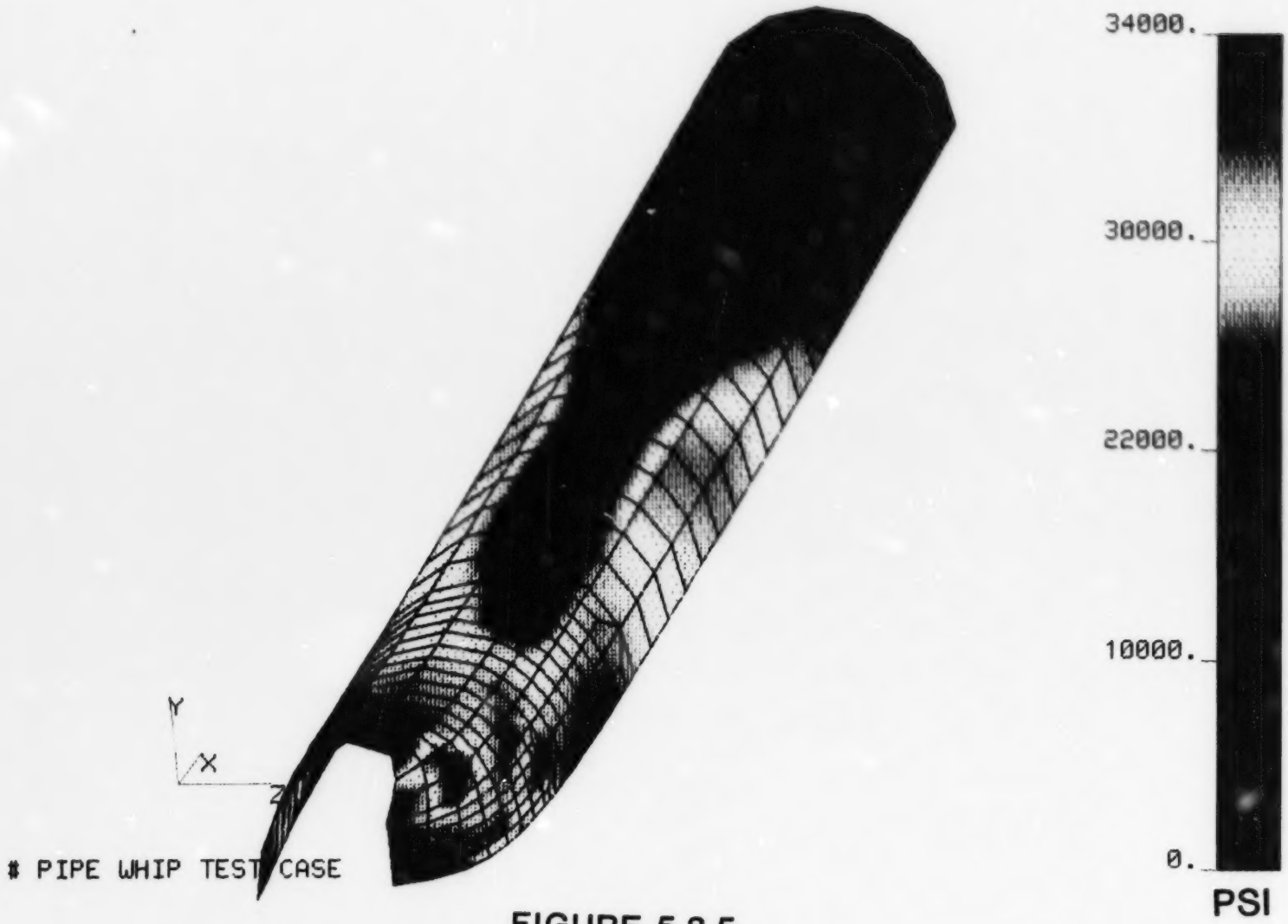

FIGURE 5.8.5
VON MISES STRESS - OUTER SHELL - TIME: 3.5 ms

FIGURE 5.8.6
VON MISES STRESS - INNER SHELL - TIME: 3.5 ms

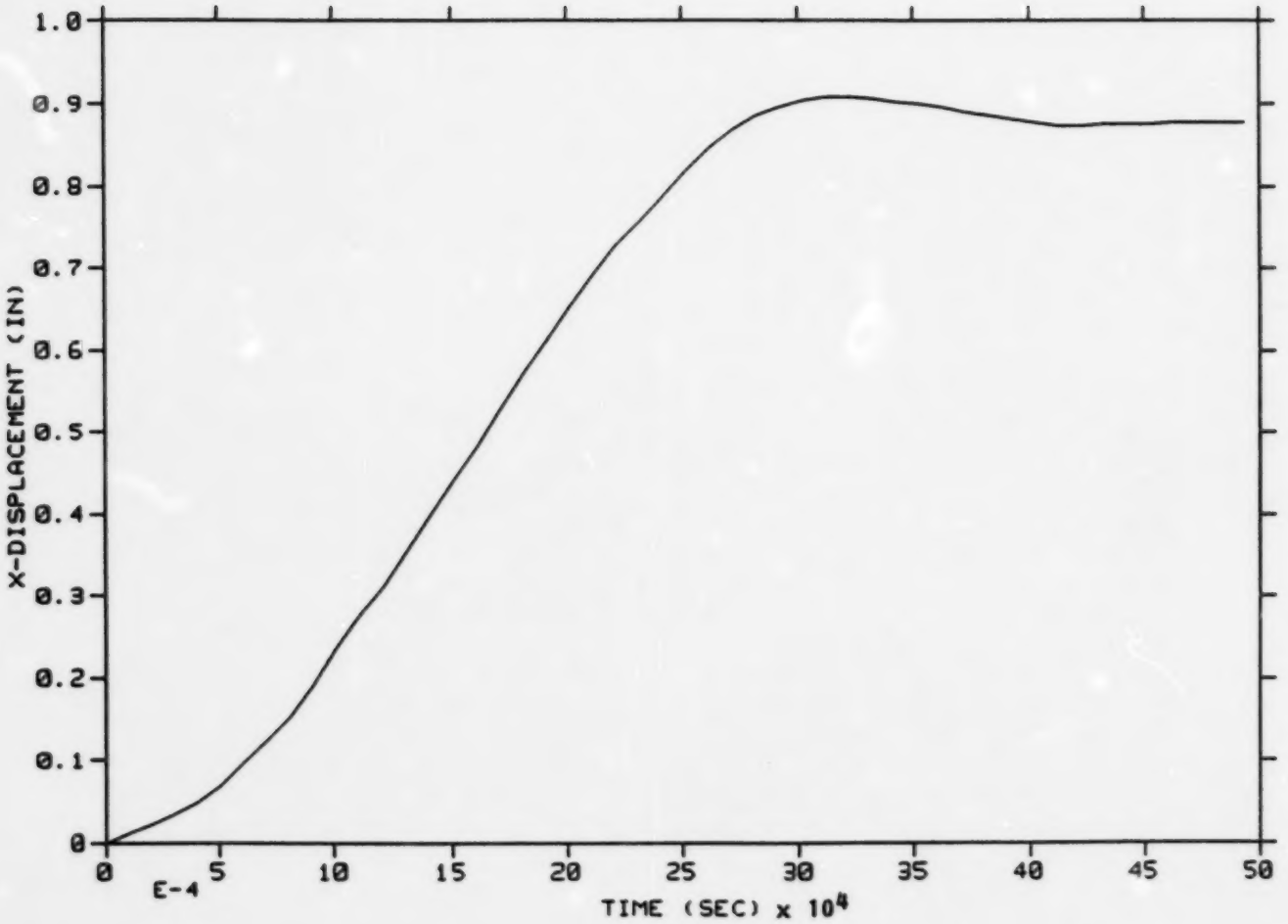

FIGURE 5.8.7

PIPE WHIP TEST
X-DISPLACEMENT TIME HISTORY OF NODE 1

89-222
161836-RD

APPENDIX A1

CENTRAL DIFFERENCE OPERATOR

CENTRAL DIFFERENCE OPERATOR
NON-LINEAR STRUCTURAL DYNAMICS

A comparison of the routine used in a standard explicit central difference operator and the routine used in non-linear structural analysis follows.

STANDARD EXPLICIT CENTRAL DIFFERENCE OPERATOR

$$\dot{x}^t = \frac{1}{2\Delta t}\left[x^{t+\Delta t} - x^{t-\Delta t}\right] \qquad \text{(velocity)}$$

$$\ddot{x}^t = \frac{\dfrac{(x^{t+\Delta t} - x^t)}{\Delta t} - \dfrac{(x^t - x^{t-\Delta t})}{\Delta t}}{\Delta t} \qquad \text{(acceleration)}$$

$$\ddot{x}^t = \frac{1}{\Delta t^2}\left[x^{t+\Delta t} - 2x^t + x^{t-\Delta t}\right]$$

$$M\ddot{x}^t = P^t - F^t \qquad \text{(damping not included)}$$

where $F^t = f(x^t)$

$$\frac{M}{\Delta t^2}\left[x^{t+\Delta t} - 2x^t + x^{t-\Delta t}\right] = P^t - F^t$$

$$\frac{M}{\Delta t^2}\,x^{t+\Delta t} = P^t - F^t + \frac{2M}{\Delta t^2}\,x^t - \frac{M}{\Delta t^2}\,x^{t-\Delta t} \qquad \text{(displacement)}$$

$$\dot{x}^t = \frac{1}{2\Delta t}\left[x^{t+\Delta t} - x^{t-\Delta t}\right] \qquad \text{(velocity)}$$

$$\ddot{x}^t = \frac{1}{\Delta t^2}\left[x^{t+\Delta t} - 2x^t + x^{t-\Delta t}\right] \qquad \text{(acceleration)}$$

Initially $x^{-\Delta t} = x_o - \dot{x}_o\Delta t + \ddot{x}_o\frac{\Delta t^2}{2}$

where x_o, $\dot{x}_o$, $\ddot{x}_o$ are the initial displacement, velocity and acceleration respectively.

From the velocity equation:

$$x^{t+\Delta t} = 2\Delta t\, \dot{x}^t + x^{t-\Delta t}$$

substituting into the equation for acceleration:

$$\Delta t^2 \ddot{x}^t = -2x^t + x^{t-\Delta t} + 2\Delta t\dot{x}^t + x^{t-\Delta t}$$

Thus;

$$x^{t-\Delta t} = x^t - \dot{x}^t\Delta t + \frac{\ddot{x}^t\Delta t^2}{2}$$

and

$$x^t = x_o \text{ initially}$$

<u>CENTRAL DIFFERENCE OPERATOR FOR NON-LINEAR F^t</u>:

$$M\ddot{x}^t = P^t - F^t$$

where: $F^t = f(x^t)$

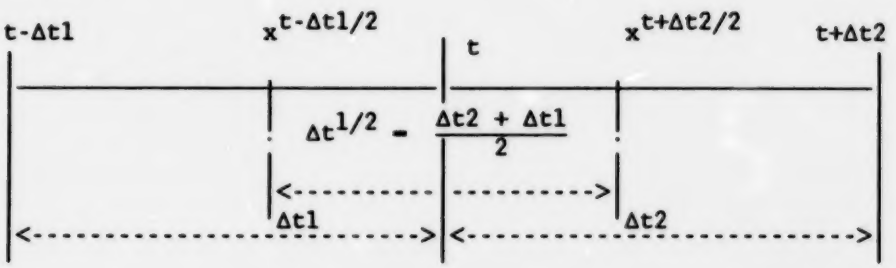

- $\ddot{x}^t = M^{-1}[P^t - F^t]$
- $\Delta t^{1/2} = \frac{\Delta t1 + \Delta t2}{2}$
- $\dot{x}^{t+\Delta t2/2} = \dot{x}^{t-\Delta t1/2} + \Delta t^{1/2}\ddot{x}^t$
- $\dot{x}^{t+\Delta t2/2} = \frac{x^{t+\Delta t2} - x^t}{\Delta t2}$

- $x^{t+\Delta t2} = x^t + \Delta t2\ \dot{x}^{t+\Delta t2/2}$
- update time t: $t + \Delta t2$
- Obtain F^t and solve for $x^{t+\Delta t2}$

Operator Stability

This operator is conditionally stable so that the time step 'Δt' must be maintained at values below a critical time step Δt_{cr} (i.e., $\Delta t < \Delta t_{cr}$).

As before:

$$\ddot{x}^t = \frac{1}{\Delta t^2}\left[x^{t+\Delta t} - 2x^t + x^{t-\Delta t} \right]$$

Therefore when:

$$p^t = 0,\ F^t = Kx^t$$

$$x^{t+\Delta t} - 2x^t + x^{t-\Delta t} + \Delta t^2 M^{-1} Kx^t = 0$$

assuming a solution of a form;

$$x^{t+\Delta t} = \lambda(x^t)$$

$$x^t = \lambda(x^{t-\Delta t})$$

$$\lambda - 2 + 1/\lambda + \Delta t^2 M^{-1} K = 0$$

letting eigenvalues $w^2 = M^{-1}K$

$$\lambda^2 + \lambda(\Delta t^2 w^2 - 2) + 1 = 0$$

$$\lambda_{1,2} = \frac{-(\Delta t^2 w^2 - 2) \pm \sqrt{(\Delta t^2 w^2 - 2)^2 - 4}}{2}$$

The roots are complex if;

$$4 > (\Delta t^2 w^2 - 2)^2$$

Thus, in the limit;

$$\Delta t^2 w^2 - 2 = 2$$

$$\underline{\Delta t_{cr} \leq \frac{2}{w}}$$

where, for structural problems (single degree of freedom system):

$$w_{max} = \left[\left| M^{-1} K^t \right|_{max} \right]^{1/2} = \left[\left| \frac{F^{t+\Delta t} - F^t}{M(x^{t+\Delta t} - x^t)} \right|_{max} \right]^{1/2}$$

$$\Delta t_{cr} \leq 2 \left[M \frac{(x^{t+\Delta t} - x^t)}{(F^{t+\Delta t} - F^t)} \right]^{1/2}$$

for shock wave problems:

$$\underline{w_{max} = \frac{2C}{L}}$$

C = speed of sound in the material

L = minimum element dimension

APPENDIX A2

THREE-DIMENSIONAL ELASTIC-PLASTIC MATERIAL MODEL WITH ISOTROPIC HARDENING

THREE-DIMENSIONAL ELASTIC-PLASTIC MATERIAL MODEL WITH ISOTROPIC HARDENING

For elastic-plastic material models the non-linear description of the material behaviour in the post-yield region entails the following:

(a) A yield criterion to determine the threshold at which plastic flow begins;

(b) A flow rule to relate plastic strain increments with total strain and stress increments; and

(c) A hardening rule to specify the modification of the yield condition during plastic flow.

For models used in the computer code H3DMAP, a von Mises yield surface and associated flow rule are adopted. The von Mises yield function is given as;

$$f(\sigma_{ij}) = J_2 - k^2$$

where J_2 is the second invariant of the stress deviator

k is the yield stress in pure shear

The bi-linear hardening model used to represent the stress strain curve is given in figure A2.1.

The deviatoric components of velocity strain and stress are given as;

$$\dot{\epsilon}'_{ij}{}^{t+\Delta t/2} = \dot{\epsilon}_{ij}^{t+\Delta t/2} - \frac{1}{3}\,\delta_{ij}\,\dot{\epsilon}_{kk}^{t+\Delta t/2}$$

$$\sigma'_{ij}{}^{t+\Delta t} = \sigma_{ij}^{t} - \delta_{ij} p^{t+\Delta t}$$

$$p^{t+\Delta t} = p^{t} + K\,\dot{\epsilon}_{ii}{}^{t+\Delta t/2}\,\Delta t$$

The radial return method/8,9/ for isotropic hardening is used in H3DMAP for the elastic plastic material models. In this method, a trial elastic deviatoric stress, S, is established. The plastic strain vector is assumed to be parallel to S. The yield condition is used to determine effective plastic strain increment $\Delta\bar{\epsilon}_p$. The updated radius of the yield surface is found and the trial elastic stress vector is returned to the new yield surface. The development of the method proceeds as follows:

i) Calculate a trial stress, S_{ij}, by updating σ'_{ij} elastically;

$$S_{ij}^{t+\Delta t} = \sigma'_{ij}{}^{t} + 2G\dot{\varepsilon}'_{ij}{}^{t+\Delta t/2}\Delta t$$

ii) Effective trial stress;

$$\bar{S} = [3J_2]^{\frac{1}{2}} = \left[\frac{3}{2} S_{ij}^{t+\Delta t} S_{ij}^{t+\Delta t} \right]^{\frac{1}{2}}$$

where J_2 is the second invariant of the stress deviator.

iii) Current yield stress $\sigma_y{}^{t}$ is obtained;

Referring to figure A2.1,

$$d\bar{\sigma} = E_t d\bar{\varepsilon}_t$$

$$d\bar{\varepsilon}_p = d\bar{\varepsilon}_t - \frac{d\bar{\sigma}}{E}$$

$$\frac{d\bar{\sigma}}{E_H} = \frac{d\bar{\sigma}}{E_t} - \frac{d\bar{\sigma}}{E}$$

$$E_H = \frac{E_t E}{E - E_t}$$

where E_H is the plastic modulus.

$$\sigma_y{}^{t} = \sigma_y{}^{o} + \bar{\varepsilon}_p^{t} E_H$$

where $\bar{\varepsilon}_p{}^{t}$ is the effective plastic strain at time 't'.

$\sigma_y{}^{o}$ is the initial yield stress.

iv) Test yield condition;

if $\bar{S} > \sigma_y{}^{t}$ yielding has occurred;

Then the stress is scaled back as follows:

$$\sigma'^{t+\Delta t}_{ij} = \frac{\sigma_y}{\bar{S}}^{t+\Delta t} S_{ij}^{t+\Delta t}$$

v) Plastic Strain Increment $\Delta\varepsilon_{p_{ij}}$:

$$\Delta\varepsilon_{pij} = \Delta\varepsilon'_{ij} - \frac{1}{2G}\left[\sigma'^{t+\Delta t}_{ij} - \sigma'^{t}_{ij}\right]$$

$$\Delta\varepsilon'_{ij} = \dot{\varepsilon}'^{t+\Delta t}_{ij}\Delta t = \frac{S_{ij}^{t+\Delta t} - \sigma'^{t}_{ij}}{2G}$$

$$\Delta\varepsilon_{p_{ij}} = \frac{1}{2G}\left[S_{ij}^{t+\Delta t} - \sigma'^{t+\Delta t}_{ij}\right]$$

$$= \left[\frac{1 - \frac{\sigma_y}{\bar{S}}^{t+\Delta t}}{2G}\right] S_{ij}^{t+\Delta t}$$

v) Effective plastic strain increment $\Delta\bar{\varepsilon}_p$;

$$\Delta\bar{\varepsilon}_p = \left[\frac{2}{3}\Delta\varepsilon_{p_{ij}}\Delta\varepsilon_{p_{ij}}\right]^{1/2}$$

$$\Delta\bar{\varepsilon}_p^2 = \frac{2}{3}\left[\left[\frac{1 - \frac{\sigma_y}{\bar{S}}^{t+\Delta t}}{2G}\right]\right]^2 S_{ij}^{t+\Delta t} S_{ij}^{t+\Delta t}$$

$$\Delta\bar{\varepsilon}_p^2 = \frac{2}{3}\left[\left[\frac{1 - \frac{\sigma_y}{\bar{S}}^{t+\Delta t}}{2G}\right]\right]^2 \frac{2}{3}\bar{S}^2$$

$$\Delta\bar{\varepsilon}_p = \frac{2}{3}\left[\left[\frac{1 - \frac{\sigma_y^{t+\Delta t}}{\bar{S}}}{2G}\right]\right]\bar{S}$$

$$= \frac{\bar{S} - \sigma_y^{t+\Delta t}}{3G}$$

$$\sigma_y^{t+\Delta t} = \sigma_y^{t} + E_H\Delta\bar{\varepsilon}_p$$

$$\Delta\bar{\varepsilon}_p = \left(\frac{\bar{S} - \sigma_y^{t+\Delta t}}{3G}\right) - \frac{\bar{S} - \sigma_y^{t} - E_H\Delta\bar{\varepsilon}_p}{3G}$$

$$\Delta\bar{\varepsilon}_p = \frac{\bar{S} - \sigma_y^{t}}{(3G + E_H)}$$

$$\bar{\varepsilon}_p^{t+\Delta t} = \bar{\varepsilon}_p^{t} + \Delta\bar{\varepsilon}_p$$

Yield at time t+Δt;

$$\sigma_y^{t+\Delta t} = \sigma_y^{t} + E_H\Delta\bar{\varepsilon}_p$$

vii) Scale back trial stress;

$$\sigma'^{t+\Delta t}_{ij} = \frac{\sigma_y^{t+\Delta t}}{\bar{S}} S_{ij}^{t+\Delta t}$$

viii) Total stress at time t+Δt;

$$\sigma_{ij}^{t+\Delta t} = \sigma'^{t+\Delta t}_{ij} + p^{t+\Delta t}\delta_{ij}$$

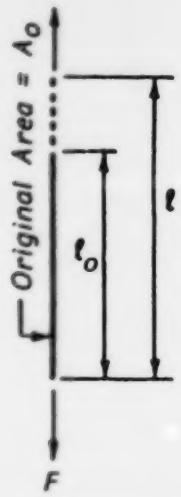

ℓ_o = Original Length
ℓ = Final Length

True Stress/Strain

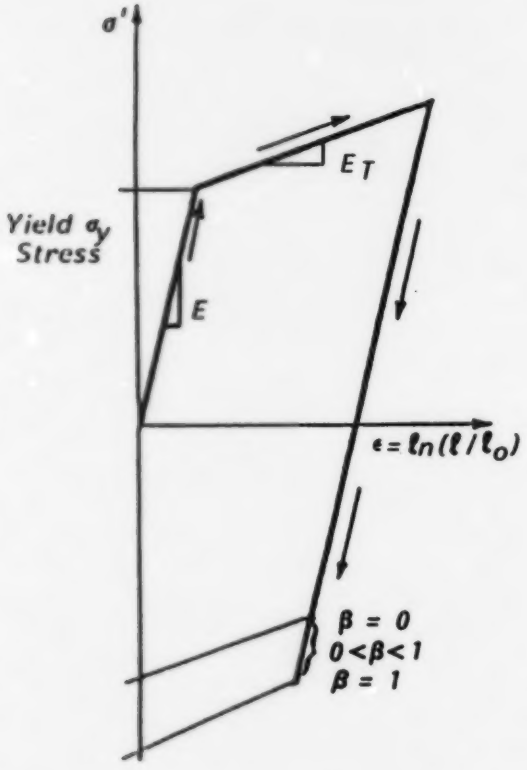

FIGURE A2.1

STRESS/STRAIN MEASURES
ELASTO-PLASTIC MATERIAL MODEL

180810-RD

89-222

APPENDIX A3

SIMPLIFICATION OF GRADIENTS IN ONE POINT GAUSS QUADRATURE

Simplification of Gradients in 1 Pt. Gauss Quadrature

The sampling points and weights for 1 and 2 pt. Gauss Quadrature are given as:

	Sampling Points		Weights
1 pt rule	r=s=0		wt = 2
2 pt rule	r	s	wt1 = 1.0
	-.577	-.577	wt2 = 1.0
	-.577	.577	
	.577	-.577	
	.577	.577	

Referring to figure 3.1, the values of the shape functions N_i described in section 3.2.1 are obtained as:

$$N_1 = 0.25(1+r)(1+s) \qquad \frac{\partial N_1}{\partial r} = 0.25(1+s) \qquad \frac{\partial N_1}{\partial s} = 0.25(1+r)$$

$$N_2 = 0.25(1-r)(1+s) \qquad \frac{\partial N_2}{\partial r} = -0.25(1+s) \qquad \frac{\partial N_2}{\partial s} = 0.25(1-r)$$

$$N_3 = 0.25(1-r)(1-s) \qquad \frac{\partial N_3}{\partial r} = -0.25(1-s) \qquad \frac{\partial N_3}{\partial s} = -0.25(1-r)$$

$$N_4 = 0.25(1+r)(1-s) \qquad \frac{\partial N_4}{\partial r} = 0.25(1-s) \qquad \frac{\partial N_4}{\partial s} = -0.25(1+r)$$

For one point Gauss quadrature r=s=0:

$$N_i = 0.25 \qquad i=1,4$$

The gradients in the local element axes are obtained from those in the natural coordinate system as;

$$\begin{Bmatrix} \frac{\partial N_i}{\partial x'} \\ \\ \frac{\partial N_i}{\partial y'} \end{Bmatrix} = [J]^{-1} \begin{Bmatrix} \frac{\partial N_i}{\partial r} \\ \\ \frac{\partial N_i}{\partial s} \end{Bmatrix}$$

$$J_{11} = \frac{\partial x'}{\partial r} = 0.25 \left[(1+s)x'_1 - (1+s)x'_2 - (1-s)x'_3 + (1-s)x'_4 \right]$$

$$J_{21} = \frac{\partial x'}{\partial s} = 0.25 \left[(1+r)x'_1 + (1-r)x'_2 - (1-r)x'_3 - (1+r)x'_4 \right]$$

$$J_{12} = \frac{\partial y'}{\partial r} = 0.25 \left[(1+s)y'_1 - (1+s)y'_2 - (1-s)y'_3 + (1-s)y'_4 \right]$$

$$J_{22} = \frac{\partial y'}{\partial s} = 0.25 \left[(1+r)y'_1 + (1-r)y'_2 - (1-r)y'_3 - (1+r)y'_4 \right]$$

$$|J| = J_{11}J_{22} - J_{12}J_{21}$$

$$J_{11}^{-1} = J_{22}/|J|$$

$$J_{12}^{-1} = -J_{12}/|J|$$

$$J_{21}^{-1} = -J_{21}/|J|$$

$$J_{22}^{-1} = J_{11}/|J|$$

For r=s=0;

$$\frac{\partial N_1}{\partial r} = 0.25 \qquad \frac{\partial N_1}{\partial s} = 0.25$$

$$\frac{\partial N_2}{\partial r} = -0.25 \qquad \frac{\partial N_2}{\partial s} = 0.25$$

$$\frac{\partial N_3}{\partial r} = -0.25 \qquad \frac{\partial N_3}{\partial s} = -0.25$$

$$\frac{\partial N_4}{\partial r} = 0.25 \qquad \frac{\partial N_4}{\partial s} = -0.25$$

$$J_{22}^{-1} = 0.25(x_1' - x_2' - x_3' + x_4')/|J|$$

$$J_{12}^{-1} = -0.25\ (y_1' - y_2' - y_3' + y_4')/|J|$$

$$J_{21}^{-1} = -0.25(x_1' + x_2' - x_3' - x_4')/|J|$$

$$J_{11}^{-1} = 0.25(y_1' + y_2' - y_3' - y_4')/|J|$$

$$\frac{\partial N_1}{\partial x'} = \frac{0.25}{|J|}\left[\, 0.25(y_1' + y_2' - y_3' - y_4') - 0.25(y_1' - y_2' - y_3' + y_4') \,\right]$$

$$= \frac{1}{8|J|}\ (y_2' - y_4')$$

$$b_{11} = \frac{\partial N_1}{\partial x'} = \frac{1}{2A}\ (y_2' - y_4')$$

where Area $A = 4|J|$ for 1 pt. quadrature,

$$A = 4|J| = \frac{1}{2}[(x'_1 - x'_3)(y'_2 - y'_4) + (x'_4 - x'_2)(y'_1 - y'_3)]$$

Similarly,

$$b_{12} = \frac{\partial N_2}{\partial x'} = \frac{1}{2A}\ (y_3' - y_1')$$

$$b_{13} = \frac{\partial N_3}{\partial x'} = \frac{1}{2A}\ (y_4' - y_2')$$

$$b_{14} = \frac{\partial N_4}{\partial x'} = \frac{1}{2A}\ (y_1' - y_3')$$

$$b_{21} = \frac{\partial N_1}{\partial y'} = \frac{1}{2A}\ (x_4' - x_2')$$

$$b_{22} = \frac{\partial N_2}{\partial y'} = \frac{1}{2A}\ (x_1' - x_3')$$

$$b_{23} = \frac{\partial N_3}{\partial y'} = \frac{1}{2A}\ (x_2' - x_4')$$

$$b_{24} = \frac{\partial N_4}{\partial y'} = \frac{1}{2A}\ (x_3' - x_1')$$

The velocity strain displacement matrix B_i presented in section 3.4 for node "i" can be written for 1 point Quadrature in the plane of the element as;

$$B_i = \begin{bmatrix} b_{1i} & 0 & 0 & 0 & zb_{1i} \\ 0 & b_{2i} & 0 & -zb_{2i} & 0 \\ b_{2i} & b_{1i} & 0 & -zb_{1i} & zb_{2i} \\ 0 & 0 & b_{1i} & 0 & N_i \\ 0 & 0 & b_{2i} & -N_i & 0 \end{bmatrix}$$

where: $z = 0.5th_i$

$N_i = 0.25$

h_i = thickness at node i